NOTICE

The quality of this microfiche is heavily dependent upon the quality of the original thesis submitted for microfilming. Every effort has been made to ensure the highest quality of reproduction possible.

If pages are missing, contact the university which granted the degree.

Some pages may have indistinct print especially if the original pages were typed with a poor typewriter ribbon or if the university sent us a poor photocopy.

Previously copyrighted materials (journal articles, published tests, etc.) are not filmed.

Reproduction in full or in part of this film is governed by the Canadian Copyright Act, R.S.C. 1970, c. C-30. Please read the authorization forms which accompany this thesis.

THIS DISSERTATION
HAS BEEN MICROFILMED
EXACTLY AS RECEIVED

AVIS

La qualité de cette microfiche dépend grandement de la qualité de la thèse soumise au microfilmage. Nous avons tout fait pour assurer une qualité supérieure de reproduction.

S'il manque des pages, veuillez communiquer avec l'université qui a conféré le grade.

La qualité d'impression de certaines pages peut laisser à désirer, surtout si les pages originales ont été dactylographiées à l'aide d'un ruban usé ou si l'université nous a fait parvenir une photocopie de mauvaise qualité.

Les documents qui font déjà l'objet d'un droit d'auteur (articles de revue, examens publiés, etc.) ne sont pas microfilmés.

La reproduction, même partielle, de ce microfilm est soumise à la Loi canadienne sur le droit d'auteur, SRC 1970, c. C-30. Veuillez prendre connaissance des formules d'autorisation qui accompagnent cette thèse.

LA THÈSE A ÉTÉ
MICROFILMÉE TELLE QUE
NOUS L'AVONS REÇUE

FLOW STRATIFICATION IN TWO-PHASE FLOW IN HORIZONTAL CHANNELS

by

Jung-Hoon Chun

A thesis submitted to the School of Graduate Studies in partial fulfillment of the requirements of the degree of

MASTER OF APPLIED SCIENCE

in the

Department of Mechanical Engineering

University of Ottawa

Ottawa, Canada

1980

ACKNOWLEDGEMENTS

The author wishes to express his most sincere gratitude to his supervisor Dr. Martha Salcudean for her invaluable guidance, support and endless encouragement throughout the course of the present study.

The author would like to pay particular thanks to Dr. D.C. Groeneveld, of A.E.C.L., who provided countless thoughtful suggestions and ideas throughout this work.

An expression of thanks is extended to technical staffs of the Mechanical Engineering Workshop at the University of Ottawa, for their cooperation.

The financial support of the Atomic Energy of Canada Research Company is also appreciated.

ABSTRACT

Two-phase flow in horizontal channels was studied using air-water flow in one-inch lucite tubes at ambient temperature. The flow pattern transitions were visually investigated, and flow pattern maps were constructed accordingly. Measurements of void distribution, mean void fraction and pressure drop were carried out.

Effects of flow obstructions on flow pattern transitions were observed. Also, effects on void distribution and pressure drop were investigated for bubbly, slug and annular flows. Two types of obstructions were used; central and peripheral, which covered an area equal to 25% of the total cross section area.

The obstruction changed flow pattern transition boundaries. The void distribution was shown to be most affected for bubbly flow. Pressure drop for all flows was higher with the central obstruction. Several other observed phenomena are also discussed such as changes of bubble sizes, pressure regeneration, etc.

The DISA 55S52 optical probe was used to measure the local void fraction with a static trigger level. This probe proved to be adequate for the investigated flow regimes, however, there was a limitation on its use for higher flow rates due to pressure fluctuations.

CONTENTS

Page

CHAPTER 3. EXPERIMENTAL APPARATUS AND PROCEDURES

CHAPTER 4. DISCUSSION OF RESULTS

LIST OF FIGURES

LIST OF TABLES

NOMENCLATURE

a	Parameter as defined in Eq.(2.24);
A	Channel flow area (m^2);
b	Parameter as defined in Eq.(2.25);
C_D	Discharge coefficient;
E	Frictional energy loss per unit mass (J/kg);
f	Frictional pressure drop coefficient;
F	Modified Frouds number as defined in Eq. (2.6);
g	Gravitational acceleration (m/sec^2);
G	Mass velocity (kg/m^2sec);
h	Height (m);
k	Head loss coefficient;
K	Product of Froude number and the square root of the superficial Reynolds number of the liquid;
L	Length (m);
P	Pressure (N/m^2);
Re	Renolds number;
S	Channel perimeter (m);
T	Parameter as defined in Eq.(2.4);
U	Velocity (m/sec);
v	Specific volume (m^3/kg)
W	Mass flow rate (kg/sec);
We	Weber number;

x	Quality;
X	Lockhart-Martinelli parameter as defined in Eq.(2.3);
y	Parameter as defined in Eq.(2.23);
Y	Parameter as defined in Eq.(2.5);
Z	Constant in Eq.(2.17);
α	Void fraction:
β	Volumetric quality;
γ	Specific weight (kg/m^2sec^2);
Γ	Chisholm-Sutherland parameter as defined in Eq.(2.15);
δ	Parameter as defined in Eq.(2.28);
η	Slip ratio;
θ	Angle between channel axis and the horizontal;
ψ	Parameter as defined in Eq.(2.2);
λ	Parameter as defined in Eq.(2.1);
μ	Absolute viscosity (kg/m sec);
ν	Kinematic viscosity (m^2/sec);
ρ	Density (kg/m^3);
σ	Surface tension (N/m);
τ	Wall shear stress (N/m^2);
Φ	Two-phase frictional multiplier;
$\frac{dp}{dx}$	Pressure gradient (N/m^3);

Superscript

S	Superficial;

Subscripts

a	Accelerational;
F	Frictional;
g	Gravitational;
G	Gas phase;
H	Homogeneous;
L	Liquid phase;
LH	Liquid phase across obstruction;
TP	Two-phase.

CHAPTER 1

INTRODUCTION

Two-phase flow* phenomena are receiving increasing attention due to their importance in the petro-chemical industry and nuclear reactors. Many studies dealing with two-phase flow have been made in order to meet the pressing need for improved and reliable design procedures.

The present thesis aims to investigate two-phase flow in horizontal channels. As the Canadian Nuclear Reactor, CANDU, has a horizontal core configuration, two-phase flow in horizontal channels is of particular importance in the CANDU design. Horizontal two-phase flow is characterized by the gravitational effects leading to an asymmetric flow.

It is a well known fact that there are natural patterns among existing flow configurations. Within each pattern the spatial location of each phase is more or less similar. As a result, one might expect a set of boundary conditions to be peculiar to a particular flow pattern. In the current study,

---

* Two-phase flow is a term covering the interacting flow of two phases where the interface between the phases is influenced by their motion, while the geometrical boundary of single phase is fixed.

the flow patterns were investigated, and void distribution and pressure drops were measured, since these data are essential to the study of two-phase flow.

Spacing devices for nuclear fuel bundles are known to have large effects on the CHF. In general, heat transfer coefficients are enhanced in the post-CHF region due to the improved subchannel mixing and the extra turbulence generated by the spacers, on the other hand pressure drops are increased significantly. As spacers are used in the CANDU reactors, one of the goals of the present study is to investigate the influence of flow obstructions on the flow patterns, void distribution and pressure drop. Two types of obstructions were used to simulate the spacers, a central and a peripheral.

In the current studies, a two-phase flow loop was designed and commissioned in order to conduct the experimental work. For void distribution measurements, a DISA 55S52 optical probe was used in conjunction with a phase indicator and void fraction unit. Quick-closing valves and a multi-column differential manometer were used to determine the mean void fraction and pressure drop respectively.

CHAPTER 2

LITERATURE SURVEY

The increasing importance of two-phase flow in industrial applications has induced extensive research, generating a number of papers with a wide range of topics. In the present survey, some of the contributions are mentioned, relating to flow pattern maps, void distributions and pressure drops, which are the topics of the present thesis.

2.1. Flow Pattern Maps in Horizontal Co-current Flow.

It is well known that there are natural groupings among a wide variety of two phases distributions which are observed. The configurations of the gas and liquid distribution are called 'FLOW PATTERNS' or 'FLOW REGIMES'. The mass flow rates of the two phases, the channel size and geometry, and the physical properties of the two phases are the factors that have been found to influence flow patterns in adiabatic two-phase flow [1].

For horizontal flows, the liquid phase tends to be

displaced towards the bottom of the channel due to the gravitational force. This results in asymmetric flow patterns. As most of the classification is based on the qualitative and subjective judgement of the observer, there are more than 60 names assigned to the particular configurations in horizontal co-current flow. Among them, six flow patterns are generally accepted as shown in Fig. 2.1. [1,2,3].

1. Stratified Flow: The liquid flows along the bottom of the channel and the gas along the top. The interface between them is smooth.
2. Wavy Flow: The liquid and gas are seperated as stratified flow, but the interface is wavy.
3. Bubby Flow: The gas is dispersed in the form of small bubbles in a continuum of the liquid. The bubbles tend to flow along the top of the channel.
4. Plug Flow: The elongated bubbles tend to move in a position adjacent to the top of the channel in a continuum of the liquid.
5. Slug Flow: The waves at the interface are picked up, resulting in frothy slugs which are propagated along the channel at a high velocity.
6. Annular Flow: The gas flows in the center of the channel, while the liquid flows through an annular section. The liquid film at the top is thinner than that at the bottom.

There are many parameters affecting the flow patterns as discussed. The controlling physical parameters differ in each pattern. Hence, each of the patterns requires a different approach to modelling of the mechanism of pressure drop and heat transfer.

As flow patterns are important to the analysis of two-phase flow characteristics, numerous flow pattern maps have been suggested in order to represent the transition from one pattern to another. In general, most of the coordinates that have been used in two-dimensional maps can be divided into two groups. One is based on the physical parameters and the other on the dimensionless group of influencing variables. However, in both cases, it is impossible to represent various transitions using only a two-dimensional plot, because it is unlikely that the same parameter would affect different transitions governed by different forces[1,4].

One of the first flow pattern maps was proposed by Bergelin and Gazley[5] using air-water in a one-inch pipe.

Baker[6] presented a map based on the data obtained by Jenkins[7], Gazley[8], Kosterin[9] and Alves[10]. He chose a number of variables such as $\frac{G_G}{\lambda}$ and $\frac{G_L \lambda \psi}{G_G}$ as the coordinates. Here,

$$\lambda = \left[\left(\frac{\rho_G}{0.075} \right) \left(\frac{\rho_L}{62.3} \right) \right]^{1/2} \qquad (2.1)$$

and

$$\psi = \frac{73.0}{\sigma}\left[\left(\frac{\mu_L}{1.0}\right)\left(\frac{62.3}{\rho_L}\right)^2\right]^{1/3} \qquad (2.2)$$

J.M. Mandhane et. al.[11] proposed a map using extensive data contained in the UC* multiphase pipe flow data bank. The physical parameters such as the superficial velocities of the liquid and gas were chosen as the coordinates.

Many other maps based on experimental data have been proposed by other investigators: amongst whom are Jenkins[7], Gazley[8], Kosterin[9], Johnson and Abou-Sabe[12], Alves[10], White and Huntington[13], Hoogendron[14], Govier and Omer[15], Scott[16] and Eaton et. al.[17].

The maps resulting from experimental data have limited ranges of validity according to the experimental conditions. This is the reason why there is a growing trend towards the development of physical models, although empirical correlation methods are widely used.

---

* UC: University of Calgary

A generalized flow pattern map based on physical modeling of the transition mechanism was presented by Taitel and Dukler[18]. Five different dimensionless groups resulted from the mathematical model used, because the mechanism for transition is different between each pair of flow patterns. They are:

$$X = \left[\frac{\left(\frac{dp}{dx}\right)_L^S}{\left(\frac{dp}{dx}\right)_G^S} \right]^{1/2} \tag{2.3}$$

where X is the parameter introduced by Lockhart and Martinelli to be discussed in section 2.2.2.

$$T = \left[\frac{\left(\frac{dp}{dx}\right)_L^S}{(\rho_L - \rho_G)\, g \cos\theta} \right]^{1/2} \tag{2.4}$$

where T is considered as the ratio of forces caused by the turbulence to forces of gravity acting on the gas.

$$Y = \frac{(\rho_L - \rho_G)\, g \sin\theta}{\left(\frac{dp}{dx}\right)_G^S} \tag{2.5}$$

where Y represents the relative forces acting on the liquid in the flow direction due to gravitational forces and pressure drop.

$$F = \sqrt{\frac{\rho_G}{\rho_L - \rho_G}} \frac{U_G^S}{\sqrt{D\ g \cos\theta}} \qquad (2.6)$$

where F is a modified Froude number multiplied by the density ratio.

$$K = F\left[\frac{D\ U_L^S}{\nu_L}\right]^{1/2} = F\left[Re_L^S\right]^{1/2} \qquad (2.7)$$

where K is the product of Froude number and the square root of the superficial Reynolds number of the liquid.

The particular transitions were shown to be controlled by the following groups as illustrated in Fig. 2.2. The groups are as follows;

Stratified to Annular	X.F.Y
Stratified to Intermittent	X.F.Y.
Intermittent to Dispersed Bubble	X.T.Y
Stratified Smooth to Stratified Wavy	X.K.Y
Annular-Dispersed Liquid to Intermittent and Dispersed Bubble	X.Y

2.2 Pressure Drop for Two-Phase Flow.

The accurate prediction of pressure head is important for the design of two-phase flow systems. Proper pumping powers are necessary to maintain a required mass flow rate. However, little information on generalized pressure drop correlations has been obtained due to the existence of complex behavior at the phases interface.

The pressure gradient for two-phase flow head in a uniform channel is given by

$$-\frac{dp}{dx} = -\frac{dp_F}{dx} - \frac{dp_a}{dx} - \frac{dp_g}{dx} \qquad (2.8)$$

where $\frac{dp}{dx}$ is the pressure gradient and $\frac{dp_F}{dx}$, $\frac{dp_a}{dx}$, $\frac{dp_g}{dx}$ are respectively the frictional, accelerational and gravitational components of the pressure gradient. Each component can be derived using a one-dimensional momentum and energy balance for slip between the phases and for no slip between the phases. These components are shown in Table 2.1.[3]

Numerous studies have been carried out to correlate the frictional component, since this component must be determined empirically, whichever equation is used.

Three basic models have been considered, that is, homogeneous flow models, separated flow models and mixed flow models.

2.2.1. Homogeneous Flow Models.

These models are based on the assumption that there is complete interaction between the phases. The single phase equations are used with suitable mean physical properties. Since the friction factor is determined as a function of homogeneous Reynolds number, the prediction for a two-phase viscosity is of great importance for the successful use of this model.

McAdams et. al.[19] proposed the equation

$$\frac{1}{\mu_H} = \frac{x}{\mu_G} + \frac{1 - x}{\mu_L} \qquad (2.9)$$

Cicchitti et. al.[20] suggested the definition

$$\mu_H = x\,\mu_G + (1 - x)\,\mu_L \qquad (2.10)$$

Dukler et. al.[21] have used the equation

$$\mu_H = \rho_H \left[x\, v_G\, \mu_G + (1 - x)\, v_L\, \mu_L\right] \qquad (2.11)$$

2.2.2. Separated Flow Models.

These models are based on the assumption that there is no interaction between the phases. It is implied that the pressure gradient in each phase when flowing together is equal to the pressure gradient produced when each phase flows separately in a channel having the same cross sectional area as that occupied originally.

Lockhart and Martinelli [22] introduced the two-phase multiplier defined as

$$\Phi_G^2 = \frac{\left(\frac{dp_F}{dx}\right)_{TP}}{\left(\frac{dp_F}{dx}\right)_G^S} \qquad \Phi_L^2 = \frac{\left(\frac{dp_F}{dx}\right)_{TP}}{\left(\frac{dp_F}{dx}\right)_L^S} \qquad (2.12) \text{ \& } (2.13)$$

By plotting Φ_G and Φ_L against X, shown in Fig. 2.3., a general correlation of two-phase frictional pressure gradient was derived.

2.2.3. Mixed Flow Models.

These models are based on the assumption that there is a certain degree of interaction between the phases.

Baroczy[23] has introduced mass-velocity correction factors to the frictional pressure drop correlation using the parameters x and Λ. Λ is defined as

$$\Lambda = \frac{\rho_G}{\rho_L} \left(\frac{\mu_L}{\mu_G}\right)^{0.2} \tag{2.14}$$

This was introduced because he was convinced that the degree of interaction between the phases seems to depend on the flow rates of each phase.

Chisholm and Sutherland[24] improved Baroczy's method in a simple way by defining a generalized parameter Γ, where Γ is given by

$$\Gamma^2 = \left(\frac{dp_F}{dx}\right)_G \Big/ \left(\frac{dp_F}{dx}\right)_L \tag{2.15}$$

2.2.4. Pressure Drop Across the Obstruction.

As the information on pressure drop across flow obstruction is essential in the design of two-phase systems, many studies have been carried out. It is difficult to obtain reliable procedures to predict the pressure drop because of lack of knowledge in analyzing the mechanism.

Pressure drop across an orifice plate was expressed by Hoopes[25] and Thom[26] as

$$\Delta p = \frac{G^2 v_L}{2 C_D^2}\left[\left(\frac{A}{A_o}\right)^2 - 1\right]\left[\frac{(1-x)^2}{1-\alpha} + \frac{v_G}{v_L}\frac{x^2}{\alpha}\right] \qquad (2.16)$$

This equation was derived under the assumption of homogeneous flow and modified by the use of two-phase multiplier. However, the accuracy of prediction was ± 50 per cent.

Chisholm and his co-workers[27] proposed a completely different and superior method under the assumption that there exists a shear force between the phases. Momentum balance across the orifice was applied to the two-phase flow. This resulted in the relation

$$\frac{\Delta p_{TP}}{\Delta p_L} = 1 + \frac{C}{X} + \frac{1}{X^2} \qquad (2.17)$$

where

$$C = Z + \frac{1}{Z}$$

However, a general procedure for predicting Z has not yet been developed.

Little information on pressure drop across a central obstruction is found in the literature.

Studies on pressure drop through enlargements, contractions and baffles have been carried out by many workers, amongst whom are; Romie[28], Ferrel and McGee[29], Geiger and Rohner[30], Fitzsimmons[31], and Couturier[32].

2.2.5. Analytical Method.

An attempt to solve the Navier-Stokes equations to obtain the pressure gradient analytically was made by Charles and Redburger[33]. The finite difference equation was applied using the relaxation procedure. As the Reynolds number of liquid phase increased, the deviation from the experimental data obtained by Russel increased. This is probably due to the fact that the analytical method cannot correctly account for the complex phenomena which occur in two-phase boundaries.

2.3. Void Fraction Correlations

The void fraction is defined as the ratio of the gas phase flow area to total flow area, and can be expressed as

$$\alpha = \frac{1}{1 + \eta \frac{1 - x}{x} \frac{\rho_G}{\rho_L}} \qquad (2.18)$$

where η is the slip ratio.[3]

In the homogeneous flow model, the void fraction can be obtained by simply setting $\eta=1$. Hence,

$$\alpha_H = \frac{1}{1 + \frac{1-x}{x}\frac{\rho_G}{\rho_L}} \tag{2.19}$$

In the separated flow model, Lockhart and Martinelli[22] proposed a void fraction correlation using the parameter X, shown in Fig. 2.3.. Tuner and Wallis[34] derived the void fraction relation based on their separate cylinders concept. It can be shown as

$$\alpha = \frac{1}{1 + X^{4/(5-n)}} \tag{2.20}$$

Zivi[35] suggested the slip ratio correlations rather than void fraction correlations as

$$\eta = \left(\frac{\rho_L}{\rho_G}\right)^{1/3} \tag{2.21}$$

In the mixed flow model, Premoli et. al.[36] correlated the slip ratio increment $\Delta\eta$ equal to $\eta-1$. The result is expressed as a function of several parameters as follows.

$$\Delta\eta = a\sqrt{\frac{y}{1+by} - by} \tag{2.22}$$

where

$$y = \frac{\alpha_H}{1 - \alpha_H} \tag{2.23}$$

$$a = 1.578\ Re_L^{-0.19}\ (\rho_L/\rho_G)^{0.22} \tag{2.24}$$

$$b = 0.0273\ We\ Re_L^{-0.51}\ (\rho_G/\rho_L)^{0.08} \tag{2.25}$$

$$Re_L = G\ D\ /\ \mu_L \tag{2.26}$$

$$We = G^2\ D\ /\sigma\rho_L \tag{2.27}$$

Bankoff [37], Hughmark [38], and Armand [39] correlated the void fraction and the volumetric quality given by

$$\delta = \frac{\alpha}{\beta} \tag{2.28}$$

It was suggested that δ increased with pressure and δ was a weak function of mass velocity.

2.4. The Measurement of Void Fraction.

Various types of two-phase flow instrumentation have been developed and utilized to determine the average and/or local void fractions. Average measurement techniques provide line, area or volume averages, while local methods provide measurements at a specific location.

The local instruments require the insertion of a probe, which detects changes in the physical properties inherent in the two-phases at the point of interest[40].

2.4.1. Isokinetic Probe.

An isokinetic probe samples the two-phase mixture under isokinetic conditions, that is, when the static pressure at the entrance of the probe is kept equivalent to the static pressure of the test section. This was designed to measure not only the local void fraction, but the velocities of each phase in certain flow regime. However, it is very difficult to obtain the isokinetic conditions because of the inherent pressure fluctuations of the two-phase flow[41,42].

2.4.2. Hot Film and Hot Wire Anemometers.

The probes make use of the fact that the heat transfer coefficient is different in the two-phase flow. The probes can be used in two-component two-phase flow, or in one-component two-phase flow with phase change to measure the local void fraction. It is also possible to measure the velocities, since heat transfer rates vary according to the velocities [43,44].

2.4.3. Optical Probe.

The optical probe detects changes in the refractive indices of the two phase mixtures, enabling measurements of local void fractions. The optical probe is probably the simplest device for obtaining information on phase distributions. Also, the small size of the U-shaped fiber sensor gives the least disturbance to the flow [43,45].

2.4.4. Electrical Probe.

The electrical probe detects the significantly different electrical conductivity of each probe. Hence, the liquid should be conducting and continuous, if this probe is to be used to measure the local void fraction. For D.C. excitation mode, electrochemical effects tend to alter the response time. Also, it is necessary for an A.C. supply to have a current frequency significantly different to that of the physical phenomenon under observation [43].

2.4.5. Photon Attenuation Techniques.

This method makes use of the principles that a stationary, homogeneous material will absorb a monochromatic beam of constant intensity. Using this method mean void fractions can

be measured without disturbing the flow[43].

2.4.6. Quick-Closing Valves.

One of the simplest ways of obtaining the mean void fraction is to stop the two-phase flow in a restricted volume by closing two gate valves simultaneously[46].

CHAPTER 3

EXPERIMENTAL APPARATUS AND PROCEDURES

3.1. Loop.

A two-phase flow loop was designed and built as shown in Fig. 3.1. in order to carry out the experiments.

The inlet section, test section and exit section were 6 m long and were supported in a horizontal position. To enable flow visualization, 25.4 mm I.D. lucite tubes were used.

3.1.1. Air-Water Mixer.

As illustrated in Fig. 3.2. schematically, the air and water flowed through a honeycomb mixer at the inlet of the test sections.

3.1.2. Test Sections.

The main test section was located at 120 hydraulic

diameters downstream from the air-water mixer. Along this section, provisions were made for measurements of the mean void fractions, local void fractions and pressure drops. Also, it was possible to rotate the test section. Flow obstructions with different shapes and sizes could be changed in the test section. Fig. 3.3. is a schematic diagram showing the locations of the optical probe and the obstruction, while Fig. 3.4. shows the locations of the pressure tappings and the obstruction.

3.1.3. Quick-Closing Valves.

Two quick-closing valves, 1.219m apart, were installed to hold up the flow over the length of the tube enclosed by the valves. Sliders connected by a mechanical linkage were operated simultaneously by a spring tension of 175 Newtons. Fig. 3.5. shows this mechanism.

3.1.4. By-Pass System

A by-pass system was devised in order to prevent damage to the experimental set-up by the high pressure resulting from the rapid flow interruption.

3.1.5. Throttling Valves.

Two ball valves were installed at the inlet and outlet of the test section. The inlet valve reduced the fluctuation of the two-phase flow, whereas the outlet valve controlled the static pressure of the test section.

3.2. Air and Water Supply System.

Air was supplied from a WAS-75 Airscrew type compressor at about 0.83 MPa, with maximum flowrate capacity of 0.2 kg/sec. This compressor was commissioned and installed for the present project. To measure the air flow rate, three rotameters and an orifice plate were installed in parallel. The ranges of the meters were 0.002-0.02 kg/sec, 0.016-0.13 kg/sec, 0.02-0.2 kg/sec and 0.00028-0.0024 kg/sec respectively. A Bourdon type pressure gauge was used to measure the static pressure at the entrances of the rotameters, whereas a U-tube manometer filled with mercury was used for the orifice plate. The calibration chart for the rotameters was supplied by the manufacturer, and is shown in Table 3.1.. However, the orifice plate was calibrated with a precise wet volume test meter, and the result is shown in Fig. 3.6..

Water was drawn from a building service line at about 1.03 MPa. A rotameter having a range of 0.16-1.7 kg/sec was installed to meter the water flow rates. By collecting the water, low flow rates were measured.

Commercial K-type thermocouples monitored the temperatures of each phase.

3.3 Instrumentation

3.3.1. Optical Probe System

The DISA 55S52 miniature optical probe in conjunction with the DISA 55S01 phase indicator unit and the DISA 55S11 void fraction unit was used to measure the local void fractions.

The optical probe comprises the probe body, the stainless steel tube and the probe tip. The probe body contains a light source placed at the end of the optical fibre and a photo transister at the other end. An optical fibre is bent at the tip to form a U-shaped sensor and mounted on the 0.003 meters diameter stainless steel tube. The fibre is 40 micrometers in diameter and the U-shaped sensor is 100 micrometers in diameter.

The probe signal is amplified in the probe body and the output is normalized so that liquid phase at the tip gives 5 volts and the gas phase gives 4.4 volts. Thus the modulation is approximately 600 $\pm$ 50 mV peak to peak and this level is preset for Air-Water measurement.

The phase indicator provides a regulated 5 volts D.C. and 12 volts D.C. to the probe and the void fraction unit respectively. This converts the probe signal into a logical signal representing the presence of the phase at the tip. Two kinds of trigger level are used; a static level and a dynamic level.

For the static output, as shown in Fig. 3.7., a fixed trigger level typically set at 4.6 volts is used. The amplitude of the input signal is compared with a fixed level in a comparator. When the probe signal is higher than 4.6 volts the phase indicator unit gives 0 volt output, representing the presence of the liquid phase.

Fig. 3.7. also shows the dynamic signal which is obtained by using two trigger levels, a high and a low level. The two trigger levels are determined as a percentage of the difference between the average maximum and the minimum values of the probe signals.

The void fraction is integrated in the void fraction unit and displayed as a percentage.

As shown in Fig. 3.8., a micrometric transverse mechanism was designed to ensure the radial displacement of the optical probe to an accuracy of ± 0.02mm. Also, a large angle divider was installed to displace the probe by angular increments of 10 degrees.

3.3.2. Pressure Drop Measurement System.

In order to measure the pressure drop, a pressure drop measurement system was built as shown in Fig. 3.9..

The Mariam 33KB35 8 tubes manometer was connected to the pressure tappings, and the pressure reservoir which was connected to the pressure tapping downstream of the test section. Mariam oil(S.G. 2.95) columns show the pressure differences between each measuring point and the reference point, that is the pressure reservoir. Toggle-operated valves were installed between the columns and the pressure tappings and also between the columns and the pressure reservoir to freeze the pressure fluctuations. A precise Bourdon type pressure gauge was mounted on the pressure reservoir to measure the static pressure at the reference point.

By-pass lines were provided to remove the air bubbles inside the connecting lines as this minimized the errors in the pressure readings.

3.4. Experimental Procedures.

3.4.1. Local Void Fraction Measurements.

1. The desired flow rates of air and water were fixed. The desired pressure was built up with the aid of a throttling valve at the end of the test section. Fluctuations due to throttling were reduced using a valve at the outlet of the air-water mixer.
2. The probe was positioned radially with a micrometric transverse mechanism, and angularly with a large angle divider. Under the assumption that the void distribution was symmetric about the vertical center line of the cross section, 95 points were located across half of the cross section. At each point, 6 readings were taken.
3. The air and water temperatures were close to the room temperature, and were sufficiently constant during the experiments. When a large variation was detected in flow rates, an additional measurement was taken.

3.4.2. Mean Void Fraction Measurements.

Flow conditions were set as previously stated. By rotating a rod which connected the triggers of each valve, two quick-closing valves were closed simultaneously. A bypass system was opened after activating the quick-closing valves to prevent damage to the experimental setup. The amount of water poured into the test section to fill the portion previously occupied by the air was metered. Three measurements were taken for each flow condition.

3.4.3. Pressure Drop Measurements.

To reduce the experimental errors, air bubbles in the pressure lines were removed. Following closure of the drain valves, the desired flow conditions were set. When the pressure differences were built up in the manometer, the quick shut-off valves between the pressure tappings and the manometer, and between the reference pressure reservoir and the manometer were closed simultaneously. The pressure differences were kept frozen in the manometer free from pressure fluctuation.

3.5. Data Reduction.

3.5.1. Void Fraction.

For a given angle, the local void fraction was interpolated linearly between 6 experimental points for the desired void fractions such as 99%, 90%, 75%, 60%, 50%, 40%, 30%, 20%, and 10%. By connecting the points with the same void values across half of the cross-section, iso-void lines were drawn.

The integrated void fraction(IVF) can be expressed as

$$IVF = \frac{2}{\pi R^2} \int_0^R \int_0^\pi \alpha(r,\theta)\, r\, d\theta\, dr \qquad (3.1a)$$

For the purpose of obtaining an integrated void fraction, the section was divided into 95 segments. In the center of each of these 95 segments, the void fraction was obtained experimentally. This experimental value was assumed to be representative of the void fraction in the whole segment. The IVF can be obtained numerically as

$$IVF = \frac{\sum (\alpha_i \times A_i)}{\sum A_i} \qquad (3.1b)$$

The mean void fraction can be easily evaluated by dividing the volume of water poured into the test section by the total test section volume.

The quality is expressed as

$$x = \frac{W_G}{W_G + W_L} \tag{3.2}$$

The real velocity of each phases can be obtained using

$$U_G = \frac{W_G}{\rho_G \alpha A}, \quad U_L = \frac{W_L}{\rho_L (1-\alpha) A} \tag{3.3 \& 3.4}$$

The slip ratio is

$$\eta = \frac{U_G}{U_L} \quad \frac{x}{1-x} \quad \frac{\rho_L}{\rho_G} \quad \frac{1-\alpha}{\alpha} \tag{3.5}$$

The superficial mass flux is defined as the mass flow rate of the phase divided by the total cross sectional area, and is expressed as

$$G_G^S = \alpha \rho_G U_G, \quad G_L^S = (1-\alpha) \rho_L U_L \tag{3.6 \& 3.7}$$

The readings of local void fraction for Fig. 4.12. and the sample calculation is presented in the Appendix.

3.5.2. Pressure Drop.

The pressure drop can be calculated by considering the difference between the column heights. This is given by

$$P = \left(\rho_{Mariam} \sigma \rho_{Water} \right) g \Delta h \qquad (3.8)$$

where Δh is the difference between the column heights.

The two-phase frictional multiplier is given by [22]

$$\Phi_L^2 = \frac{\left(\frac{dp_F}{dx}\right)_{TP}}{\left(\frac{dp_F}{dx}\right)_L} \qquad (3.9)$$

The head loss coefficient for water across the obstruction is defined as

$$k = \frac{\frac{(\Delta P)_L}{\rho_L}}{\frac{U_L^2}{2g}} \qquad (3.10)$$

The two-phase multiplier for the head loss coefficient is calculated with the relation

$$\Phi_{LH}^2 = \frac{\frac{(\Delta P)_{TP}}{\gamma_L}}{k \frac{U_L^S{}^2}{2g}} \qquad (3.11)$$

The frictional coefficient for single phase flow is expressed as

$$f = \frac{\Delta P}{\gamma} \frac{D}{L} \frac{2g}{U^2} \qquad (3.12)$$

CHAPTER 4

DISCUSSION OF RESULTS

4.1. Flow Pattern Map

Although there are some widely used flow pattern maps for air-water flows in 0.0254 m I.D. tubes, a flow pattern map for the plain tube was constructed using a visual investigation method to enable consistent decision making for the various flow pattern transitions, in order to evaluate flow obstruction influence more accurately.

A strobe light was used to freeze the movement of bubbles, so that the sizes and numbers of the bubbles could be easily investigated. Also, some photographs were taken, and the photographs for each regime is shown in Fig. 4.1.. Void redistribution for bubbly flow past a peripheral obstruction is shown in Fig. 4.2.. The superficial velocities of water and air were used as coordinates.

4.1.1. Flow Pattern Map for Plain Tube.

In the transition boundary regions, 152 points were investigated, and are shown in the form of a flow pattern map in Fig. 4.3.. Table 4.1. shows the superficial velocities of air and water at 152 experimental points.

In the figure, this map is compared with others which have been proposed by Mandhane et. al. [11] and Dukler et. al. [18] . Stratified and wavy to mixed(plug and slug) transition occurs in lower liquid velocities. Also, mixed to bubbly transition appears in lower liquid velocities. In the case of slug to annular transition, there is a fairly good agreement for lower liquid velocities with Mandhane's results, but in higher liquid velocities there are some discrepancies. However, stratified to wavy and wavy to annular transitions show very good agreement with their results. The observer's criteria on transitions would probably cause the discrepancy in plug to slug transition.

4.1.2. The Effects of Flow Obstructions on Flow Pattern Transitions.

Figs. 4.4. and 4.5. show the flow pattern maps for the test sections with peripheral and central obstructions respectively.

The flow obstruction ratio was 25% and visual investigation for 152 points in the transition boundaries was conducted in the region following the obstruction. Tables 4.2. and 4.3. show the superficial velocities of air and water at 152 experimental points for central and peripheral obstructions respectively.

Fig. 4.6. illustrates the comparison of the transitions with those in the plain tube.

1. Stratified to wavy transition:

   This occurs at lower gas velocities, since obstructions disturb the two-phase flow resulting in a wave at the surface of the water. The peripheral obstruction mainly disturbs the water flow, while the central obstruction increases the gas velocity and disturbs the interface between the gas and liquid. The results show that the central obstruction has a stronger effect.

2. Wavy to slug transition:

   This takes place at lower liquid velocities. As the flow is disturbed by the obstruction, the waves are generated at lower liquid velocities and are consequently picked up to form a frothy slug. The central obstruction has a stronger effect as previously explained.

3. Slug to annular transition:

This appears at lower gas velocities. It can be explained by observing that liquid phase is pushed out to the wall after it passes the obstructions, so that an annulus can be easily formed. In this transition, the peripheral obstruction shows a stronger effect, because the central obstruction helps the flow homoginization and reduces its effect on transition boundaries.

4.2. Optical Probe Performance.

Using an optical probe, local void fractions were measured for nine different inlet conditions. These measurements were carried out in the 1.219 m long test section enclosed by the quick-closing valves. The probe was mounted at the middle of the test section. The distance between the probe and the air-water mixer was kept at 144 hydraulic diameters under the assumption that there was little evolution of two-phase flow compared to the development near the mixer.

4.2.1. Dynamic Trigger Level.

Table 4.4. and Figs. 4.7., 4.8. show the result of measurements using the dynamic trigger level.

It was found that with the dynamic trigger level the optical probe gave a considerably lower void fraction than that obtained using the quick-closing valves. It is believed that the disagreement was caused by the fact that the dynamic trigger level is not suitable for the flow regimes under consideration. According to the system description, the dynamic trigger level could cause difficulties in cases where there are periods longer than one second with the gas phase at the probe tip. As flow separation increases, a larger discrepancy occurs.

4.2.2. Static Trigger Level.

The static trigger level, however, gave good agreement between the integrated void fractions, obtained using an optical probe, and the mean void fractions, obtained using the quick-closing valves, as shown in Table 4.5.. Figs. 4.9.-4.15. show the obtained void distribution. The iso-voidage lines are fairly horizontal throughout the cross section and tend to move upwards near the wall. As expected, the water film at the bottom of the channel was thicker than that at the top due to the force of gravity. As the air flow rate was increased, the air phase tended to flow through the middle of the the cross section resulting in a more symmetrical void distribution.

The void fractions were calculated according to the homogeneous model, Zivi model and Premoli model for the corresponding inlet conditions. As shown in Table 4.5., experimentally obtained values were close to those predicted by the models of Zivi and Premoli, so that one can conclude that the homogeneous model does not represent the observed flow. These models have been proposed based on the mixed flow model and are discussed in section 2.3..

4.2.3. Limitation on the use of Optical Probes.

There were several failures of the probe tip for considerably high flow rates; air: 59.2 kg/m^2sec, water: 592 kg/m^2sec. This seems to be due to the pressure fluctuations of two-phase mixture, since the tip performed properly in an equivalent single phase flow, either air or water.

4.3. Effects of Flow Obstructions on the Void Distributions.

4.3.1. Bubbly Flow.

In bubbly flow, void distributions and the integrated void fraction were considerably changed due to the flow obstructions.

1. Peripheral obstruction.

Fig. 4.16. illustrates the change of void distribution along the test section. Void distribution at Tap 1 where the flow is not yet disturbed is characterized by the air phase tending to move along the top of the channel.

As the flow approaches the obstruction, the increase of voidage can be found. This is probably due to the following mechanism; the air bubbles are slowed down by the obstruction more than the liquid phase, since the air bubbles have smaller kinetic energy per unit volume. As a result, the slip is decreased, and the voidage is increased.

Following the obstruction, considerable flow homogenization can be observed at the bottom of the channel resulting in an increase of voidage. The change of the paths of air bubbles causes the decrease of their momenta in the direction of flow, and consequently the ratio of inertial forces to the surface tension forces is decreased. This introduces a larger number of bubbles with smaller diameters, resulting in an increase of voidage. The obstruction also introduces turbulence which is known to produce breaking up of the bubbles because of momentum redistribution.

At 12 hydraulic diameters downstream from the obstruction, the iso-voidage lines become similar to those at Tap 1. However, air phase was still detected at the lower part of the channel. It could be observed that the length of disturbed flow was about 20 hydraulic diameters.

2. Central obstruction.

The general influence of the obstruction is similar to the peripheral case, but the effect is much stronger as shown in Fig. 4.17. because of the following reasons.

Although the ratios of obstruction are the same for both cases, the area affecting the two-phase mixtures is larger in the case of the central obstruction. This caused the slowing down of bubbles, resulting in a slip ratio of less than one. Also, the central obstruction increases the bubble breakdown, therefore smaller sizes of air bubbles were observed. In addition, three supporting bars, required to hold the obstruction, help the flow homogenization.

At Tap 3, the voidage distribution was still quite far from the non-disturbed distribution observed at Tap 1, since the flow homogenization was largely achieved by the central obstruction. The flow was recovered at about 30 hydraulic

diameters downstream from the obstruction.

One can thus conclude that for bubbly flow the central obstruction has a stronger effect.

4.3.2. Annular Flow.

The effects of flow obstruction on the annular flow were less pronounced than on the bubbly flow. The reason for the decreased effect of the obstruction is due to the lesser importance of surface tension phenomena when compared to bubbly flow. However, changes of void distribution could be observed.

1. Peripheral obstruction.

Fig. 4.18. shows the change of void distribution along the test section. In the undisturbed void distribution, the air phase flows in the central part of the test section and the liquid phase forms an annulus. The distribution is asymmetric, since air phase tends to move upward. Many small air bubbles were entrained in the water film at the top of the channel.

For the peripheral obstruction, two contrary trends can be considered:

i. Because of its compressibility and the geometry of the obstruction, the air phase is accelerated more rapidly through the obstruction. This increases the slip ratio and leads to decrease of voidage. On passing the obstruction, two-phase flow also encounters the mixing procedure. As a result, a great number of small air bubbles are entrained in the water film. This decreases the area available for the flow of air in the separated central core. Hence, the voidage is decreased.

ii. On the other hand, the air entrainment in the water film results in homogenization in the region close to the wall. Due to this homogenization, the slip is lowered and voidage is increased.

Between the two trends, the voidage decrease seems to be slightly stronger as illustrated in Fig. 4.18.

At Tap 3, the two-phase mixture is recovering the original phase distribution. However, the water film at the top of the channel is still thicker than in the undisturbed case, resulting in decrease of voidage. The void distribution was recovered within 15 hydraulic diameters.

2. Central obstruction.

Central obstruction has stronger effects on both void fraction and void distribution as shown in Fig. 4.19..

As the obstruction is located in the middle of the channel, it introduces much stronger separation of the mixture, resulting in a decrease of voidage and more symmetric phase distribution compared to the peripheral obstruction.

4.3.3. Slug Flow.

Figs. 4.20. and 4.21. show the changes of void distribution along the test section for peripheral and central obstructions respectively. The behavior of the slug flow is closer to the annular flow than to the bubbly flow. The reason is that the surface tension forces are correspondingly lower as compared with the inertial forces.

As the slugs are formed in the upper part of the test section, the peripheral obstruction shows a stronger effect. On passing both obstructions, clear separation occurs. Thus, air flows in the core of the test section, and water is present in the upper part of test section continuously.

Approaching Tap 3, the flow tends to have initial void distribution, that is, air forms slugs in the upper part of the test section.

4.4. Pressure Drop.

Pressure drops were measured in a plain test section and a test section with central and peripheral obstructions. The areas of flow obstruction were 25% of the cross sectional area. To verify the method of obtaining pressure drop measurements for two-phase flow, single phase flow was also investigated.

Fig. 4.22. illustrates the single phase pressure drop for a plain test section and for test sections with central and peripheral obstructions. Using Eq.(3.12) , pressure drop coefficients were calculated to be 0.0231 and 0.030 as compared with the values of 0.0225 and 0.028 obtained from Moody diagram respectively.

The pressure profile across the obstruction shows an increase in pressure before the obstruction due to curvatures of the streamlines. Following the obstruction, the pressure reached a minimum value. As the velocity decreases, the pressure regenerates then continues to drop linearly.

Head loss coefficients for central and peripheral obstructions were calculated using Eq. (3.10) and are given in Table 4.6.. The central obstruction which causes distrubances at the core of the flow has a stronger effect, because the higher momentum region is disturbed.

In the two-phase flow experiments, two different water flow rates were set and the air flow rates were varied accordingly. The typical pressure distributions for bubbly and annular flows are shown in Figs. 4.23. and 4.24. respectively.

Two-phase multipliers for linear pressure drops upstream and downstream from the obstructions were obtained using Eq. (3.9) and are given in Table 4.6., and two-phase multipliers for pressure drop across obstructions were calculated using Eq.(3.11) and are shown in Table 4.6..

Fig. 4.25. shows the comparison of two-phase multiplier Φ_L^2, for linear pressure drop with Baroczy's correlation. For the investigated flow region, there was a fairly good agreement. Fig. 4.26. shows a graph of the two-phase multiplier Φ_{LH}^2 versus the superficial gas velocity for each of the various obstructions. As quality increases, the multiplier increases.

An analysis of the data leads to the following results:

1. The head loss coefficients of obstructions were higher for central obstructions than for peripheral obstructions for all flows. This is because of the fact that the higher velocity region was affected by the central obstructions. More turbulence was generated for the central obstructions, while in the case of peripheral obstructions higher velocity fluid continued to flow as 'vena contracta'.

2. The pressure drop profile in two-phase flow seems to be affected strongly by the void distribution. It was found that the length of pressure regeneration following the obstruction was larger in the bubbly flow. As discussed in the previous section, the effect of the obstruction on the void distribution was stronger in the bubbly flow. For bubbly flow, central obstruction caused a longer regeneration region, while peripheral obstruction introduced a longer regeneration region in the case of annular flow. Also, different void distributions resulted in the changes of pressure drop upstream and downstream from the obstruction.

CHAPTER 5

CONCLUSIONS AND SUGGESTIONS

5.1. Conclusions.

Two-phase flows were studied experimentally in horizontal channels using air and water. The effects of flow obstructions were investigated, and the results obtained lead to the following conclusions:

1. The flow pattern transition boundaries were changed noticeably with the addition of obstructions. The transitions affected were those between stratified and wavy, wavy to slug, and slug and annular flow. The central obstruction showed more influence than the peripheral one.

2. Void distributions were changed due to the effects of the flow obstructions. Although the distribution was affected in all flow patterns, the bubbly flow proved to be affected most. The central obstruction had a

stronger effect on bubbly and annular flow, while the peripheral obstruction showed a stronger effect on slug flow.

3. The pressure drop was higher in the region upstream from the obstruction as compared to the downstream region. As the length of disturbed flow increased, the length of pressure regeneration increased. The two-phase multipliers increased with increasing gas superficial velocities.

4. The DISA 55S52 optical probe used for the measurements of void distributions proved to be adequate using the static trigger level. In the investigated flows, the dynamic trigger level could not be used. The optical probe had serious limitations for higher flow rates as it could not withstand the pressure fluctuations inherent to two-phase flow.

5.2. Suggestions for Further Research.

1. The obstructions used in this work covered an area equal to 25% of the total cross section area: Further study is suggested for different obstruction ratios, to investigate the effect of the obstruction areas on the flow.

2. Further work is required for the different types of obstructions.

3. In the present experimental set-up, air and water were supplied from the building service lines directly. Pressure regulators need to be installed at the inlets of each phase.

REFERENCES

1. H.C. Simpson, et. al., "Flow Patterns in Two-Phase Flow.- Part 1. Literature Survey and Design Recommendations for Gas-Liquid Flows in Closed Channels", A.E.R.E.-R. 8120, 1975.

2. Y. Taitel, et. al., "Trandient Gas-Liquid Flow in Horizontal Pipes: Modelling the Flow Pattern Transition, A.I.Ch. E. Journal, Vol. 24, pp. 920-933, 1978.

3. J.G. Collier, "Convective Boiling and Condensation ", McGraw-Hill, 1972.

4. D. Butterworth and G.F. Hewitt, " Two-Phase Flow and Heat Transfer", Oxford Press, 1977.

5. O.P. Bergelin and C. Gazley, "Co-current Gas/Liquid Flow: Part 1. Flow in Horizontal Tubes", Proc. Heat Transfer and Fluid Mechanics Inst., A.S.M.E. Berkley, California, pp. 5-18, 1949.

6. O. Baker, "Multiphase Flow in Pipelines", Oil and Gas J., pp. 156-167, 1958.

7. R. Jenkins, "Two-phase Two-component Flow of Air and Water", M.S. Thesis, University of Delaware, 1947.

8. C. Gazley, "Interfacial Shear and Stability in Two-phase Flow", Ph.D. Thesis, University of Delaware, 1949.

9. S.I. Kosterin, " An Investigation of the Influence of the Diameter and the Position of a Tube on the Hydraulic Resistance and the Structure of Flow of Gas/Liquid Mixture", IZV. AKAD. NAUK. Otd. Tekh., Nauk., No.12, pp. 1824-1831, 1949.

10. G.E. Alves, "Co-current Liquid/Gas Flow in a Pipe Line Contractor", Chem. Eng. Prog., Vol. 50, No. 9, pp. 449-456, 1954.

11. J.M. Mandhane, et. al., "A Flow Pattern Map for Gas/Liquid Flow in Horizontal Pipes", Int. J. of Multiphase Flow, Vol. 1, No. 4, pp. 537-553, 1974.

12. H.A. Johnson and A.H. Abou-Sabe, "Heat Transfer and Pressure Drop for Turbulent Flow of Air/Water Mixtures in a Horizontal Pipe", Trans. A.S.M.E., Vol. 74, pp. 977-987, 1952.

13. P.D. White and R.L. Huntington, "Horizontal Co-current Two Phase Flow of Fluids in Pipe Lines", The Petroleum Eng., Vol. 27, No. 9, pp. D40-D45, 1955.

14. C.J. Hoogendron, "Gas/Liquid Flow in Horizontal Pipes", Chem. Eng. Sci., Vol. 9, pp. 205-217, 1959.

15. G.W. Govier and M.M. Omer, "The Horizontal Pipeline Flow of Air/Water Mixtures", Can. J. Chem. Eng., Vol. 40, pp. 93-104, 1962.

16. D.S. Scott, "Properties of Co-current Gas/liquid Flow", Advances in Chem. Eng., Vol. 4, pp. 199-277, Academic Press, N.Y., 1963.

17. B.A. Eaton, et. al., "The Prediction of Flow Patterns, Liquid Holdup and Pressure Losses Occuring During Continuous Two Phase Flow in Horizontal Pipelines", Trans. Soc. Pet. Eng., A.I.M.E., Vol. 240, pp. 815-828, 1967.

18. Y. Taitel and A.E. Dukler, "A Model for Predicting Flow Regime Transitions in Horizontal and Near Horizontal Gas-Liquid Flow", A.I.Ch.E.Journal, Vol. 22, pp. 47-55, 1976.

19. W.H. McAdams, et. al., "Vaporization inside Horizontal Tubes-II-Benzene-Oil Mixtures", Trans. A.S.M.E., Vol. 64, p. 193, 1942.

20. A. Cicchitti, et. al., "Two-Phase Cooling Experiments-Pressure Drop, Heat Transfer and Burnout Measurements", Energia Nucleare, Vol. 7, No. 6, pp. 407-425, 1960.

21. A.E. Dukler, et. al., "Pressure Drop and Holdup in Two-Phase Flow", A.I.Ch.E. Journal, Vol. 10(1), pp. 38-51, 1964.

22. R.W. Lockhart and R.C. Martinelli, "Proposed Correlation of Data for Isothermal Two-Phase, Two-Component Flow in Pipes", Chem. Eng. Prog., Vol. 45, pp. 39-48, 1949.

23. C.J. Baroczy, " A System Correlation for Two Phase Pressure Drop", A.I.Ch.E. Reprint No. 37, Paper presented at 8th Nat. Heat Transfer Conference, Los Angeles, 1965.

24. D. Chisholm and L.A. Sutherland, "Prediction of Pressure Gradients in Pipeline Systems during Two-Phase Flow", Paper presented at Symposium on Fluid Mechanics and Measurements in Two-Phase Flow Systems, Uni. of Leeds, 1969.

25. J.W. Hoopes, "Flow of Steam-Water Mixtures in a heated Annulus and through Orifices", A.I.Ch.E. Journal, Vol. 3, No. 2, pp. 268-275, 1957.

26. J.R.S. Thom, "Some Experiences on the Two-Phase Flow of Water and Steam through a Sharp-edged Orifice", NEL R-217, 1966.

27. D. Chisholm, et. al., "The Flow of Steam/Water Mixtures through Sharp-edged Orifices", NEL R-213, 1966.

28. J.G.Collier, "Convective Boiling and Condensation", McGraw-Hill.

29. J.K. Ferrel and J.W. McGee, "Two-Phase Flow through Abrupt Expansions and Contractions", TID-23394, Vol. 3, Rayleigh, N.C., North Carolina State Uni., 1966.

30. G.E. Geiger and W.M. Rohner, "Sudden Contractions Losses in Two-Phase Flow", J. of Heat Transfer, pp. 1-9, 1966.

31. D.E. Fitzsimmons, "Two-Phase Pressure Drop in Piping Components", HW 80970, Rev. 1, 1964.

32. M.F. Couturier, "Effect of Flow Disturbances on Phase Velocities, Droplet Trajectories and Pressure Drop", CRNL, 1978.

33. M.E. Charles and P.J. Redburger, "The Reduction of Pressure Gradients in Oil Pipe Lines by the Addition of Water; Numerical Analysis of Stratified Flow", Can. J. Chem. Eng., pp. 70-75, 1962.

34. J.M. Tuner and G.B. Wallis, "The Separate-Cylinders Model of Two-Phase Flow", NYO-3114-6, Thayer School of Eng., Partmouth College, Hanover, New Hampshire, 1965.

35. S.M. Zivi, "Estimation of Steady State Steam Void Fraction by Means of the Principle of Minimum Entropy Production", J. of Heat Transfer, Vol. 86, pp. 247-252, 1964.

36. A. Premoli, et. al., "A Dimensionless Correlation for Determining the Density of Two-phase Mixtures", Thermotecnica, Vol. 25(1), pp. 17-26, 1971.

37. S.G. Bankoff, "A Variable Density Single-fluid Model of Two-Phase Flow with Particular Reference to Steam-Water Flow", Trans. A.S.M.E. J. Heat Transfer, Vol. 82, No. 2, pp. 265-272, 1960.

38. G.A. Hughmark, "Hold-up in Gas Liquid Flow", Chem. Eng. Prog., Vol. 58, No. 4, pp. 62-65, 1962.

39. A.A. Armand, "The Resistance during the Movement of a Two-Phase System in Horizontal Pipes", English Trans. N.L.L., M 882, Boston Spa., Yorks, 1946.

40. A. Abuaf, et. al., "Responce Characteristics of Optical Probes", A.S.M.E. Paper 78-WA/HT-3, 1978.

41. G.L. Shires and P.J. Riley, "The Measurement of Radial Voidage Distribution in Two-Phase Flow by Isokinetic Sampling", AEEW-M650, 1966.

42. N. Adorni, et. al., "An Isokinetic Sampling Probe for Phase and Velocity Distribution Measurements in Two-Phase Flow Near the Wall of the Conduit", C.I.S.E.-R. 89, 1963.

43. O.C. Jones, Jr. and J.M. Delhaye, "Transient and Statistical Measurement Techniques for Two-Phase Flows: A Critical Review", Int. J. Multiphase Flow, Vol. 3, pp. 89-116, 1976.

44. D. Boulay, "Void Profiles in a Horizontal Two-Phase Air-Water Flow in a 38 mm I.D. Tube", CRNL-1779.

45. DISA Instruction Mannual.

46. W.T. Howatt, et. al., "Two-phase Control Absorber Development Program: Quick-shutoff Valves for Void-fraction Measurements", CRNL-1558, 1977

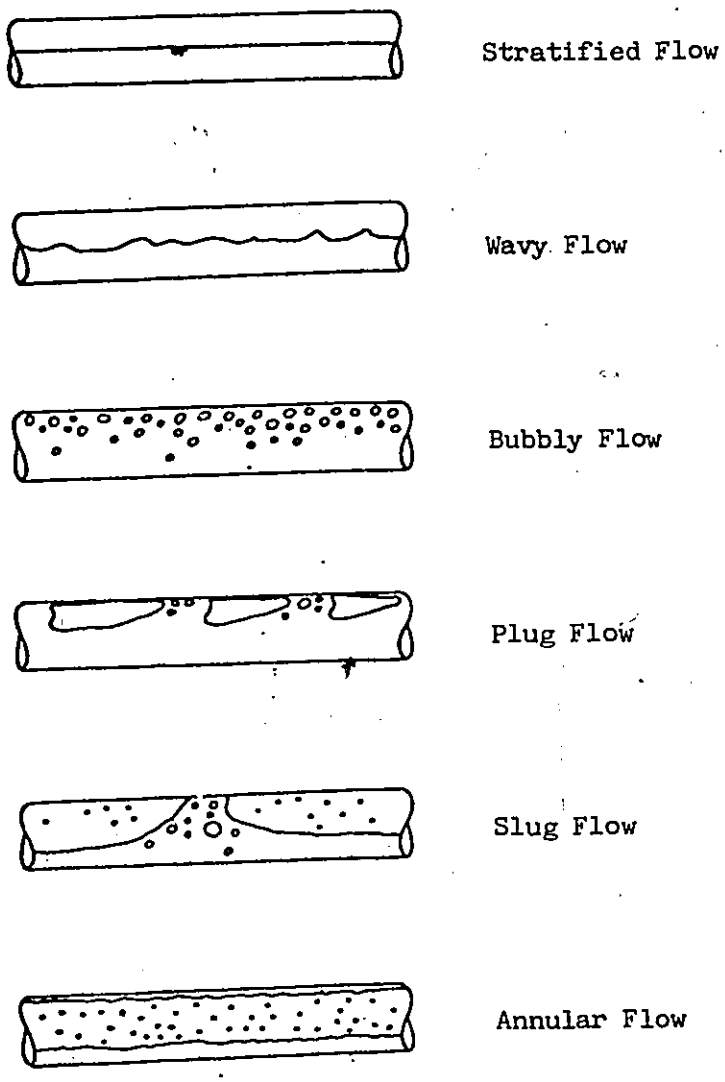

Fig.2.1. Flow patterns in horizontal co-current flows

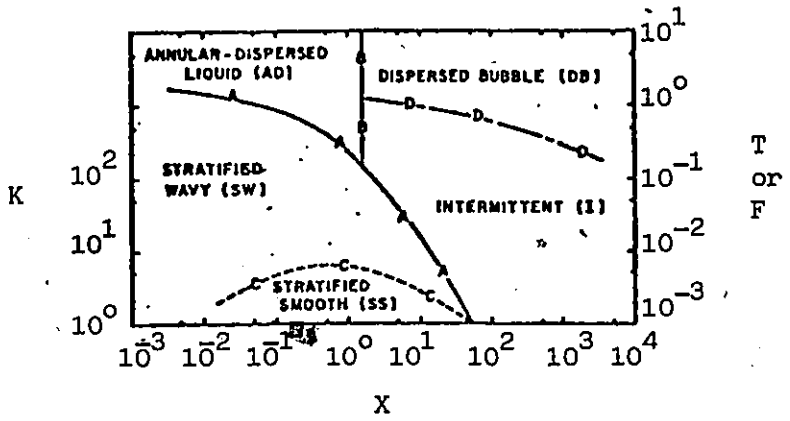

Fig. 2.2. Generalized flow pattern map, horizontal flow.

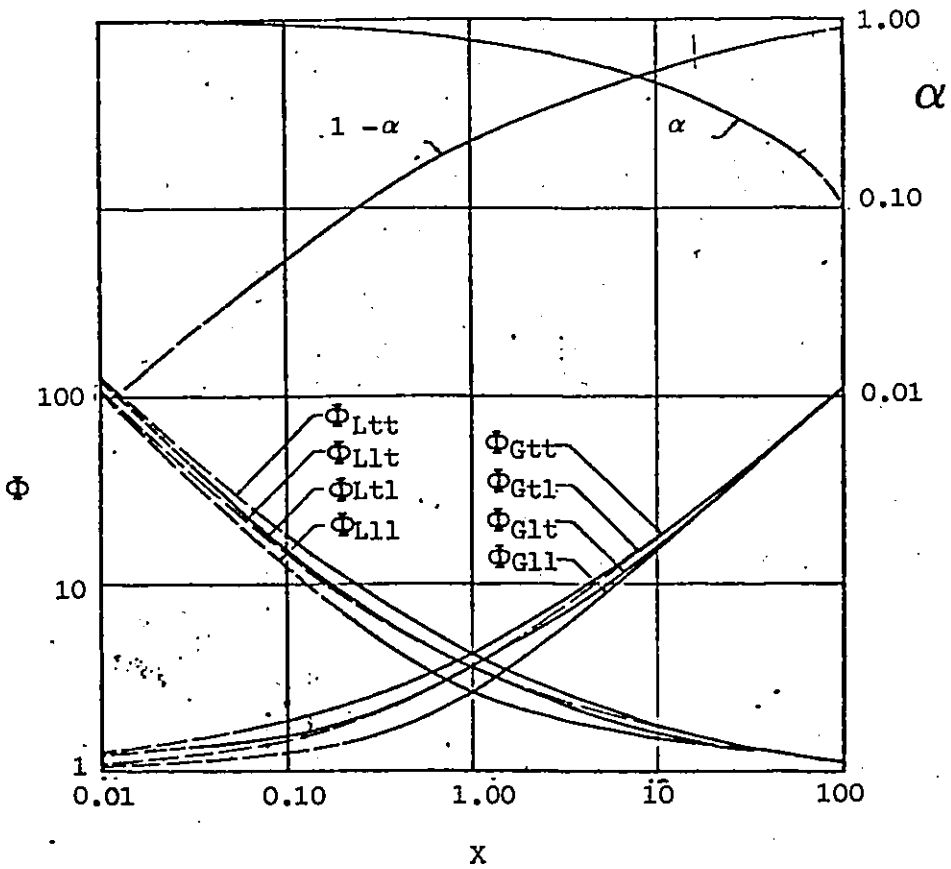

Fig. 2.3. Faired curves showing relation between Φ_L, Φ_G, α for all flow mechanisms.

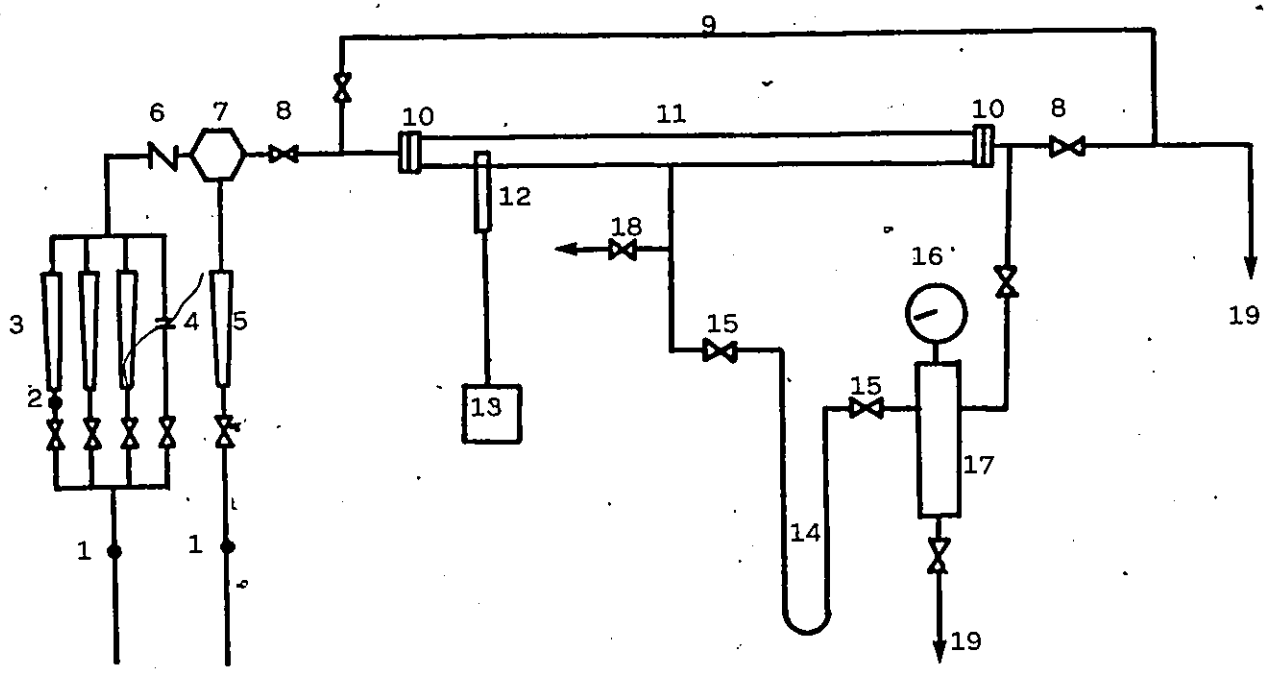

1. Thermocouple
2. Pressure Gauge
3. Rotameter (Air)
4. Orifice Plate (Air)
5. Rotameter (Water)
6. Check Valve
7. Air-Water Mixer
8. Throttle Valve
9. By-pass Line for Test Section
10. Quick-closing Valve
11. Test Section
12. Optical Probe
13. Electronics for Optical Probe
14. Manometer
15. Quick Shut-off Valve
16. Pressure Gauge
17. Pressure Reservoir
18. By-pass Line for Pressure Line
19. To Drain

Fig. 3.1. Schematic diagram of the loop.

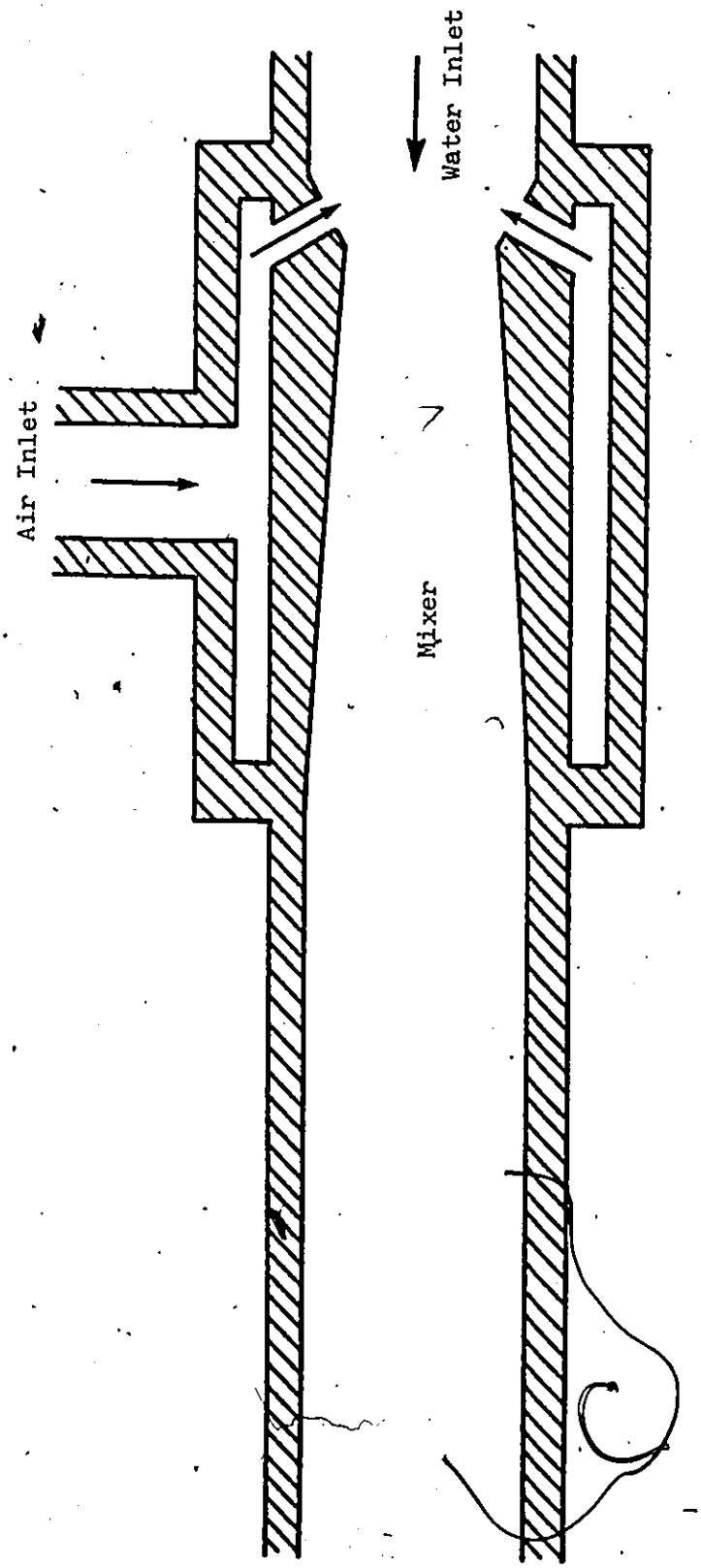

Fig. 3.2. Schematic diagram of the Air-Water Mixer

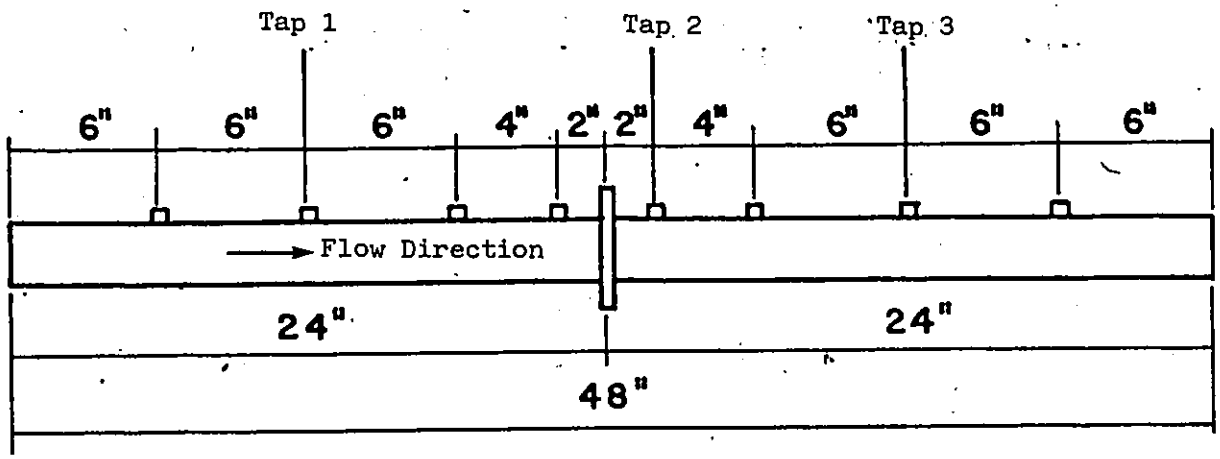

(i) Peripheral Obstruction

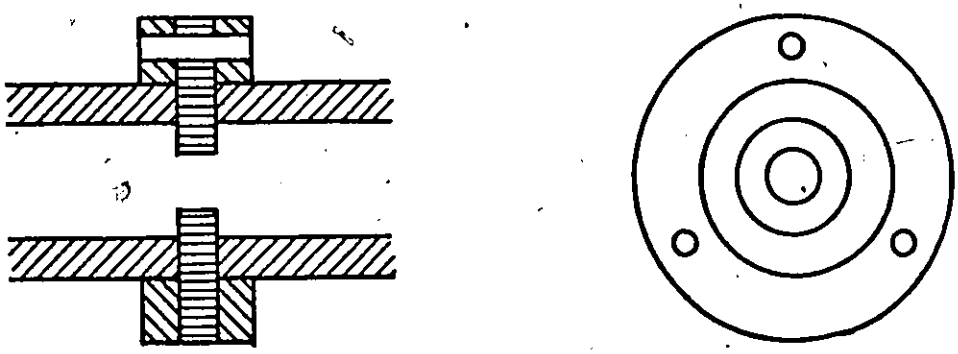

(ii) Central Obstruction

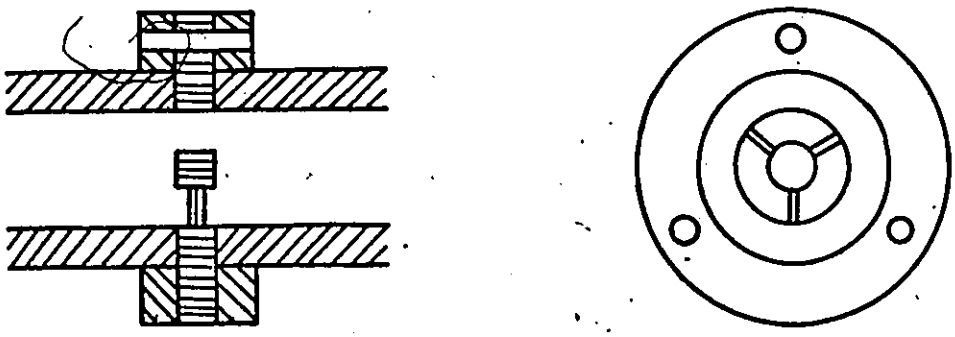

Fig. 3.3. Locations of the optical probe and obstructions

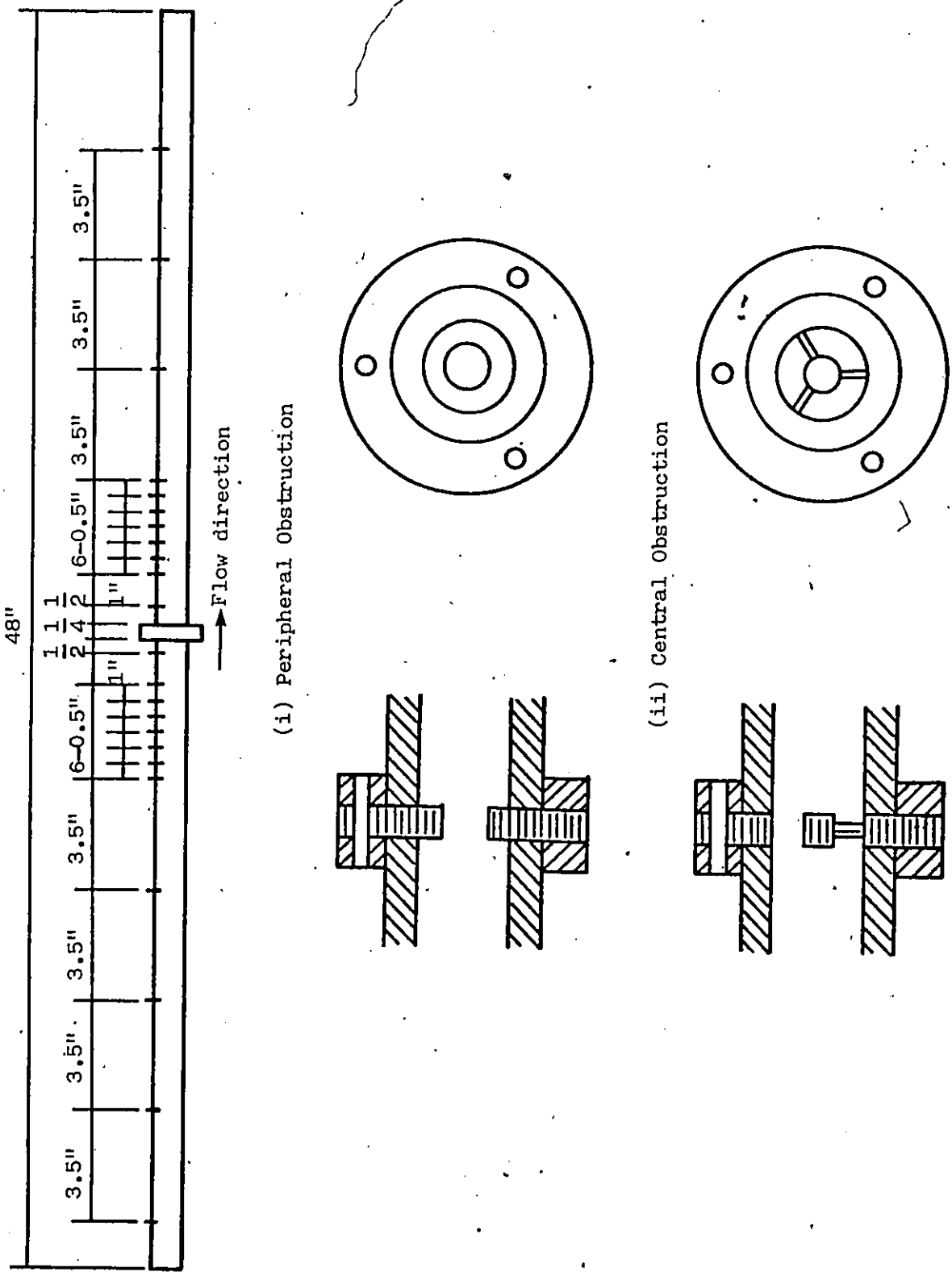

Fig. 3.4. Locations of pressure tappings and obstructions

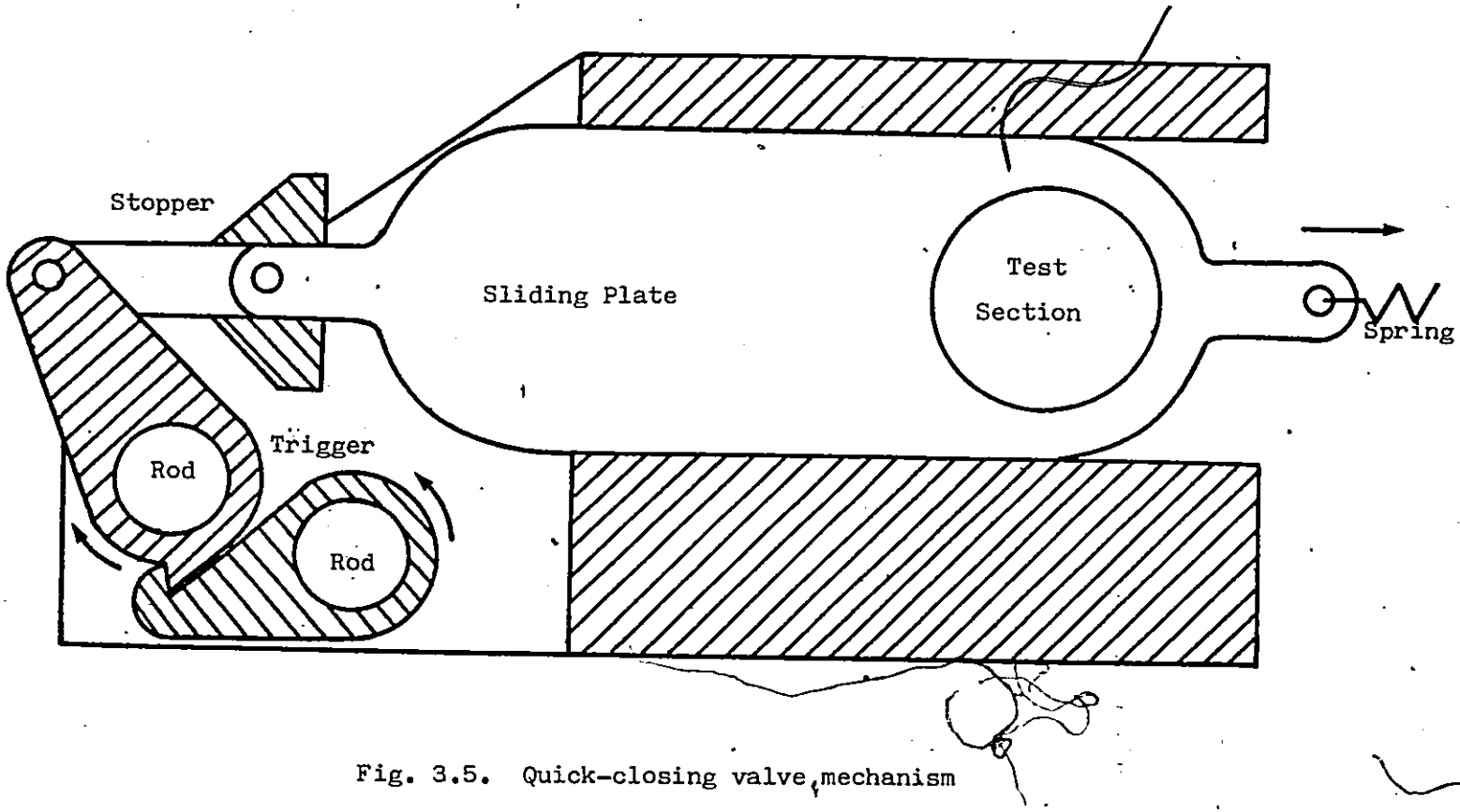

Fig. 3.5. Quick-closing valve mechanism

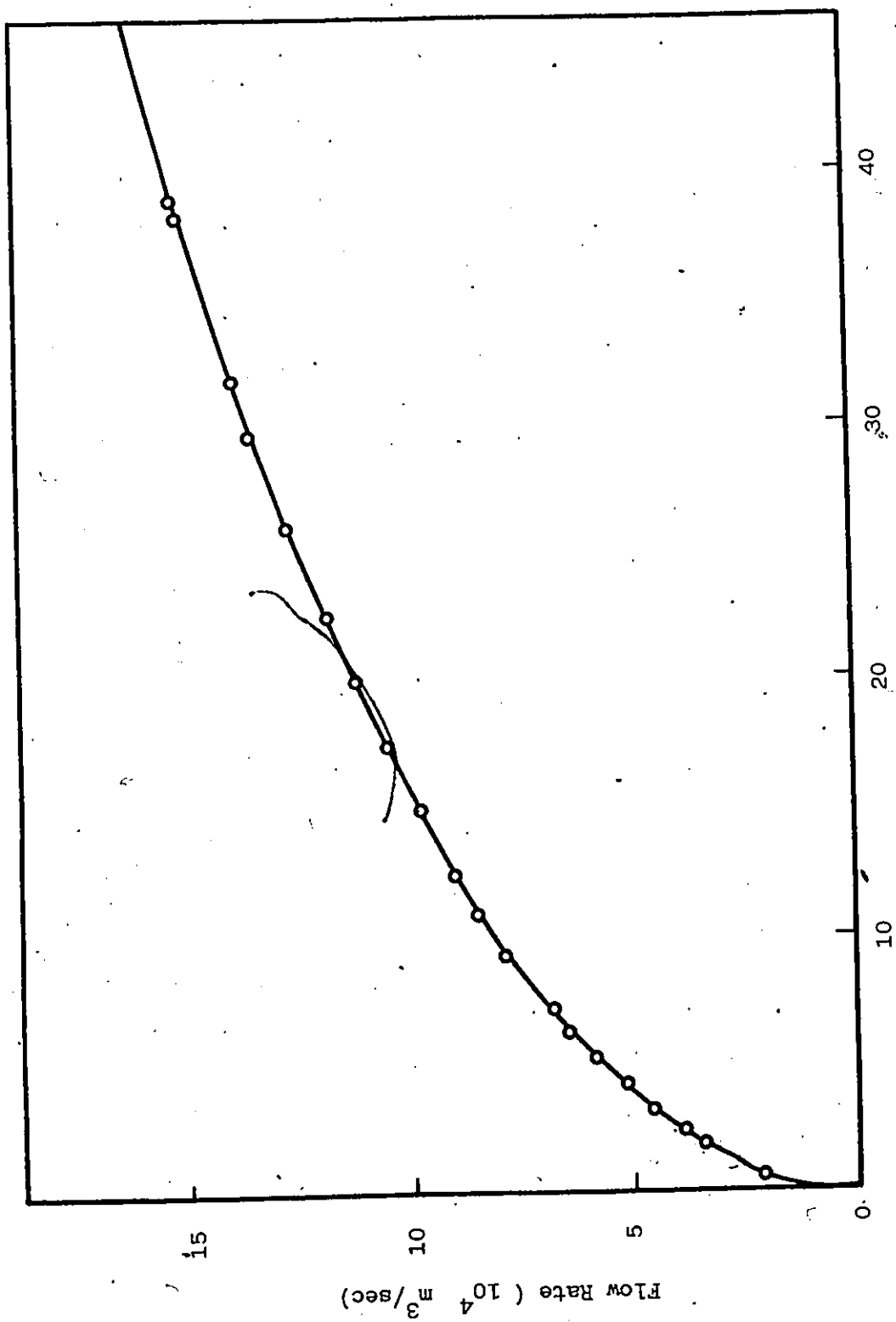

Fig. 3.6. Calibration chart for orifice plate

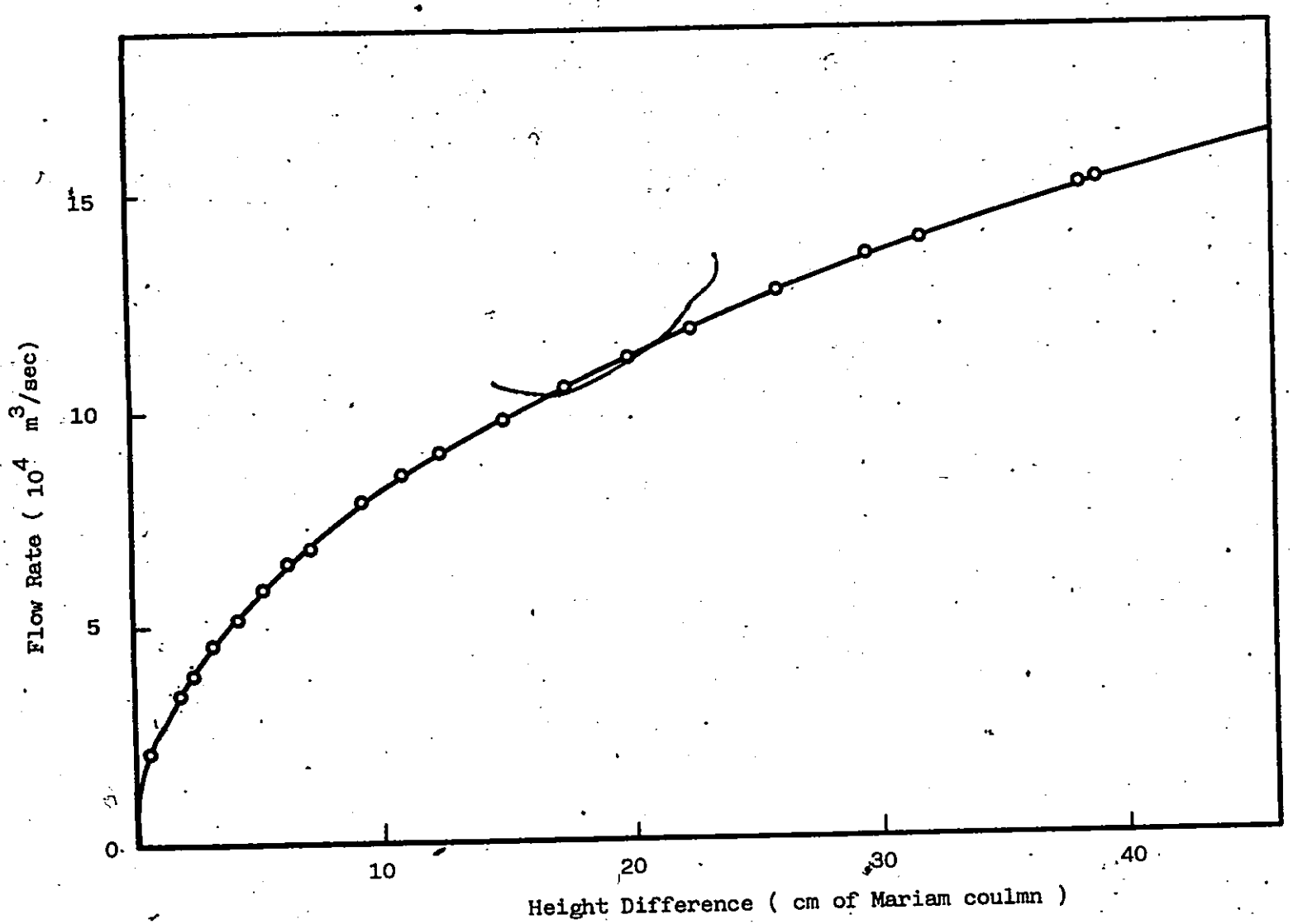

Fig. 3.6. Calibration chart for orifice plate

(i) Static

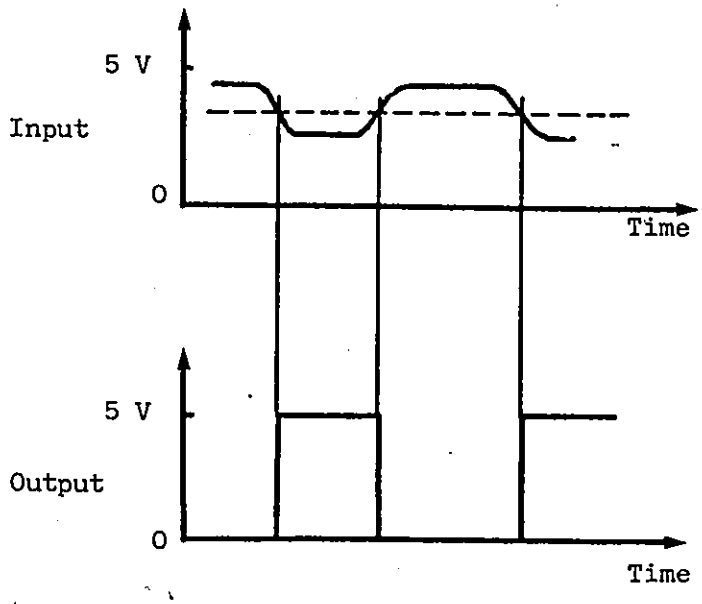

(ii) Dynamic

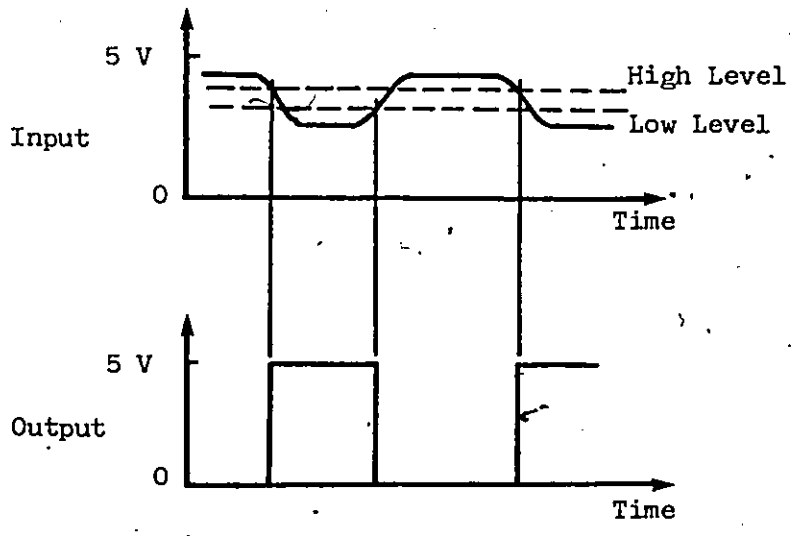

Fig. 3.7. Input and output for static and dynamic signals

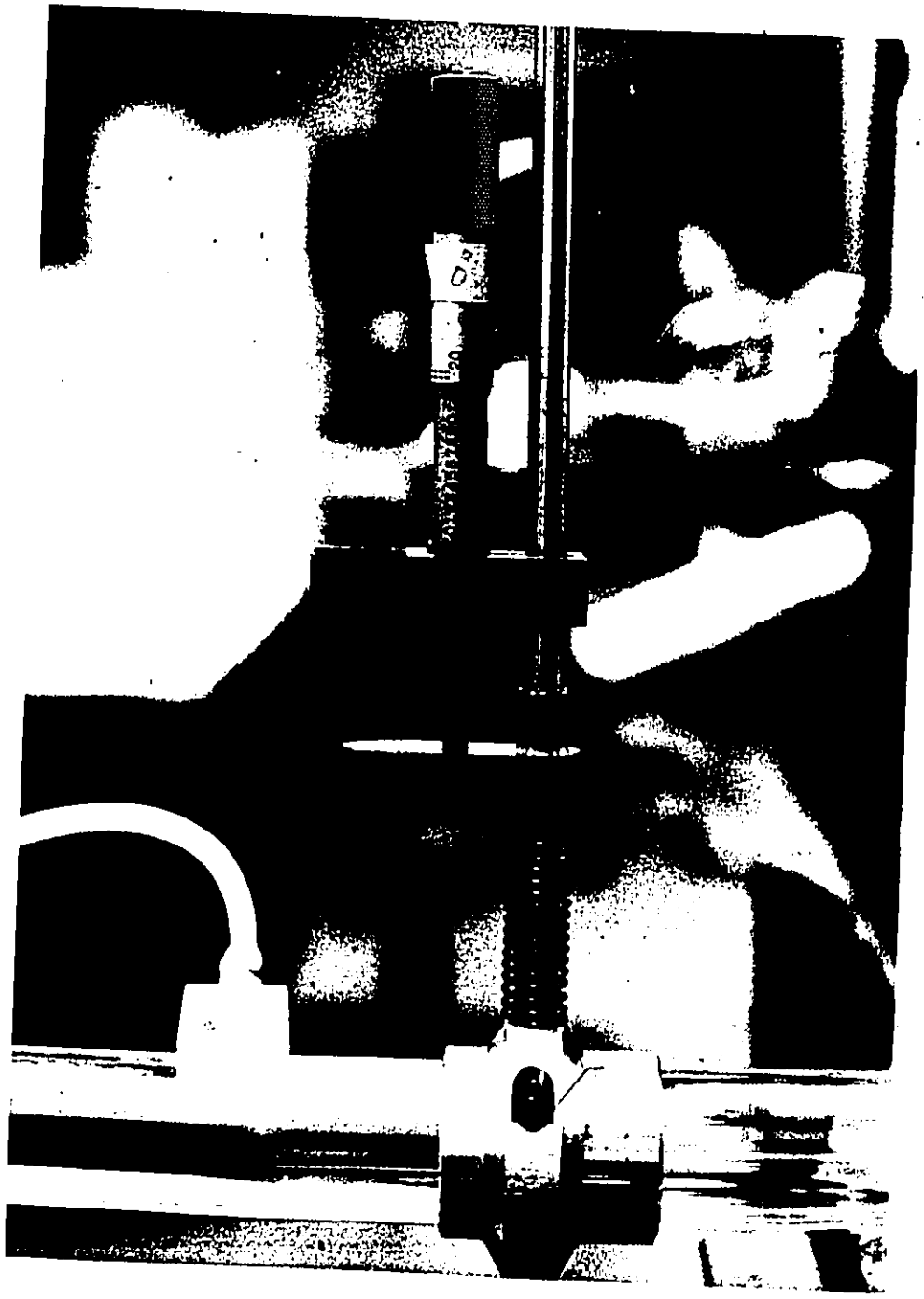

Fig. 3.8. Transverse Mechanism

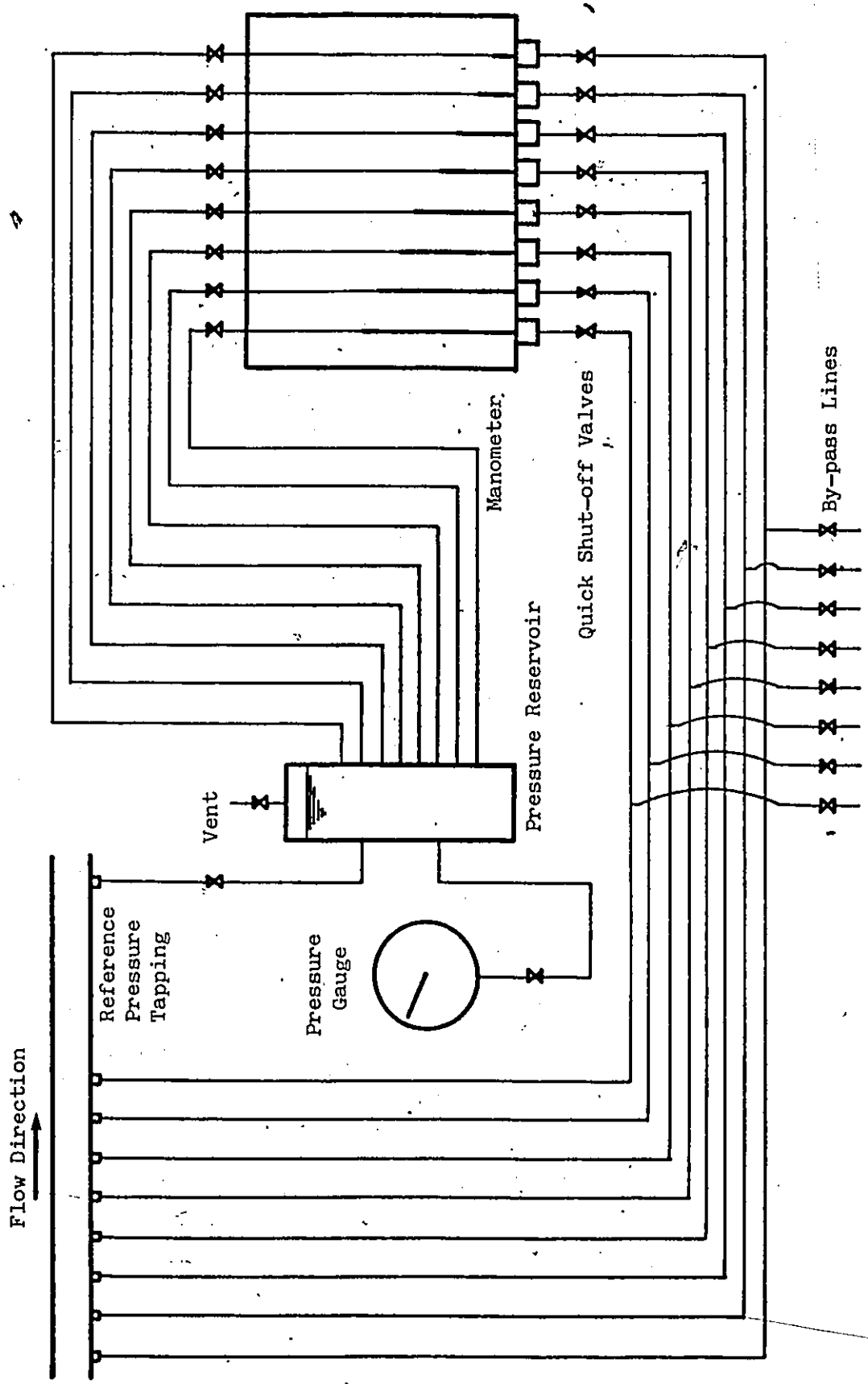

Fig. 3.9. Pressure measurements system

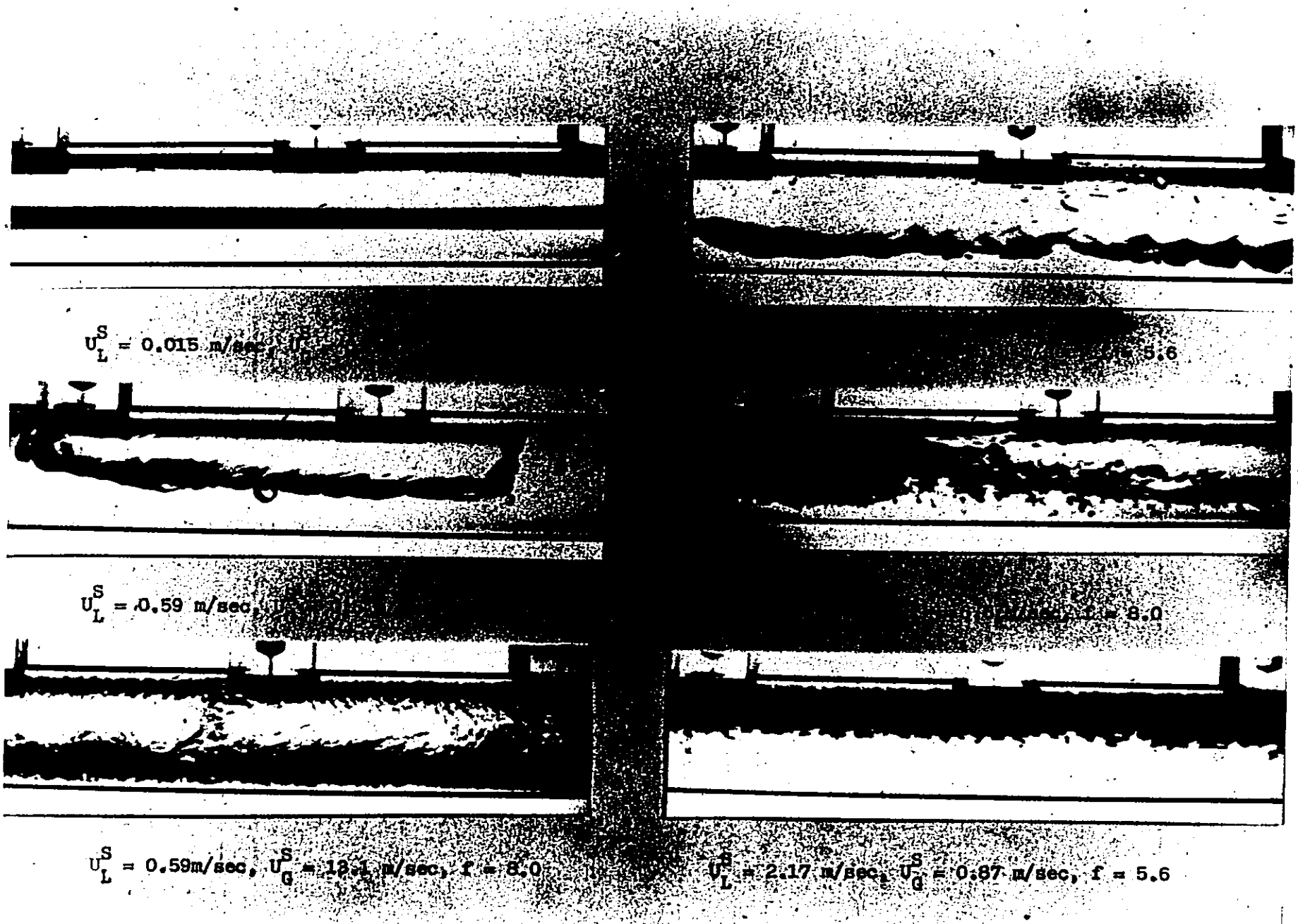

Fig. 4.1. Photographs of flow patterns

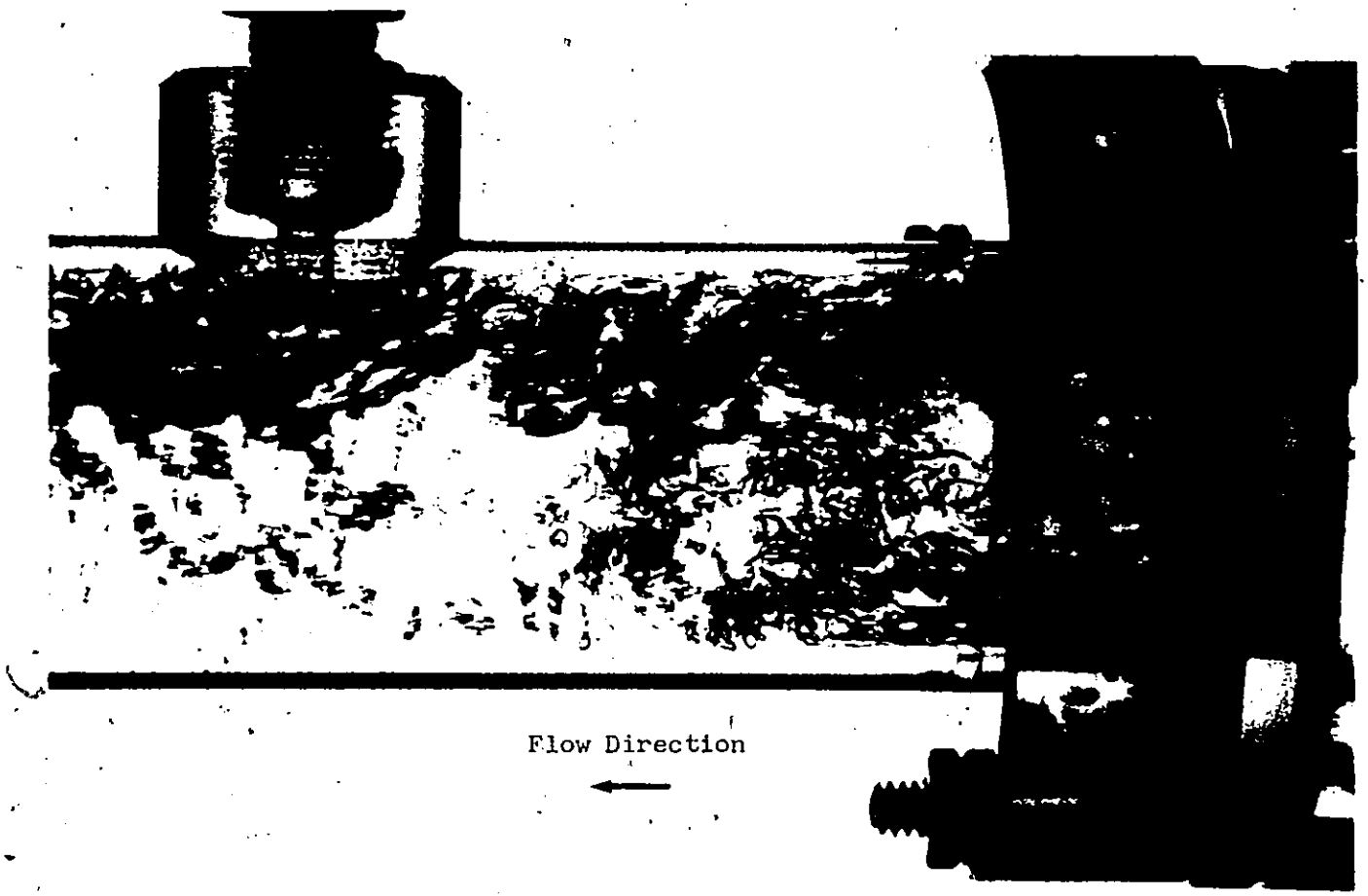

Fig. 4.2. Photograph showing void redistribution:

Bubbly flow past peripheral obstruction

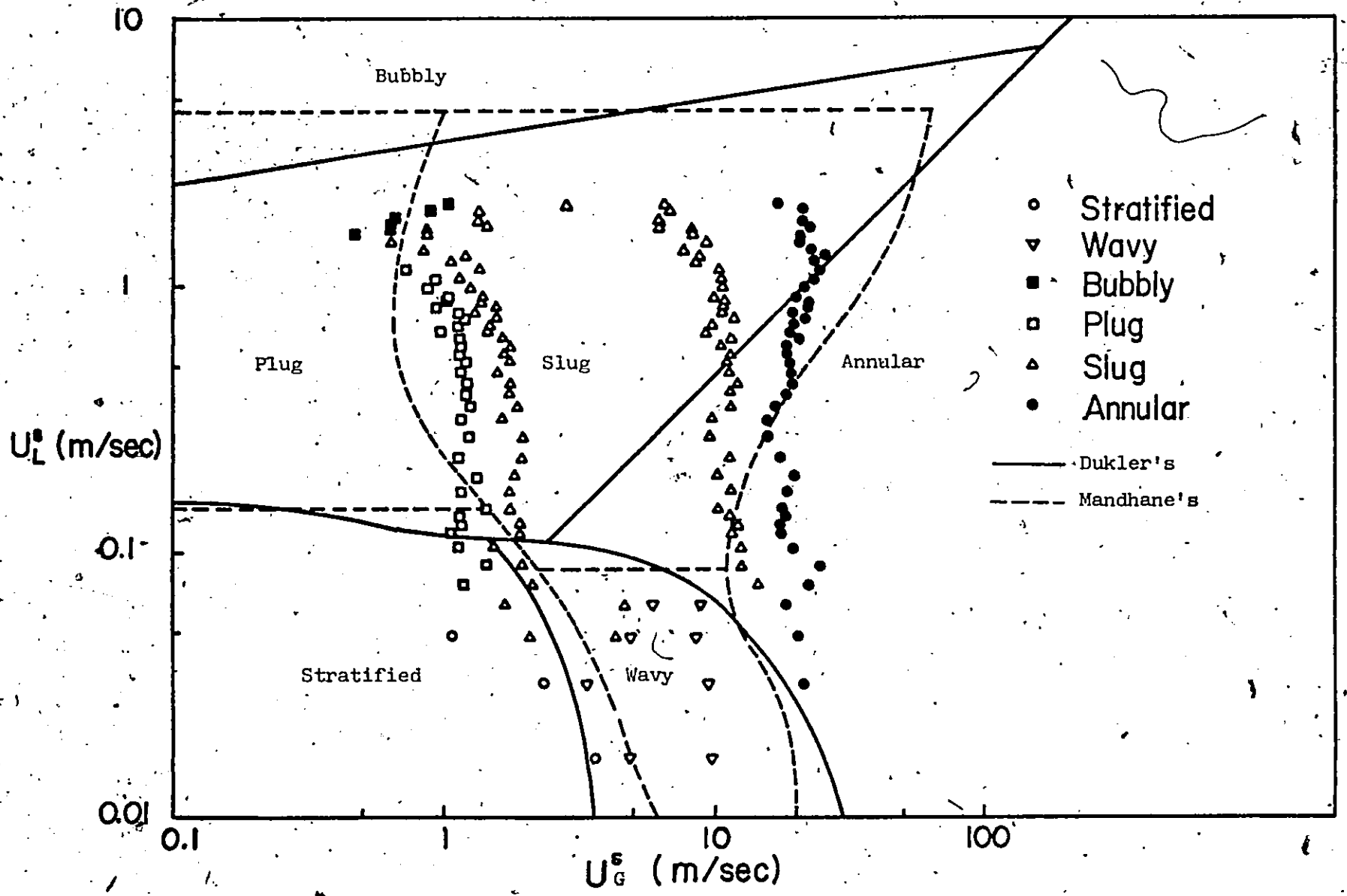

Fig. 4.3. Flow pattern map in an 1"I.D. horizontal channel: Comparison with Mandhane's and Dukler's

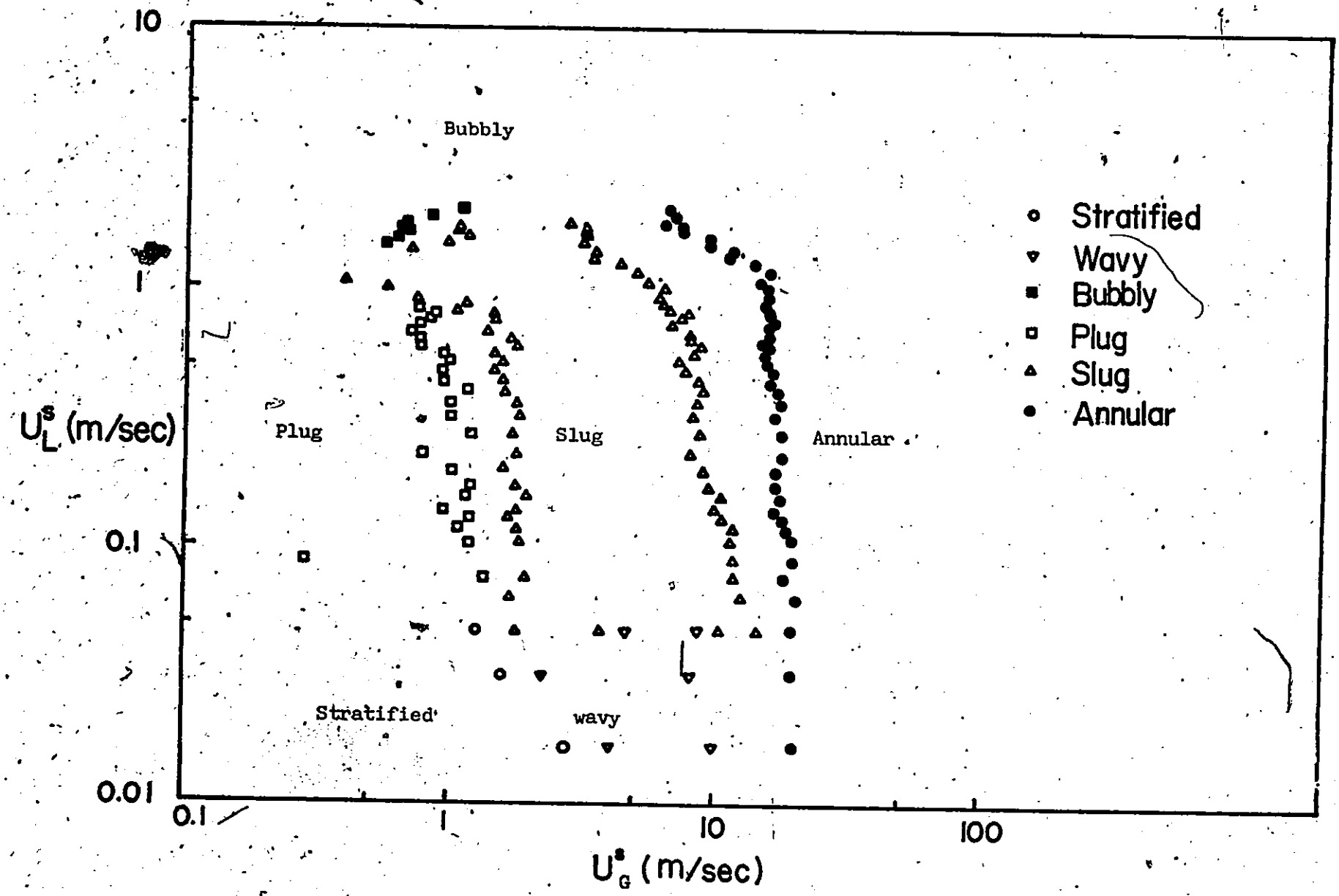

Fig. 4.4. Flow pattern map in an 1" I.D. horizontal channel with a peripheral obstruction

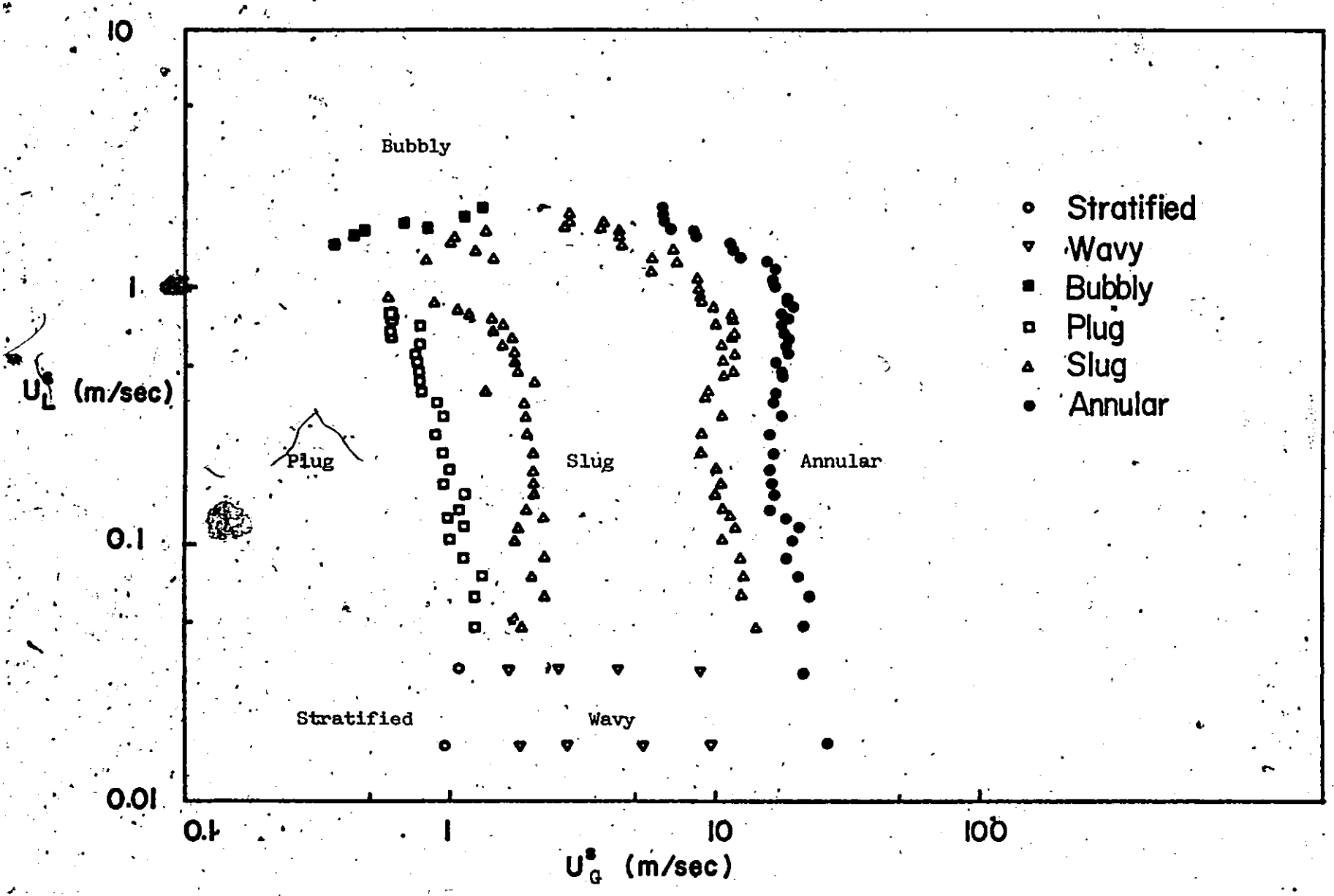

Fig. 4.5. Flow pattern map in an 1" I.D. horizontal channel with a central obstruction

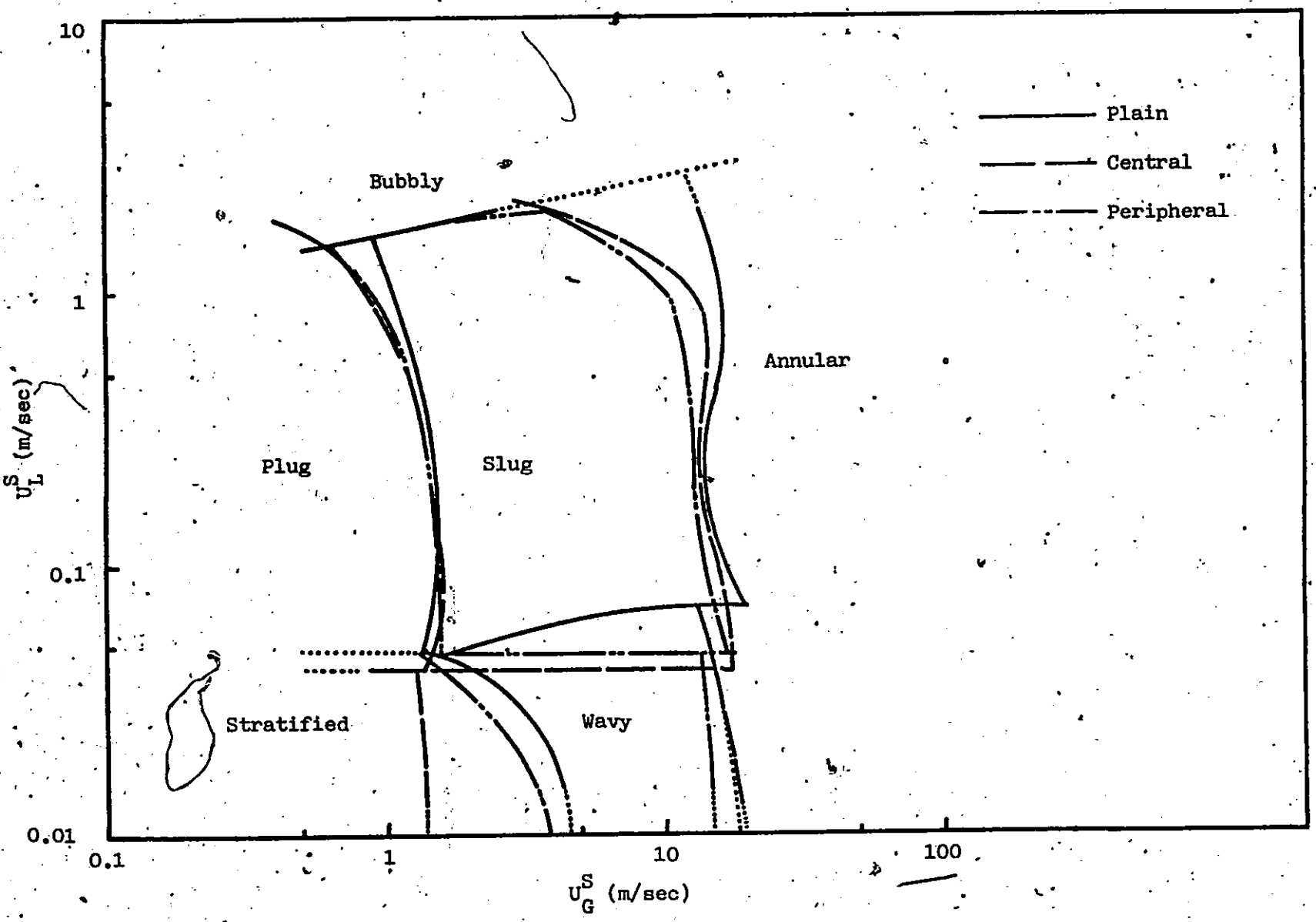

Fig. 4.6. Comparison of flow pattern transition boundaries: plain, central and peripheral

1. Flow Rate (kg/sec)
   Water 0.4
   Air 0.0091
2. Void Fractions (%)
   Integrated 37.8
   Mean 66.6
3. Iso-voidage Lines (%)

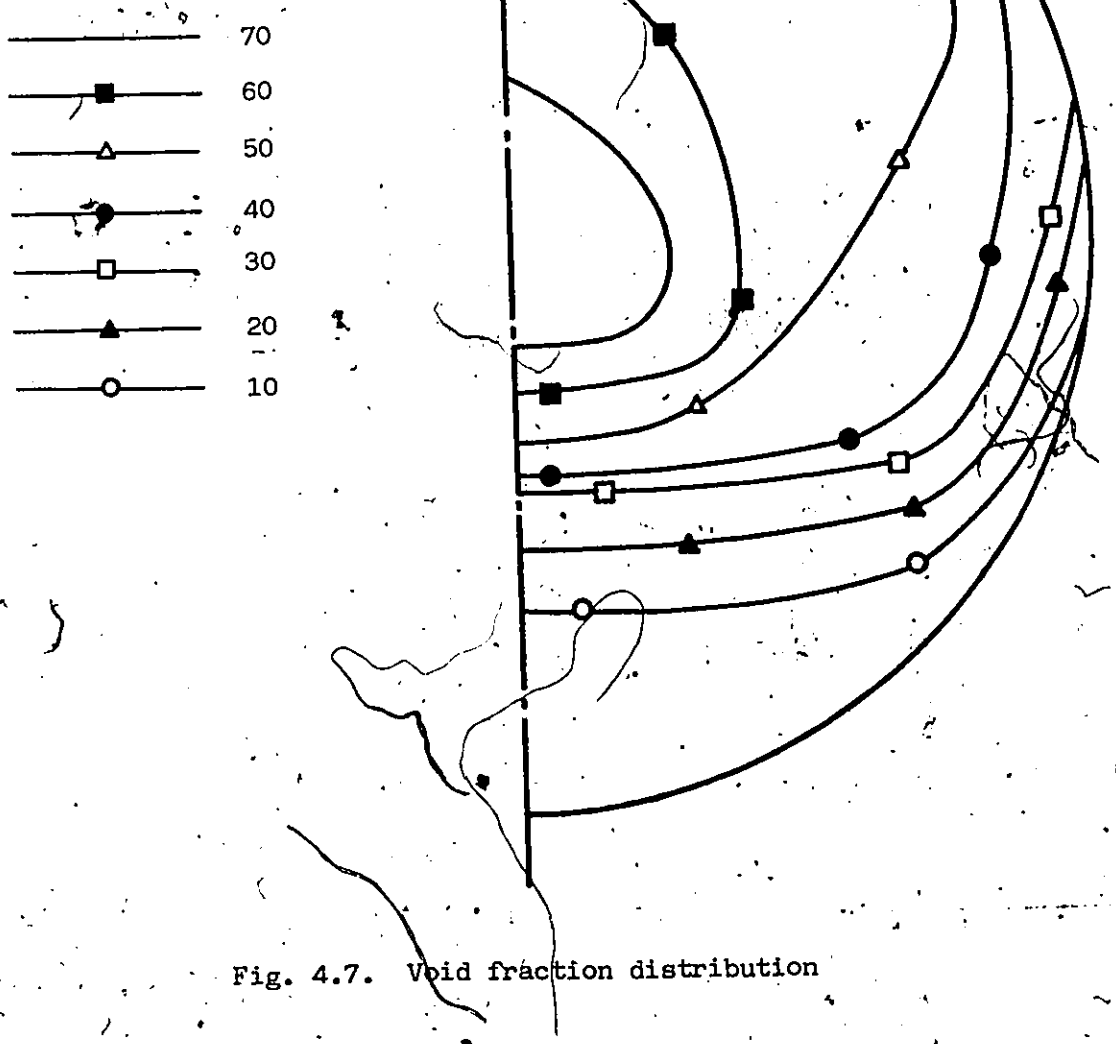

Fig. 4.7. Void fraction distribution

1. Flow Rates (kg/sec)
   Water 0.4
   Air 0.019
2. Void Fractions (%)
   Integrated 51.0
   Mean 83.0
3. Iso-voidage Lines (%)

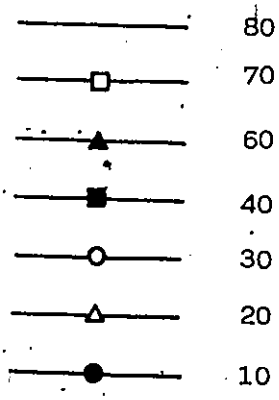

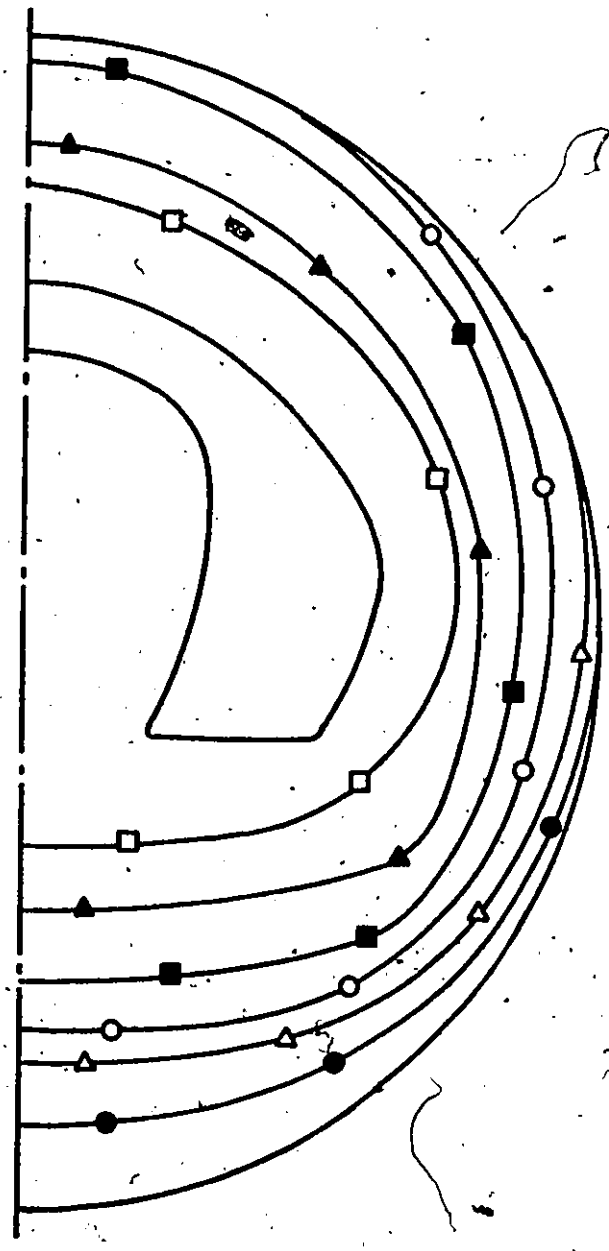

Fig. 4.8. Void fraction distribution

1. Flow Rates (kg/sec)
   Water 0.44
   Air 0.0217
2. Void Fractions (%)
   Integrated 75.1
   Mean 77.4
3. Iso-voidage Lines (%)

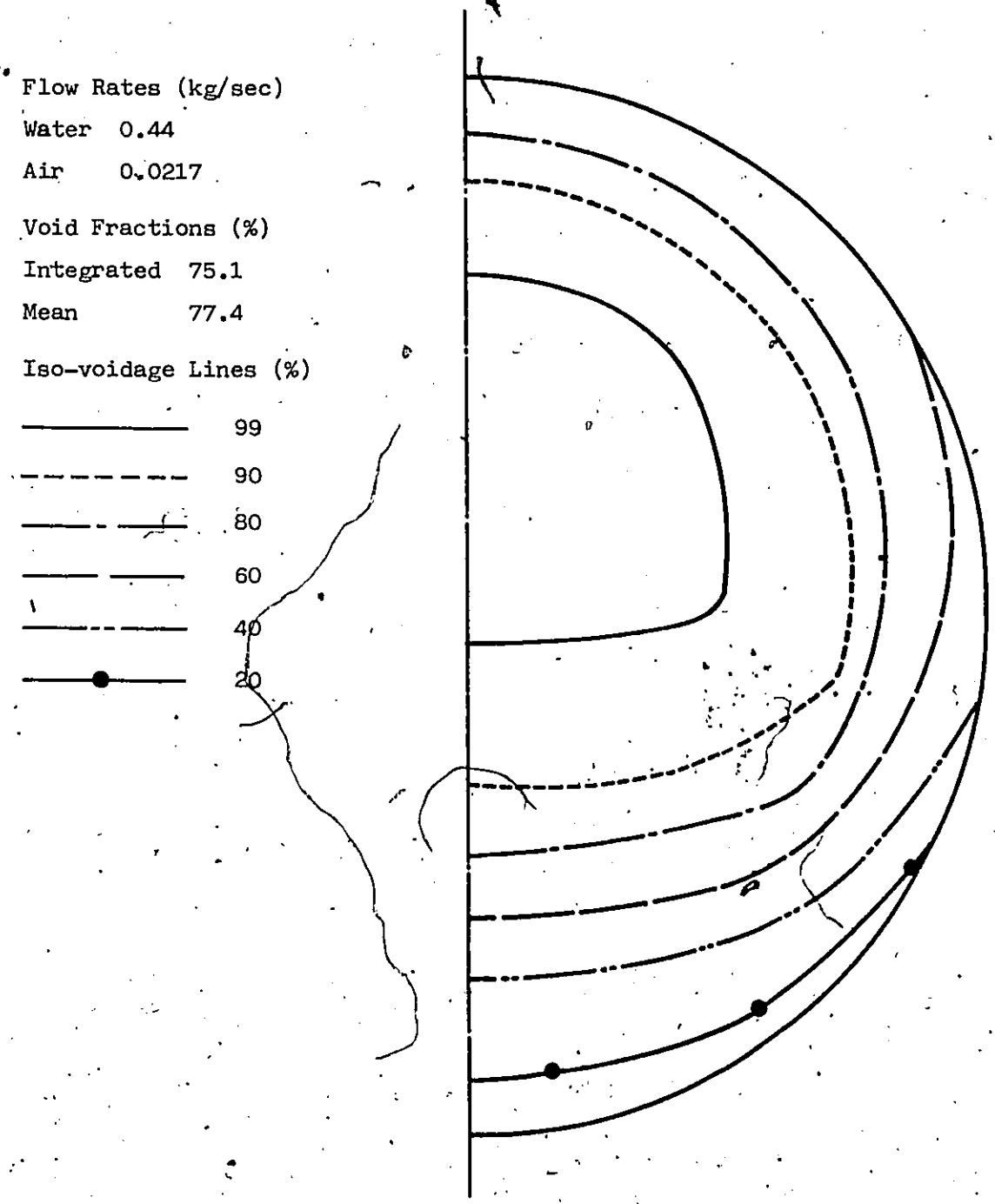

Fig. 4.9. Void fraction distribution

1. Flow Rates (kg/sec)
   Water 0.44
   Air 0.015
2. Void Fractions (%)
   Integrated 73.2
   Mean 76.7
3. Iso-voidage Lines (%)
   99
   90
   80
   60
   40
   20

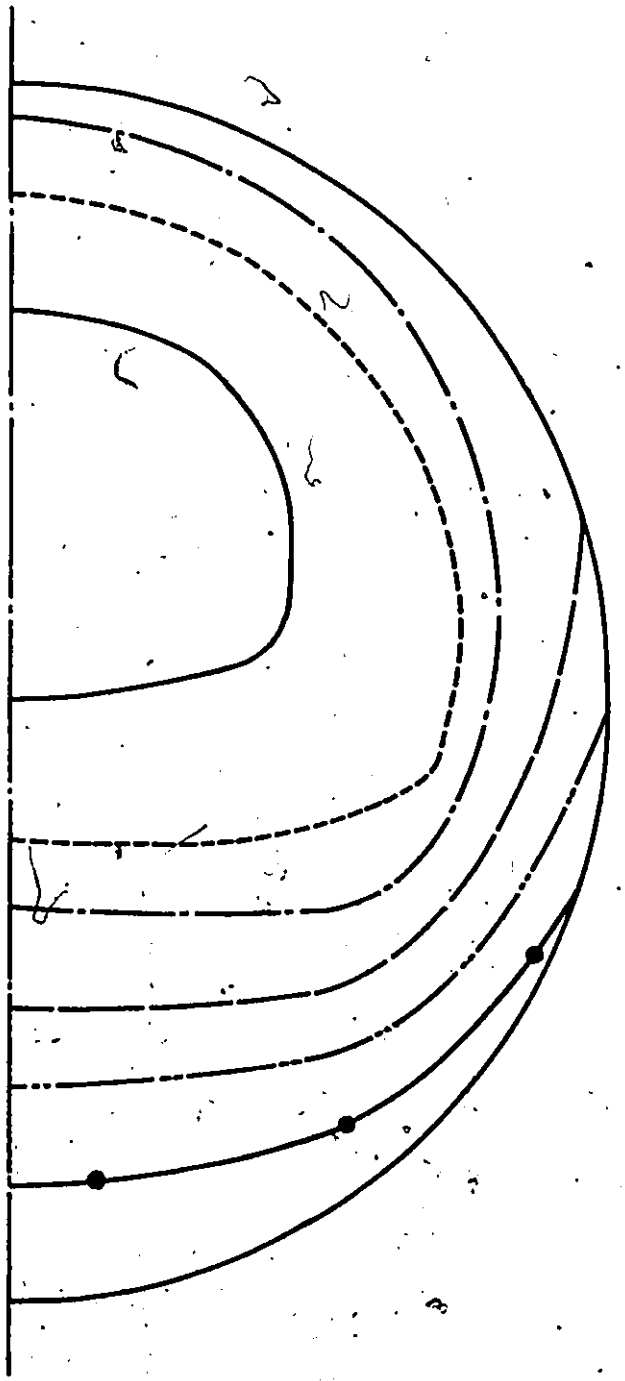

Fig. 4.10. Void fraction distribution

1. Flow Rates (kg/sec)
   Water 0.44
   Air 0.015
2. Void Fractions (%)
   Integrated 69.4
   Mean 69.2
3. Iso-voidage Lines (%)

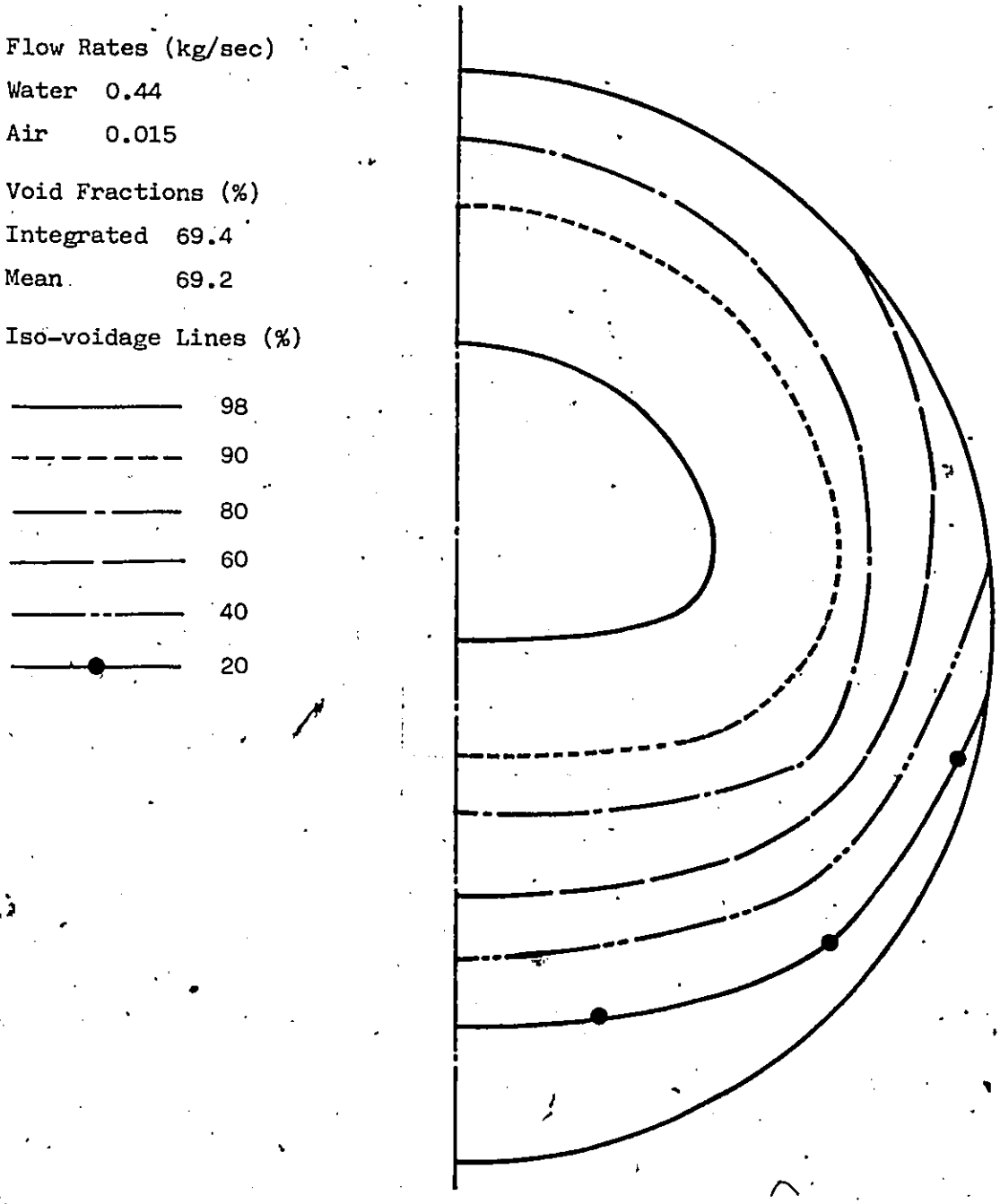

Fig. 4.11. Void fraction distribution

1. Flow Rates (kg/sec)
   Water 0.4
   Air 0.0215
2. Void Fractions (%)
   Integrated 76.9
   Mean 75.0
3. Iso-voidage Lines (%)

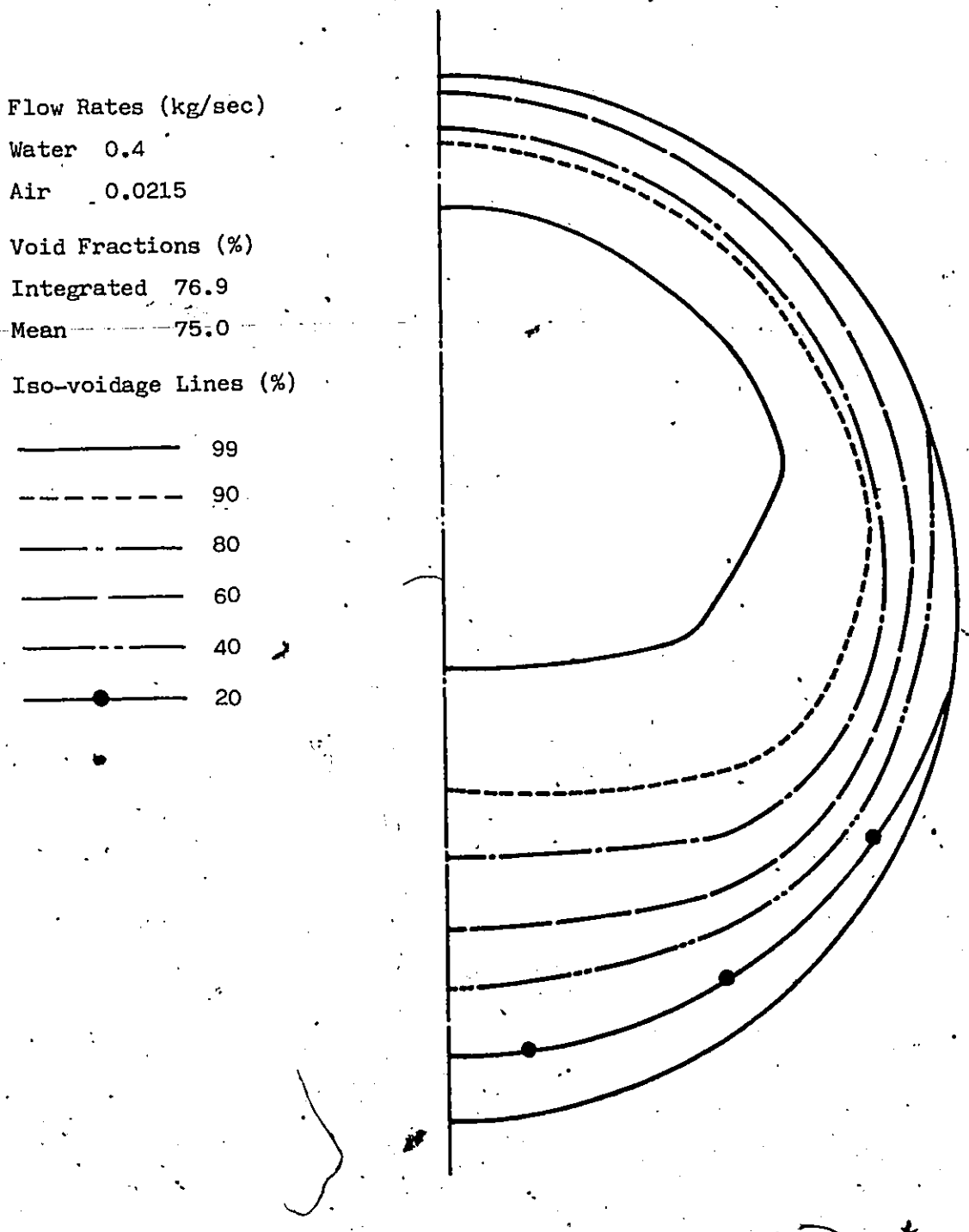

Fig. 4.12. Void fraction distribution

1. Flow Rates (kg/sec)
   Water 0.4
   Air 0.0215
2. Void Fractions (%)
   Integrated 78.9
   Mean 75.0
3. Iso-voidage Lines (%)

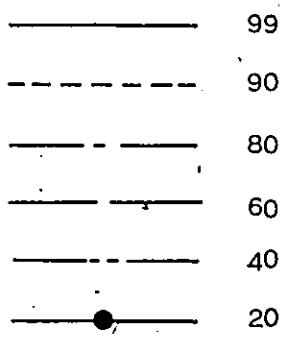

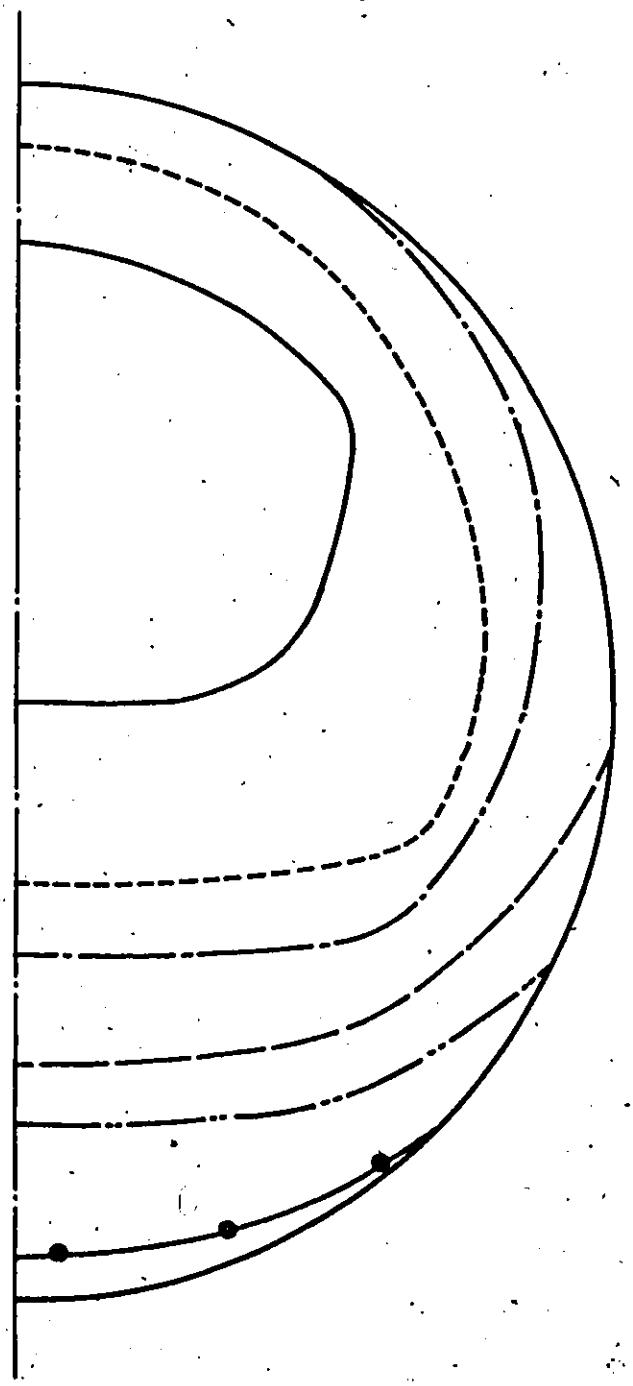

Fig. 4.13. Void fraction distribution

1. Flow Rates (kg/sec)
   Water 0.4
   Air 0.0215
2. Void Fractions (%)
   Integrated 80.6
   Mean 75.0
3. Iso-voidage Lines (%)
   99
   90
   80
   60
   40
   20

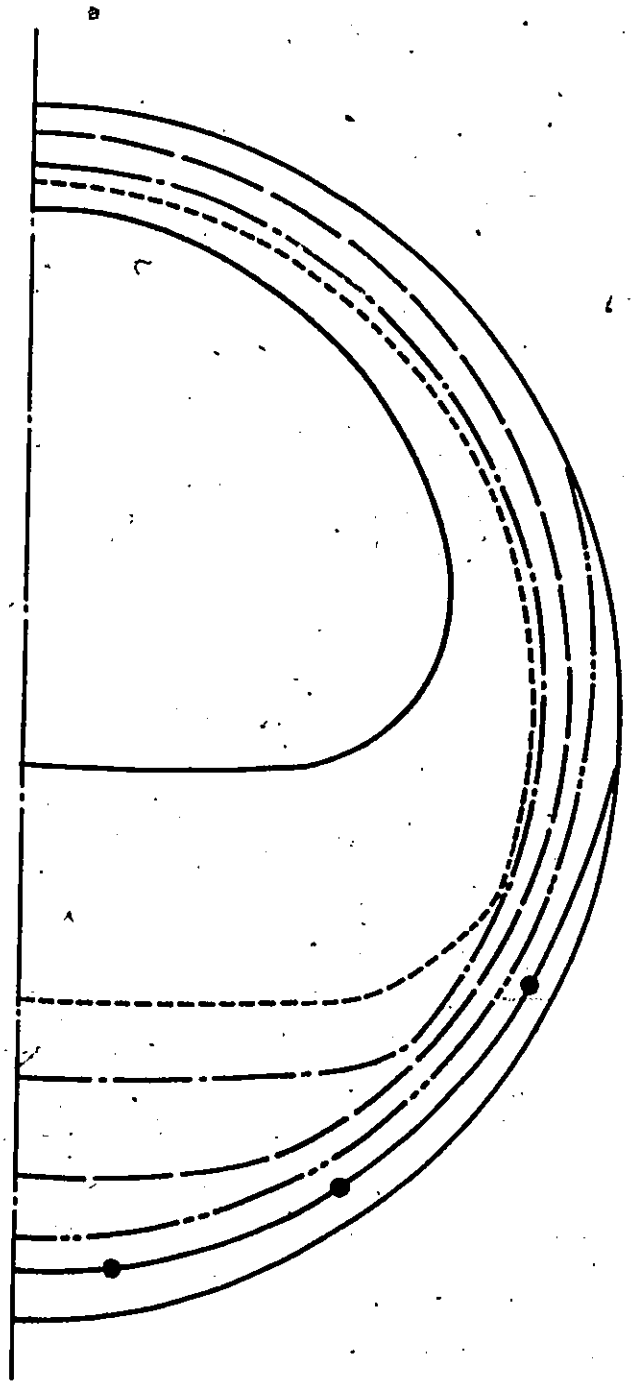

Fig. 4.14. Void fraction distribution

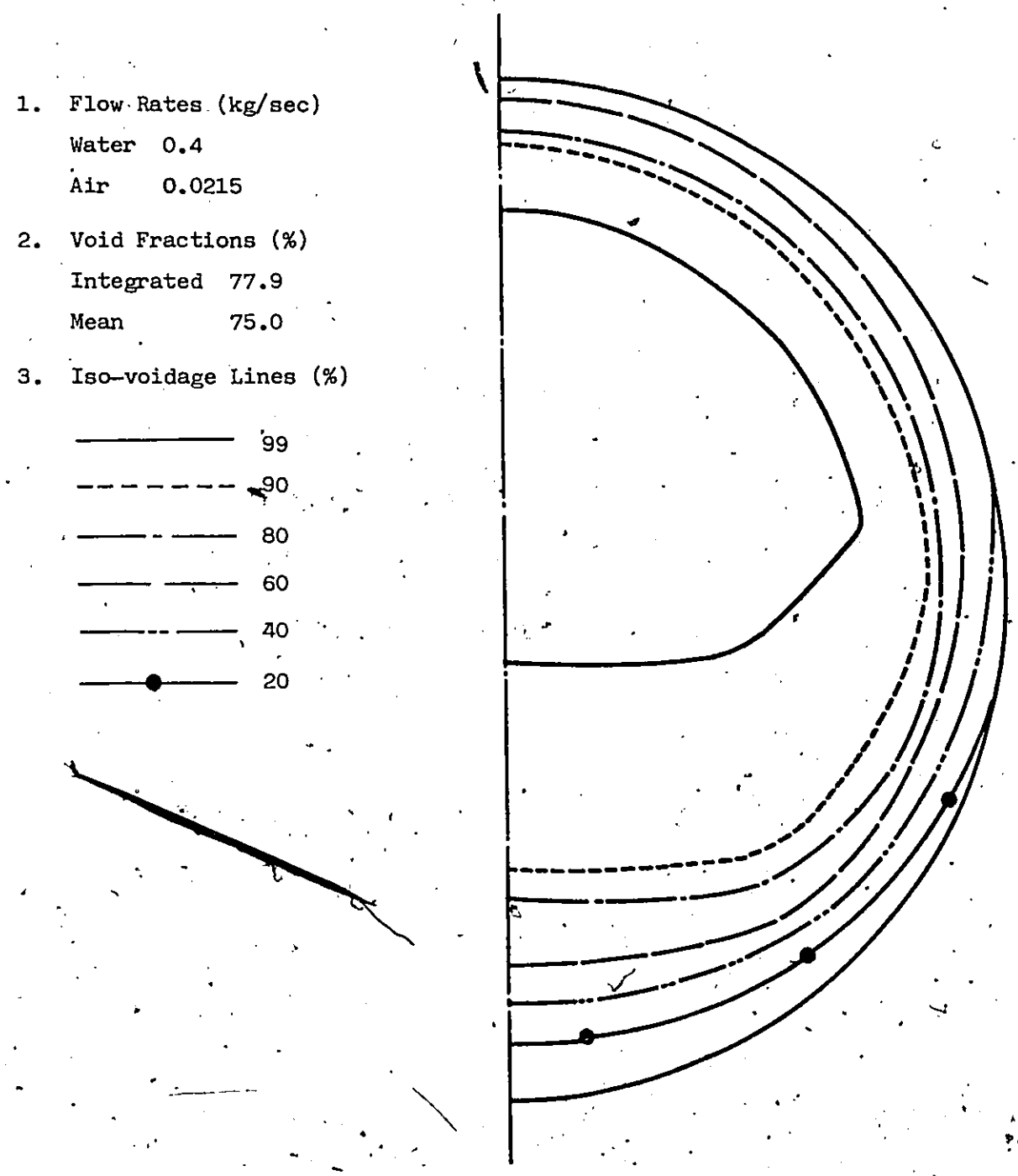

Fig. 4.15. Void fraction distribution

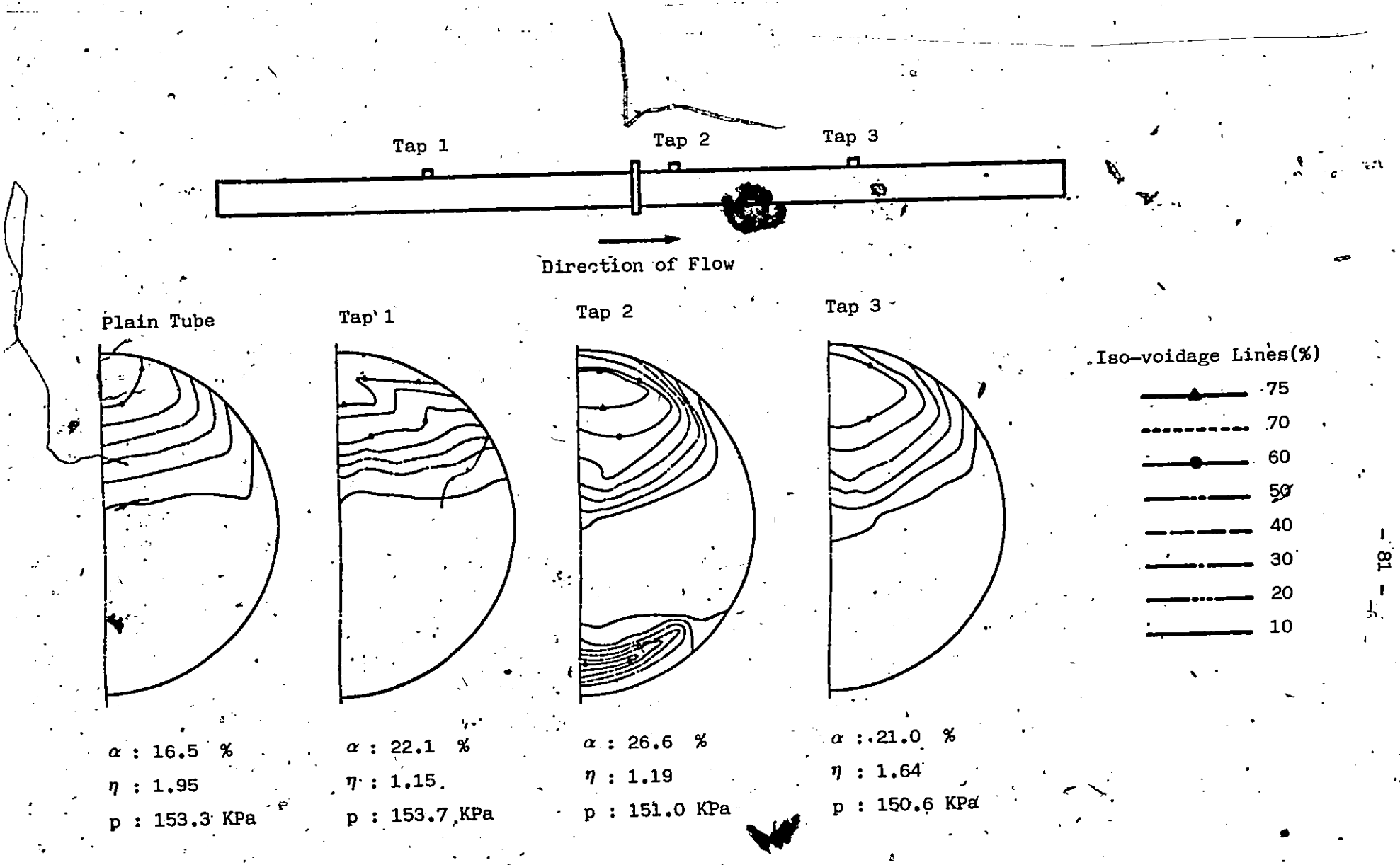

Fig. 4.16. Change of void distribution-Peripheral Obstruction (bubbly flow)
Water: 1.1 kg/sec, Air: 0.000775 kg/sec, Quality: 0.0704 %

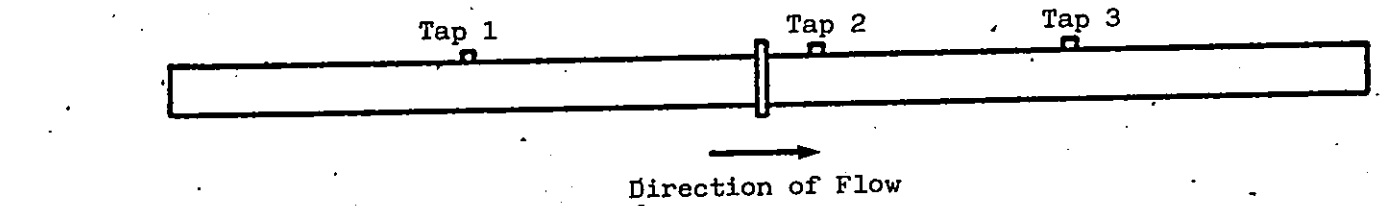

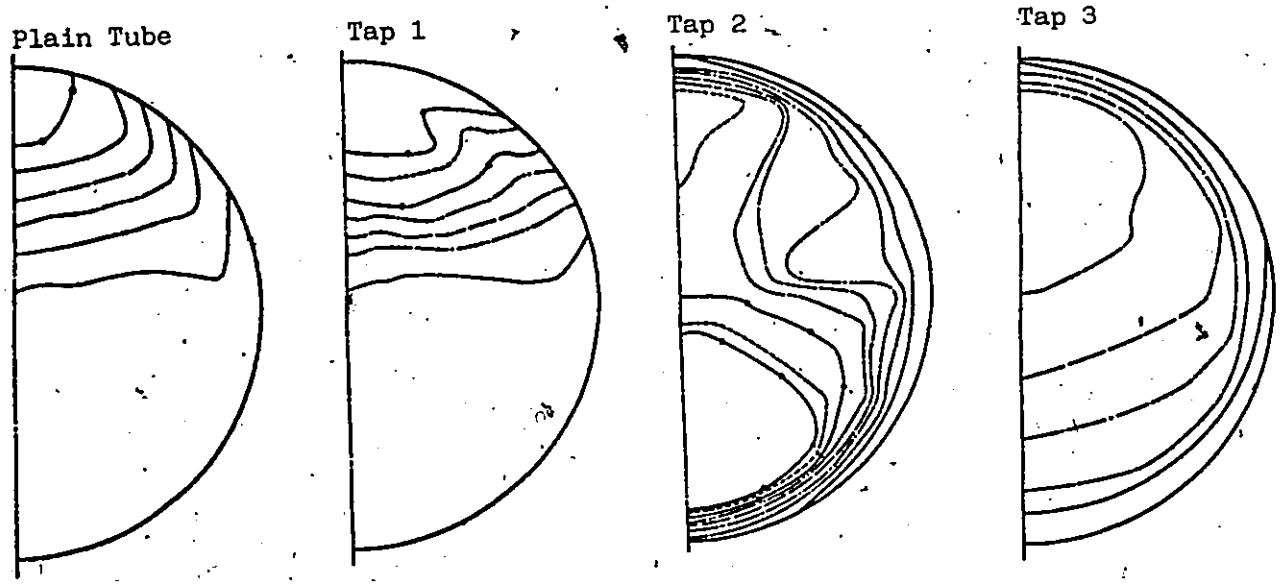

Plain Tube	Tap 1	Tap 2	Tap 3
α : 16.5 %	α : 25.6 %	α : 54.0 %	α : 37.4 %
η : 1.95	η : 1.10	η : 0.34	η : 0.66
p : 153.3 KPa	p : 155.7 KPa	p : 148.3 KPa	p : 149.4 KPa

Fig. 4.17. Change of void distribution-Central Obstruction (bubbly flow)
Water: 1.1 kg/sec, Air: 0.000775 kg/sec, Quality:0.0704 %

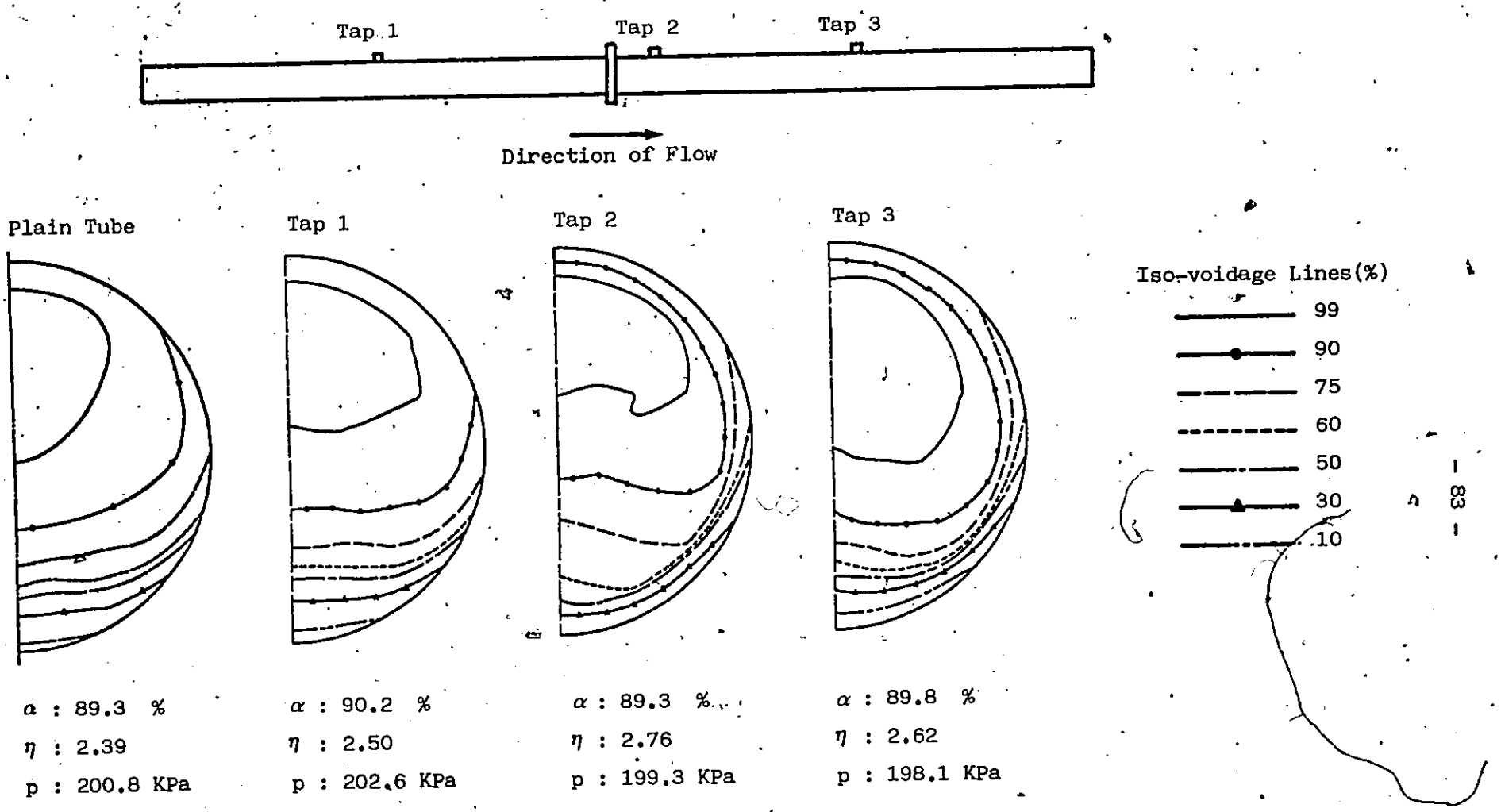

Fig. 4.18. Change of void distribution-Peripheral Qbstruction (annular flow)
Water: 0.3 kg/sec, Air: 0.0143 kg/sec, Quality: 4.55 %

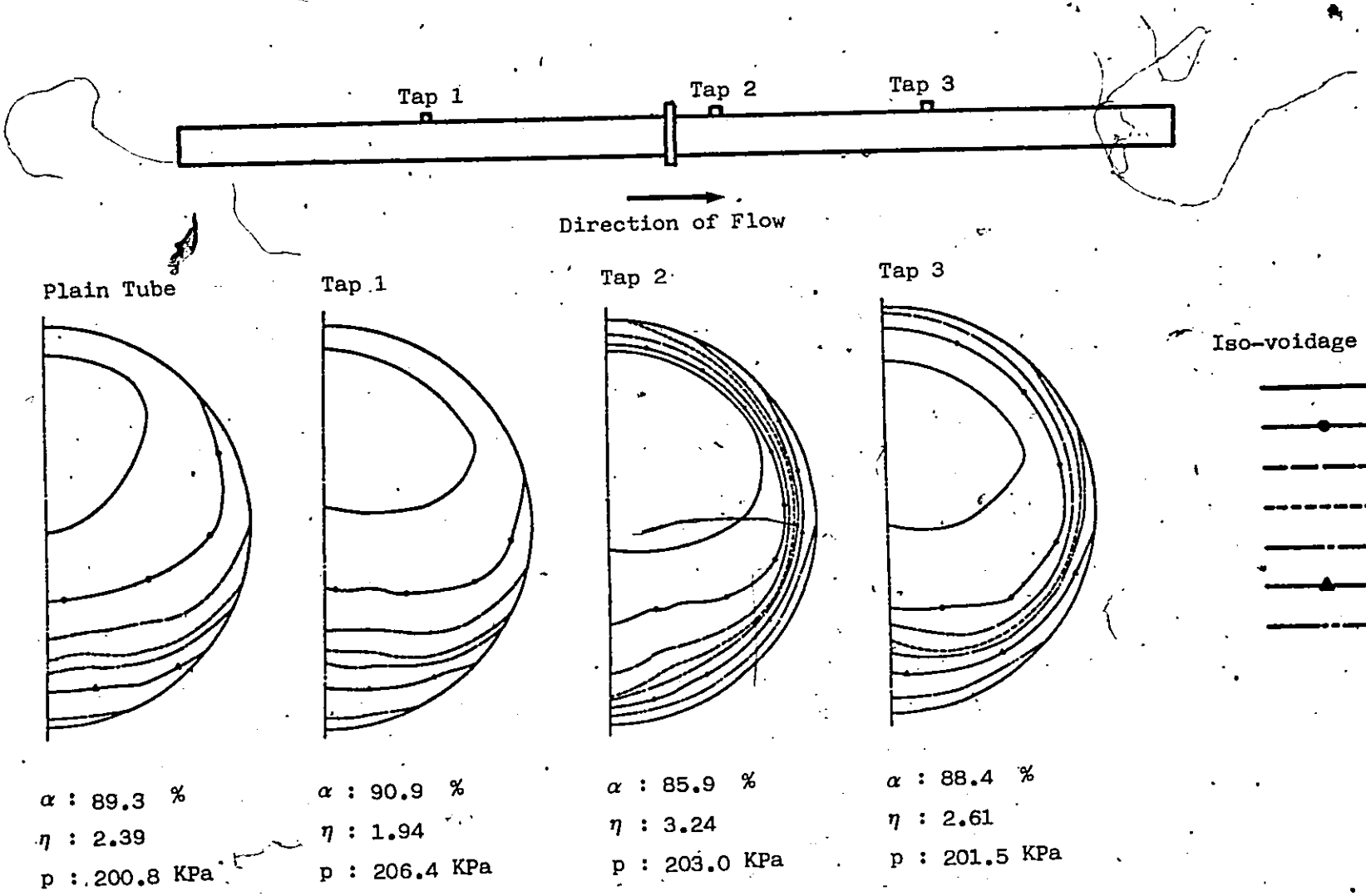

Fig. 4.19. Change of void distribution-Central Obstruction (annular flow)
Water: 0.3 kg/sec, Air: 0.0143 kg/sec, Quality: 4.55 %

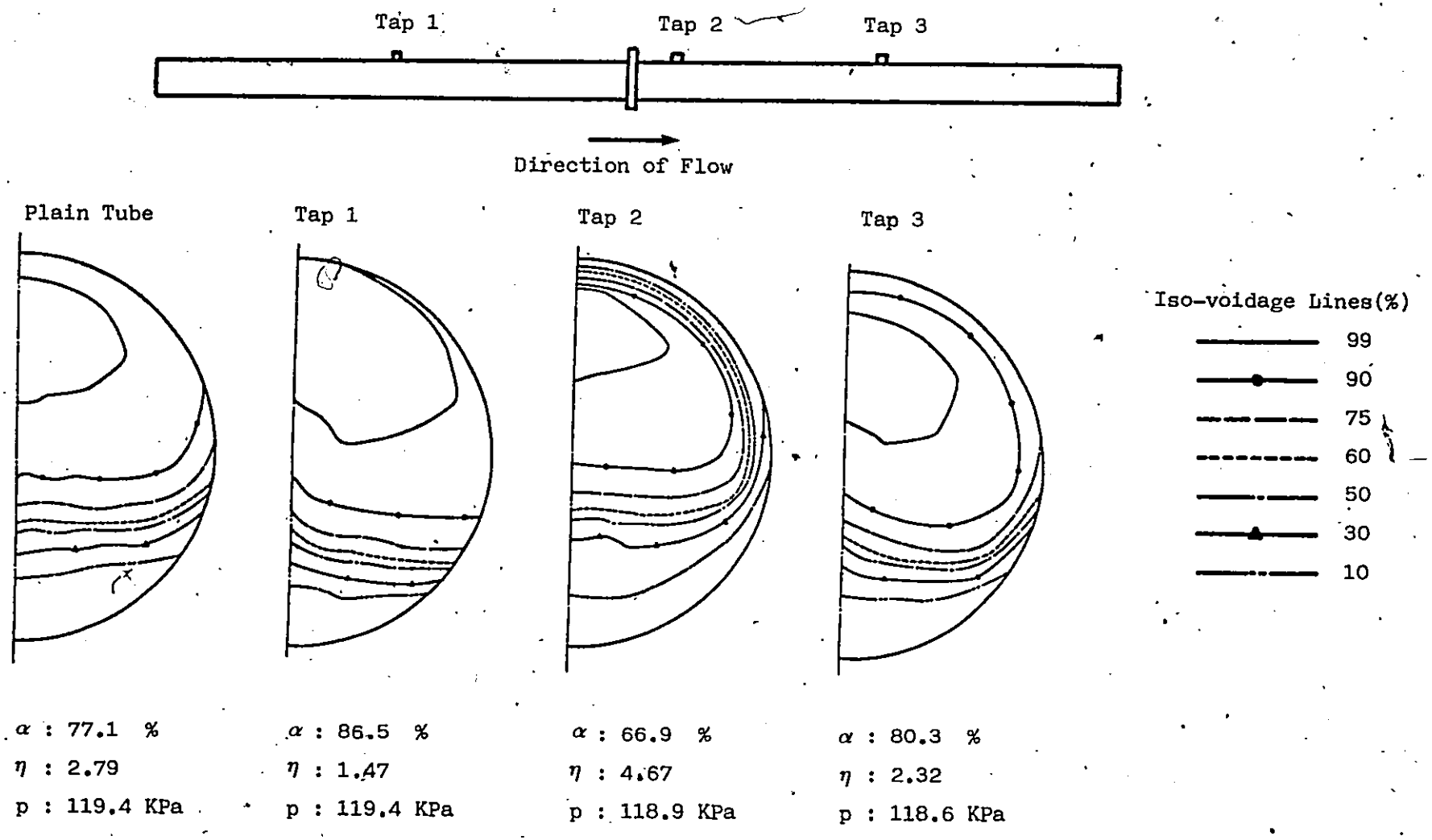

Fig. 4.20. Change of void distribution-Peripheral Obstruction (slug flow)
Water: 0.2 kg/sec, Air: 0.00268 Kg/sec, Quality: 1.32 %

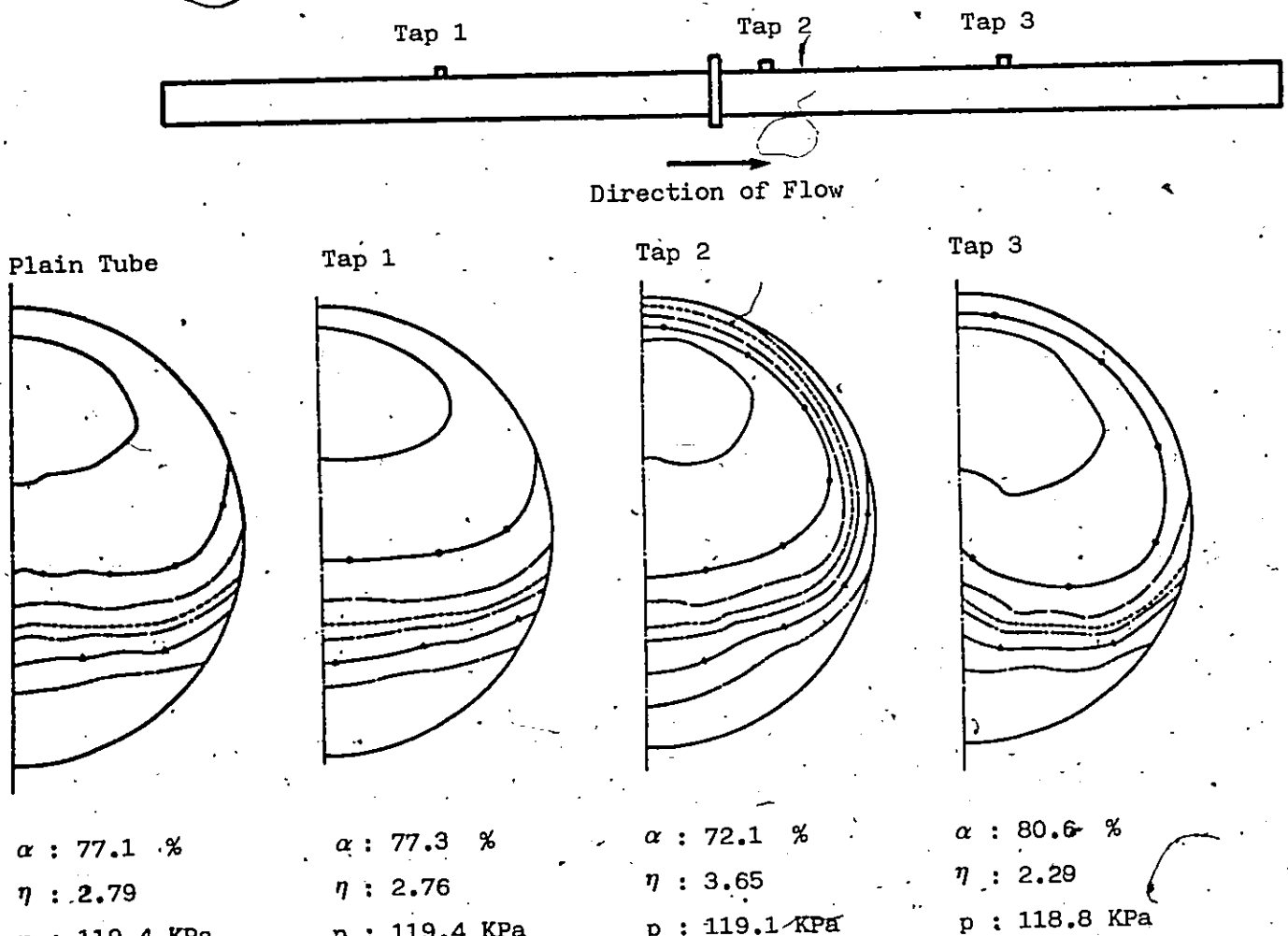

Fig. 4.21. Change of void distribution-Central Obstruction (slug flow)
Water: 0.2 kg/sec, Air; 0.00268 kg/sec, Quality: 1.32 %

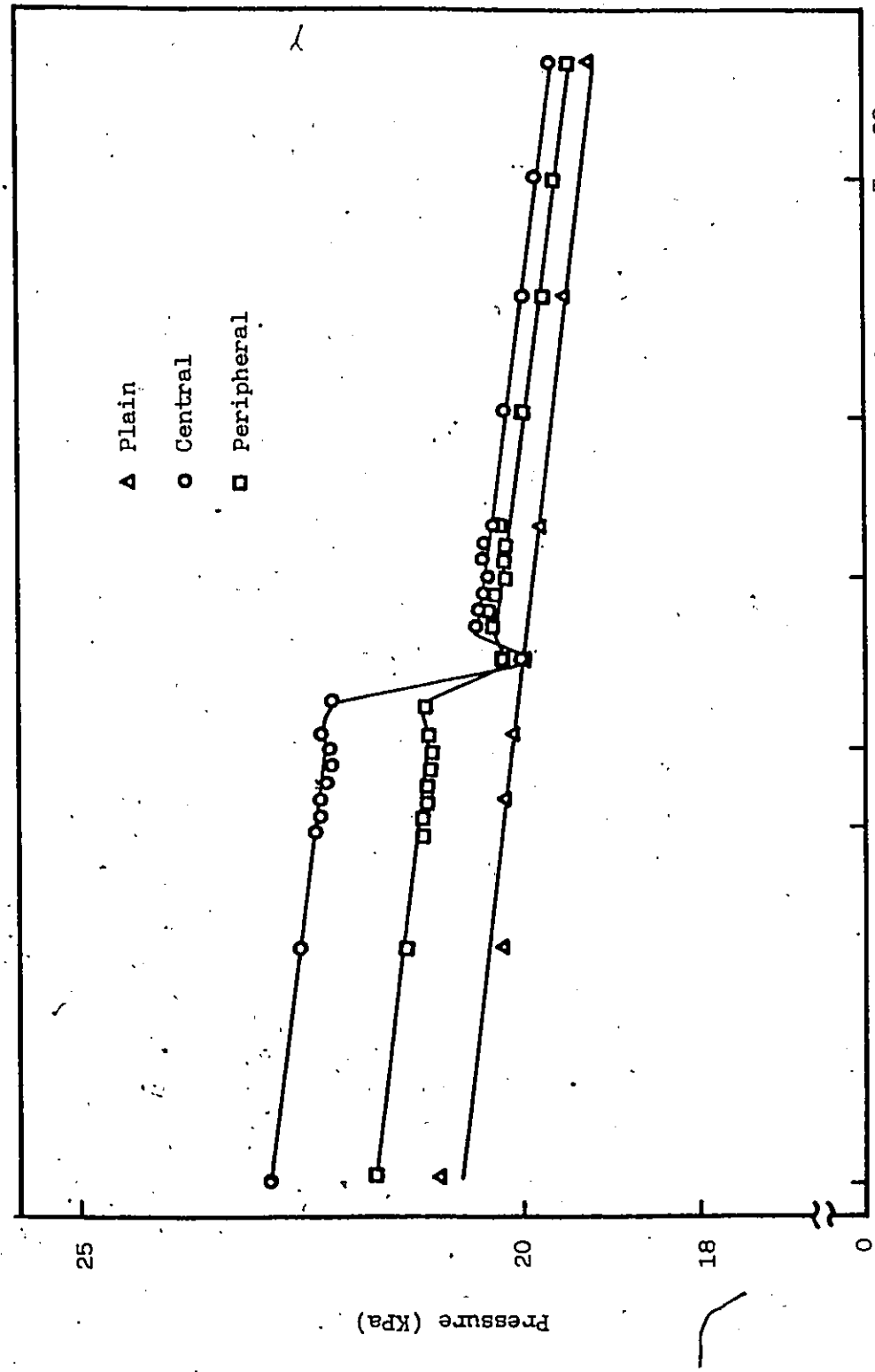

Fig. 4.22. Pressure profile

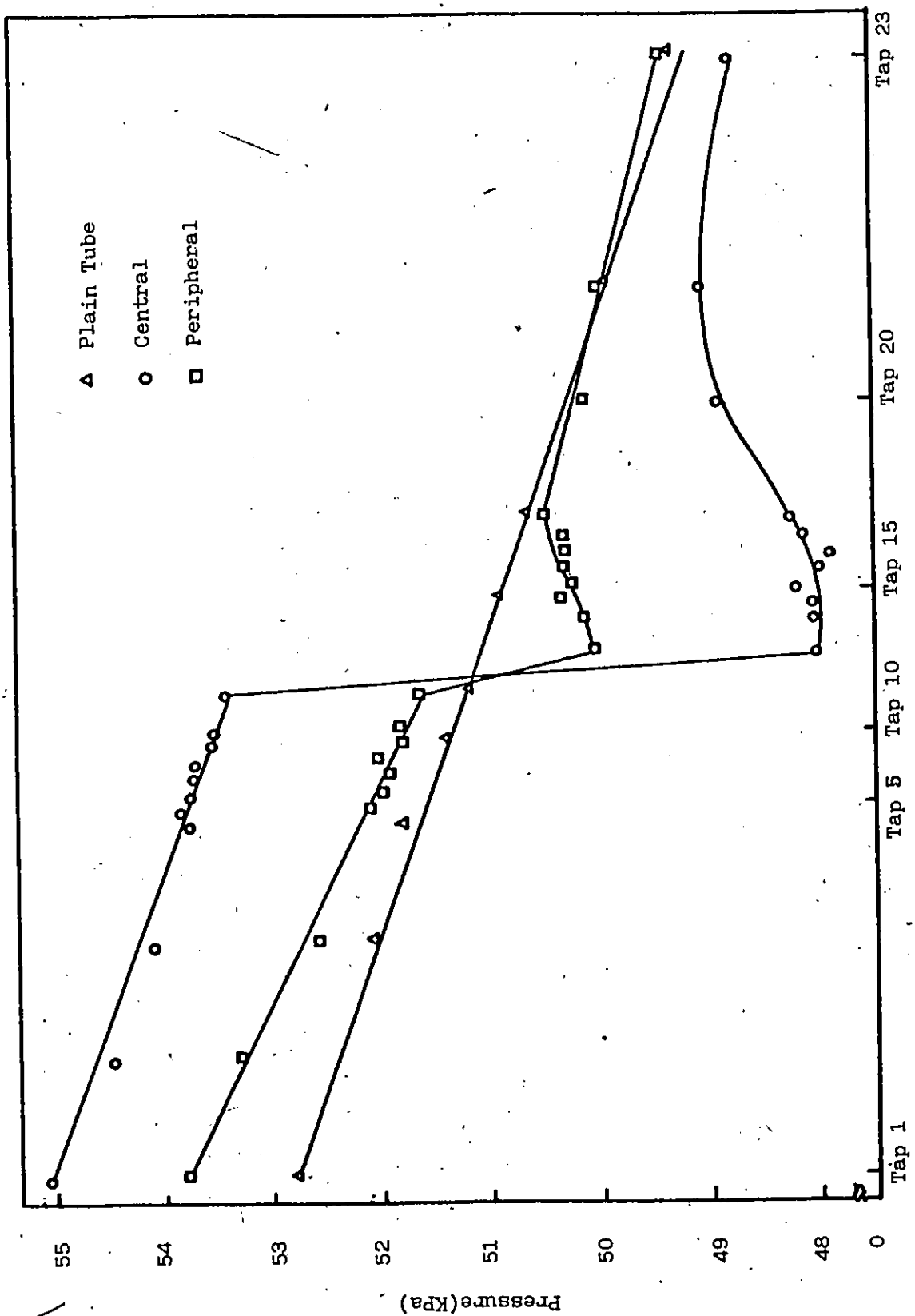

Fig. 4.23. Pressure profile (bubbly flow)
Water: 1.1 kg/sec, Air: 0.000775 kg/sec

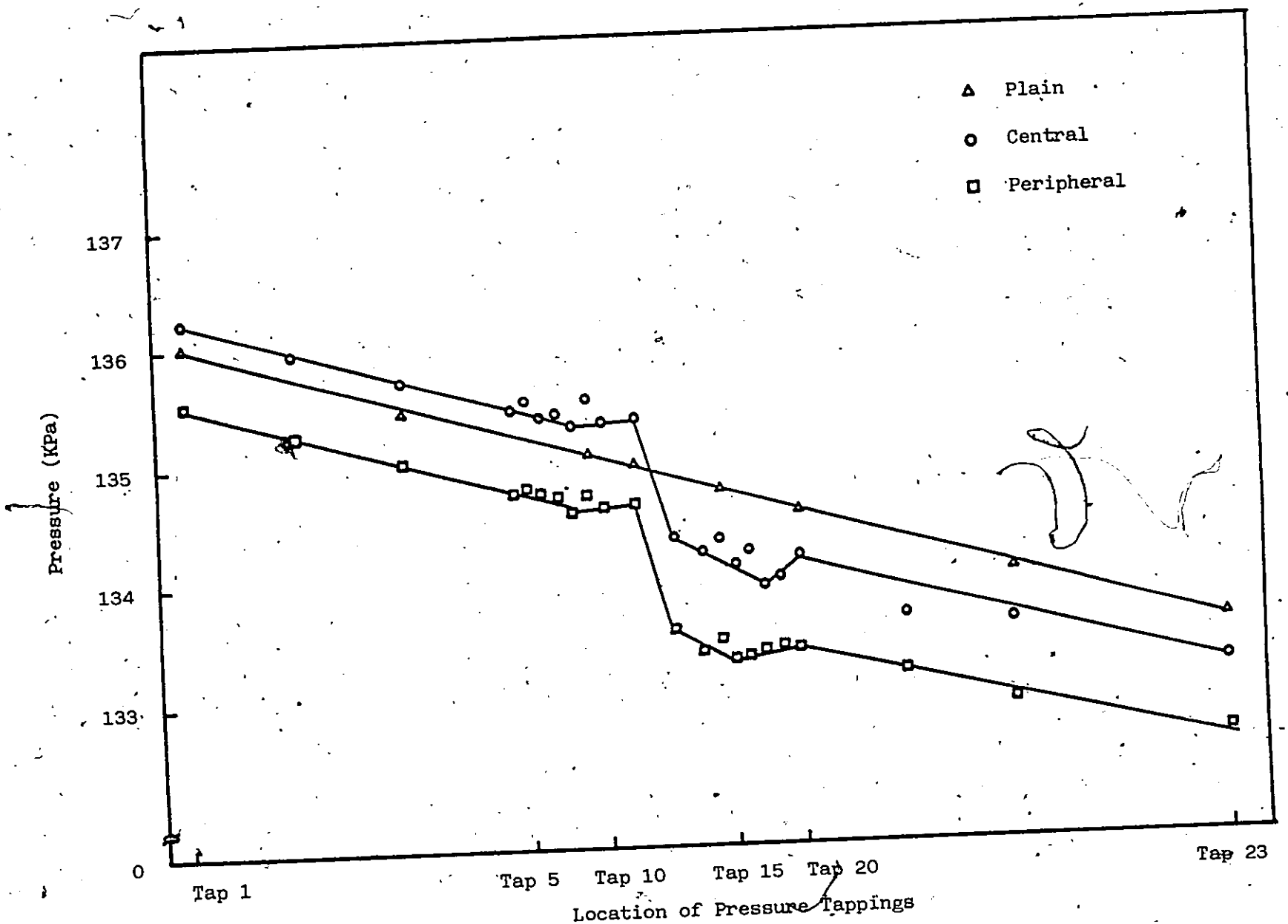

Fig. 4.24. Pressure profile (annular flow)
Water: 0.3 kg/sec, Air: 0.0143 kg/sec

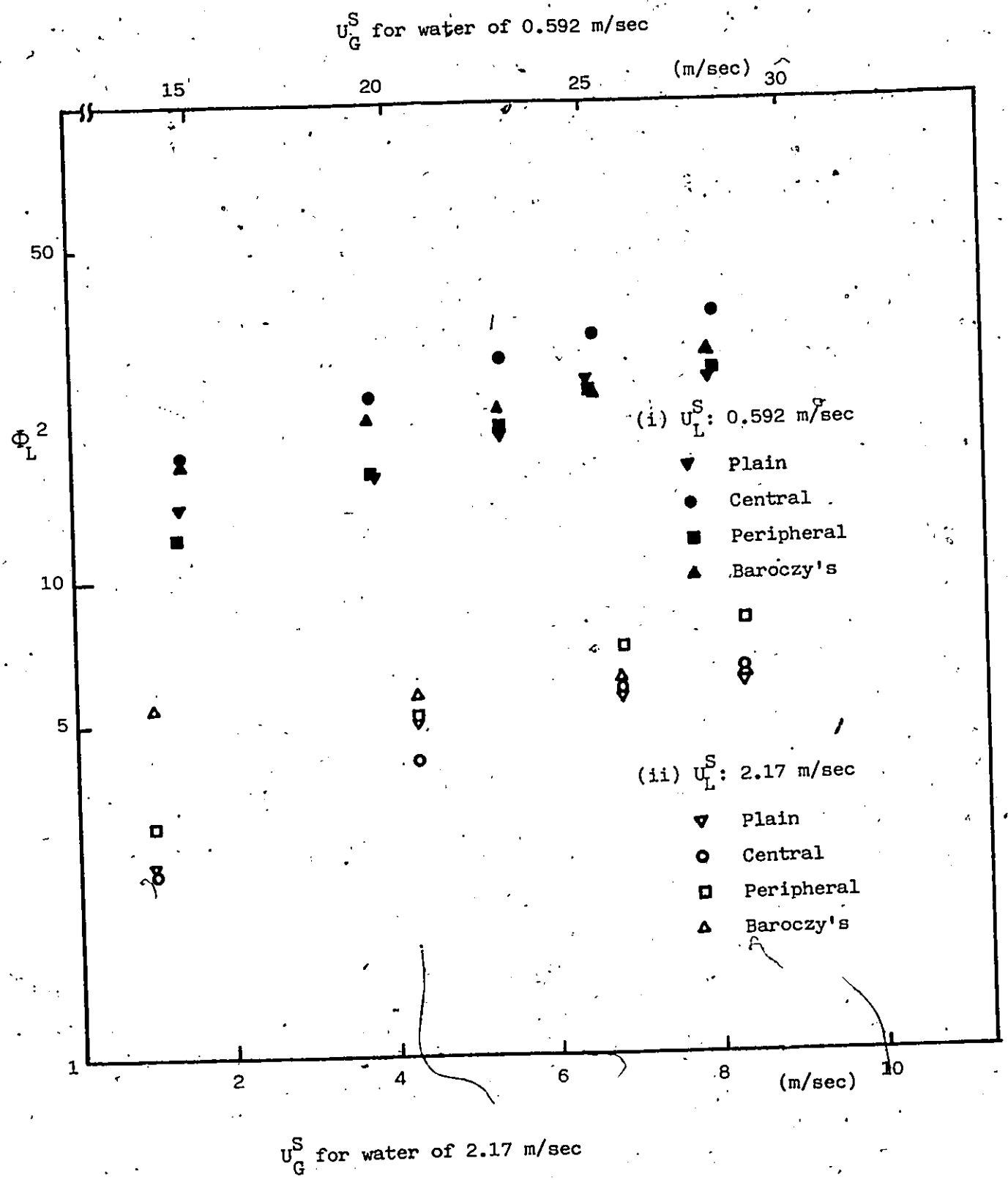

Fig. 4.25. Two-phase pressure drop multiplier Φ_L^2:

Comparison with Baroczy's.

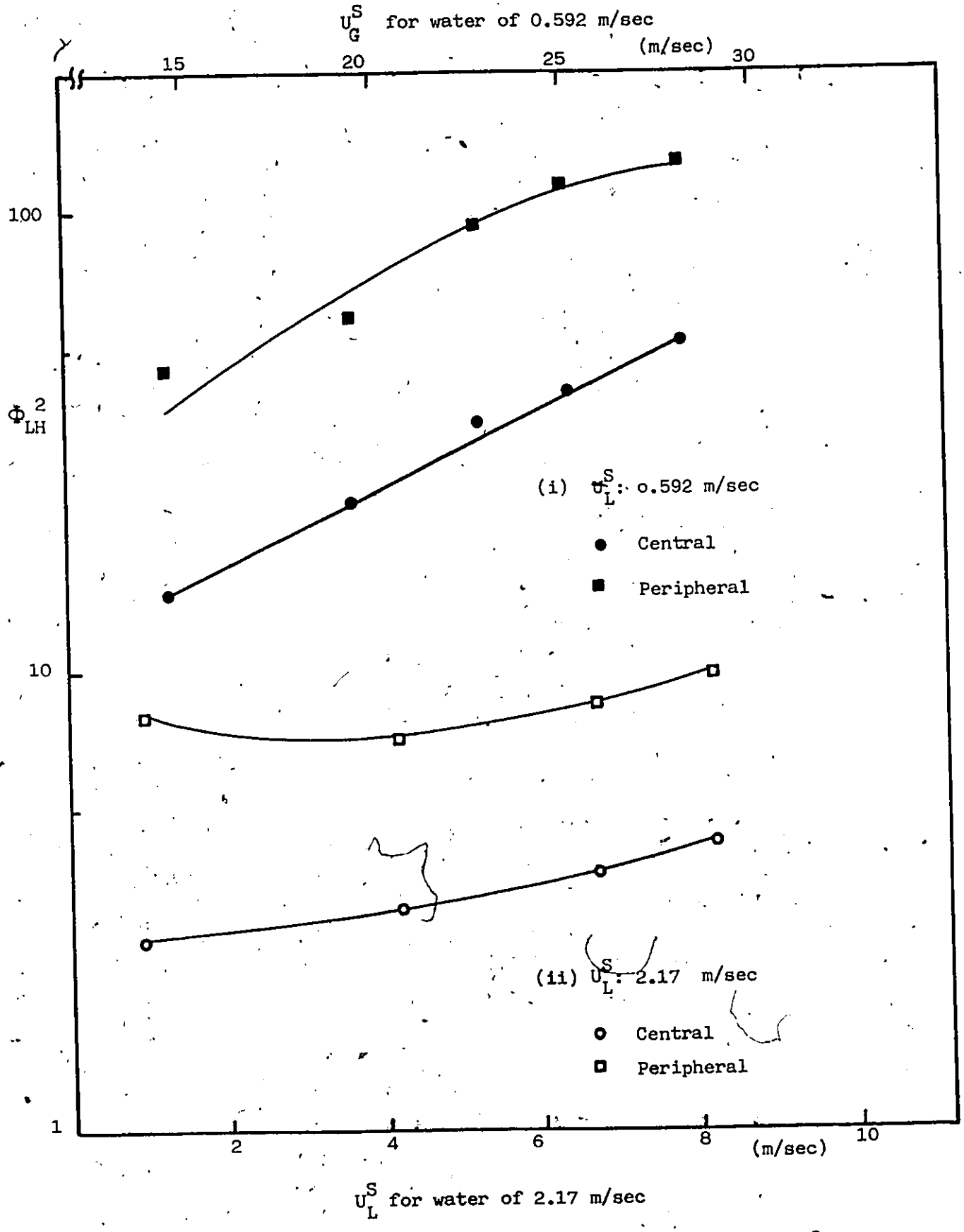

Fig. 4.26. Two-phase pressure drop multiplier Φ_{LH}^2 for obstructions

TABLE 4.5.

Comparison of Void Fractions obtained from the Optical Probe, Q.C.V., Homogeneous Model, Premoli's Model, and Zivi's Model.

Experimental	Water Flow Rate kg/sec	Air Flow Rate kg/sec	Pressure KPa	Void Fraction					Ref.
				Optical Probe	Q.C.V.	Homogeneous	Premoli	Zivi	
1	0.44	0.0217	239	0.751	0.774	0.946	0.710	0.819	Fig. 4.9.
2	0.44	0.015	193	0.732	0.767	0.937	0.662	0.802	Fig. 4.10.
3	0.44	0.015	239	0.694	0.692	0.923	0.630	0.775	Fig. 4.11.
4	0.4	0.0215	230	0.769	0.750	0.952	0.733	0.830	Fig. 4.12.
5	0.4	0.0215	230	0.789	0.750	-	-	-	Fig. 4.13.
6	0.4	0.0215	230	0.806	0.750	-	-	-	Fig. 4.14.
7	0.4	0.0215	230	0.779	0.750	-	-	-	Fig. 4.15.

TABLE 2.1.

Pressure-gradient components in the Momentum, Energy, and Homogeneous Flow equations

	Momentum Equation	Energy Equation	Homogeneous Flow Equation
$-\frac{dp_F}{dx}$	$\frac{aS}{A}\tau$	$\rho_H \frac{dE}{dx}$	$\frac{S}{A}\tau$ or $\rho_H \frac{dE}{dx}$
	determined empirically	determined empirically	determined empirically
$-\frac{dp_a}{dx}$	$G^2 \frac{d}{dx}\left\{\frac{x^2}{\alpha \rho_G} + \frac{(1-x)^2}{(1-\alpha)\rho_L}\right\}$	$\frac{\rho_H G^2}{2}\frac{d}{dx}\left\{\frac{x^3}{\alpha^2 \rho_G^2} + \frac{(1-x)^3}{(1-\alpha)^2 \rho_L^2}\right\}$	$G^2 \frac{dv_H}{dx}$
	where α is determined empirically	where α is determined empirically	
$-\frac{dp_g}{dx}$	$g \sin\theta\{\alpha \rho_G + (1-\alpha)\rho_L\}$	$\rho_H g \sin\theta$	$\rho_H g \sin\theta$
	where α is determined empirically		

TABLE 3.2. PRESSURE CORRECTION FACTORS

SCHUTTE & KOERTING CO. INSTRUMENT DIVISION, CORNWELLS HEIGHTS, BUCKS COUNTY, PA.

PRESSURE (PSIG) FOR WHICH ROTAMETER IS CALIBRATED	PRESSURE (PSIG) FOR WHICH CORRECTION IS TO BE MADE																								
	0	2	4	6	8	10	15	20	25	30	35	40	50	60	70	80	90	100	120	140	160	180	200	220	240	260
0	1.000	1.066	1.128	1.187	1.243	1.296	1.421	1.536	1.643	1.744	1.838	1.929	2.098	2.254	2.400	2.538	2.669	2.793	3.027	3.244	3.447	3.639	3.822	3.996	4.163	4.323
2	.938	1.000	1.058	1.114	1.166	1.217	1.334	1.442	1.542	1.636	1.725	1.810	1.967	2.114	2.251	2.381	2.504	2.621	2.839	3.043	3.234	3.413	3.583	3.749	3.905	4.056
4	.887	.945	1.000	1.052	1.102	1.149	1.261	1.362	1.457	1.546	1.631	1.710	1.860	1.999	2.128	2.251	2.366	2.476	2.683	2.876	3.056	3.226	3.387	3.543	3.691	3.833
6	.843	.898	.951	1.000	1.047	1.093	1.198	1.295	1.385	1.469	1.549	1.625	1.767	1.900	2.022	2.138	2.248	2.354	2.550	2.733	2.905	3.066	3.219	3.368	3.508	3.643
8	.805	.858	.908	.955	1.000	1.043	1.144	1.235	1.323	1.403	1.480	1.552	1.688	1.814	1.932	2.043	2.148	2.247	2.435	2.610	2.774	2.928	3.073	3.215	3.350	3.479
10	.771	.822	.870	.915	.958	1.000	1.096	1.185	1.268	1.345	1.418	1.488	1.618	1.739	1.852	1.959	2.059	2.155	2.335	2.502	2.658	2.806	2.946	3.083	3.211	3.335
15	.704	.750	.793	.835	.874	.912	1.000	1.081	1.156	1.227	1.293	1.357	1.476	1.586	1.690	1.786	1.877	1.965	2.129	2.282	2.424	2.559	2.687	2.811	2.928	3.041
20	.651	.693	.734	.772	.808	.844	.925	1.000	1.070	1.135	1.197	1.255	1.365	1.467	1.562	1.652	1.737	1.818	1.970	2.111	2.243	2.368	2.486	2.601	2.709	2.814
25	.609	.649	.686	.722	.756	.789	.865	.935	1.000	1.061	1.119	1.174	1.277	1.371	1.460	1.544	1.623	1.700	1.842	1.974	2.098	2.215	2.323	2.431	2.533	2.630
30	.573	.611	.647	.681	.713	.743	.815	.881	.943	1.000	1.055	1.106	1.204	1.292	1.376	1.455	1.530	1.603	1.736	1.860	1.977	2.087	2.190	2.291	2.387	2.474
35	.544	.579	.613	.646	.676	.705	.773	.835	.894	.948	1.000	1.049	1.142	1.226	1.305	1.380	1.451	1.520	1.646	1.764	1.874	1.979	2.077	2.173	2.264	2.351
40	.518	.552	.585	.615	.644	.672	.736	.797	.852	.904	.953	1.000	1.089	1.168	1.243	1.315	1.383	1.448	1.569	1.682	1.787	1.887	1.980	2.071	2.158	2.241
50	.477	.508	.538	.566	.592	.618	.678	.733	.784	.831	.876	.919	1.000	1.075	1.144	1.210	1.272	1.331	1.443	1.546	1.643	1.735	1.822	1.905	1.984	2.061
60	.444	.473	.500	.526	.551	.575	.631	.682	.729	.773	.816	.856	.931	1.000	1.065	1.126	1.184	1.239	1.343	1.439	1.529	1.615	1.695	1.773	1.847	1.918
70	.417	.444	.470	.494	.518	.540	.592	.640	.685	.726	.766	.804	.874	.939	1.000	1.057	1.112	1.164	1.261	1.351	1.436	1.516	1.594	1.665	1.734	1.801
80	.394	.420	.444	.468	.489	.511	.560	.605	.648	.687	.724	.760	.826	.888	.946	1.000	1.052	1.100	1.192	1.278	1.358	1.434	1.505	1.574	1.640	1.703
90	.375	.399	.423	.445	.466	.486	.533	.576	.616	.654	.689	.723	.786	.845	.899	.951	1.000	1.046	1.134	1.216	1.292	1.364	1.432	1.497	1.560	1.620
100	.359	.382	.404	.425	.445	.464	.509	.550	.588	.624	.658	.691	.751	.807	.859	.909	.956	1.000	1.084	1.161	1.234	1.303	1.368	1.430	1.490	1.548
120	.330	.352	.373	.392	.411	.428	.470	.508	.543	.576	.608	.637	.693	.745	.793	.839	.882	.923	1.000	1.072	1.138	1.202	1.262	1.320	1.375	1.428
140	.308	.329	.348	.366	.383	.400	.438	.474	.507	.538	.567	.594	.647	.695	.740	.782	.822	.861	.933	1.000	1.063	1.122	1.177	1.232	1.283	1.333
160	.290	.309	.327	.344	.360	.376	.413	.446	.477	.506	.534	.560	.609	.654	.696	.736	.774	.810	.879	.941	1.000	1.055	1.108	1.159	1.207	1.254
180	.275	.293	.310	.326	.342	.356	.391	.422	.452	.479	.505	.530	.576	.619	.660	.697	.733	.767	.832	.891	.948	1.000	1.049	1.098	1.144	1.188
200	.262	.279	.295	.311	.325	.339	.372	.402	.430	.456	.481	.505	.549	.590	.629	.664	.698	.731	.792	.850	.903	.953	1.000	1.046	1.089	1.131
220	.250	.267	.282	.297	.311	.324	.356	.385	.411	.436	.460	.483	.525	.564	.601	.635	.668	.699	.758	.812	.863	.911	.957	1.000	1.042	1.083
240	.240	.256	.271	.285	.299	.311	.342	.369	.395	.419	.442	.463	.504	.542	.577	.610	.641	.671	.727	.779	.828	.874	.918	.960	1.000	1.039
260	.231	.247	.261	.275	.288	.300	.329	.355	.380	.403	.425	.446	.485	.522	.555	.587	.617	.646	.700	.750	.798	.842	.884	.924	.963	1.000

For Rotameter Calibrated in Free Units – Rotameter Scale Reading X Factor = Corrected Flow for New Condition

For Rotameter Calibrated in Actual Units – Rotameter Scale Reading X $\frac{1}{\text{Factor}}$ = Corrected Flow for New Condition

TABLE 4.1.

Co-ordinates for Transition Boundaries of Flow Map shown in Fig. 4.3.

Transition Boundary	U_L^S m/sec	U_G^S m/sec
Stratified to Wavy	0.0165	3.709 - 4.837
	0.033	2.465 - 3.411
Wavy to Annular	0.033	9.498 - 21.574
	0.0478	8.583 - 20.700
	0.0626	8.983 - 18.467
Wavy to Slug	0.0478	4.354 - 4.992
	0.0626	4.680 - 5.947
Plug to Slug	0.0755	1.190 - 2.118
	0.0884	1.430 - 1.930
	0.103	1.132 - 1.508
	0.118	1.076 - 1.901
	0.128	1.182 - 1.992
	0.138	1.182 - 1.835
	0.154	1.425 - 1.765
	0.170	1.179 - 1.759
	0.196	1.312 - 1.835
	0.227	1.124 - 1.904
	0.269	1.226 - 1.973
	0.341	1.171 - 1.629
	0.353	1.251 - 1.882
	0.393	1.214 - 1.728

(continued)

Transition Boundary	U_L^S m/sec	U_G^S m/sec
Plug to Slug	0.432	1.214 - 1.744
	0.471	1.157 - 1.581
	0.511	1.203 - 1.703
	0.550	1.146 - 1.698
	0.589	1.146 - 1.735
	0.628	1.140 - 1.563
	0.668	0.955 - 1.458
	0.707	1.133 - 1.498
	0.746	1.198 - 1.541
	0.785	1.120 - 1.295
	0.825	0.943 - 1.566
	0.864	1.014 - 1.398
	0.903	1.037 - 1.393
	0.982	0.879 - 1.270
	1.060	0.827 - 1.162
	1.139	0.718 - 1.378
	1.217	1.088 - 8.714
Slug to Annular	0.0755	14.358 - 22.328
	0.0884	12.846 - 24.890
	0.103	12.991 - 19.827
	0.118	11.831 - 17.824
	0.128	12.307 - 17.661
	0.138	11.538 - 18.235
	0.154	10.940 - 17.983
	0.170	11.340 - 18.440
	0.196	10.256 - 19.748
	0.227	11.573 - 17.542

(continued)

Transition Boundary	U_L^S m/sec	U_G^S m/sec
Slug to Annular	0.269	9.637 - 15.806
	0.314	9.637 - 15.982
	0.353	11.442 - 16.883
	0.393	11.182 - 18,360
	0.432	12,042 - 19.021
	0,471	11.290 - 19.124
	0.511	11.187 - 19.047
	0.550	11.667 - 18.790
	0.589	10.610 - 18.525
	0.628	11.509 - 20.621
	0.668	9.293 - 19.126
	0.707	9.922 - 19.878
	0.746	11.947 - 21.425
	0.785	10.613 - 19.692
	0.825	10.809 - 22.024
	0.864	10.907 - 22.324
	0.903	9.978 - 20.109
	0.982	10.942 - 21.641
	1.060	10.597 - 23.175
	1.139	10.591 - 24.845
	1.217	8.714 - 23.259
	1.296	8.798 - 25.524
	1.375	7.644 - 23.445
	1.453	9.379 - 20.628
	1.532	8.257 - 20.746
	1.610	8.257 - 22.138
	1.689	6.178 - 21.185
	1.767	6.276 - 21.288

(continued)

Transition Boundary	U_L^S m/sec	U_G^S m/sec
Slug to Annular	1.866	6.881 - 21.127
	1.963	6.472 - 17.014
Bubbly to Slug	1.532	0.477 - 0.868
	1.610	0.632 - 0.864
	1.689	0.627 - 1.477
	1.767	0.664 - 1.363
	1.866	0.902 - 1.346
	1.963	1.038 - 2.831

TABLE 4.2.

Co-ordinates for Transition Boundaries of Flow Map shown in Fig. 4.5.

Transition Boundary	U_L^S m/sec	U_G^S m/sec
Stratified to Wavy	0.0165	0.945 - 1.817
	0.033	1.081 - 1.542
Wavy to Annular	0.0165	9.536 - 26.190
	0.033	8.873 - 21.663
Plug to Slug	0.478	1.244 - 1.831
	0.0626	1.269 - 2.240
	0.0755	1.322 - 2.009
	0.0884	1.110 - 2.267
	0.103	0.996 - 1.738
	0.118	1.110 - 1.794
	0.128	0.996 - 2.261
	0.138	1.076 - 1.922
	0.154	1.130 - 2.045
	0.170	0.938 - 2.057
	0.196	0.993 - 2.038
	0.227	0.938 - 2.082
	0.269	0.772 - 1.946
	0.314	0.932 - 1.893
	0.353	0.877 - 1.893
	0.393	0.767 - 1.340
	0.432	0.763 - 2.037

(continued)

Transition Boundary	U_L^S m/sec	U_G^S m/sec
Plug to Slug	0.471	0.763 - 1.786
	0.511	0.734 - 1.755
	0.550	0.733 - 1.766
	0.589	0.756 - 1.563
	0.628	0.596 - 1.674
	0.668	0.594 - 1.454
	0.707	0.746 - 1.583
	0.746	0.590 - 1.416
	0.785	0.588 - 1.165
Slug to Annular	0.0478	14.037 - 21.574
	0.0626	12.296 - 22.077
	0.0755	12.737 - 20.006
	0.0884	12.809 - 18.338
	0.103	10.542 - 19.501
	0.118	11.798 - 20.231
	0.128	11.124 - 18.235
	0.138	10.787 - 16.925
	0.154	9.910 - 16.557
	0.170	10.113 - 16.005
	0.196	9.831 - 15.822
	0.227	8.814 - 16.333
	0.269	8.888 - 15.982
	0.314	10.119 - 17.889
	0.353	9.118 - 16.389
	0.393	9.376 - 16.903
	0.432	10.670 - 17.628
	0.471	11.290 - 17.960

(continued)

Transition Boundary	U_L^S m/sec	U_G^S m/sec
Slug to Annular	0.511	10.161 - 16.736
	0.550	11.667 - 18.624
	0.589	10.302 - 18.201
	0.628	11.400 - 18.525
	0.668	11.619 - 17.633
	0.707	9.827 - 17.512
	0.746	11.458 - 18.828
	0.785	11.429 - 17.619
	0.825	9.706 - 19.698
	0.864	8.814 - 18.630
	0.903	8.897 - 18.891
	0.982	8.572 - 16.884
	1.060	8.481 - 16.057
	1.139	5.769 - 16.986
	1.217	7.067 - 15.530
	1.296	5.715 - 12.110
	1.375	6.833 - 11.644
	1.453	4.407 - 11.334
	1.532	4.324 - 8.403
	1.610	4.273 - 8.132
	1.689	3.606 - 6.672
	1.767	3.674 - 6.227
	1.866	2.778 - 6.325
Bubbly to Slug	1.453	0.360 - 0.989
	1.532	0.427 - 1.026
	1.610	0.473 - 1.384
	1.689	0.715 - 2.693

(continued)

Transition Boundary	U_L^S m/sec	U_G^S m/sec
Bubbly to Slug	1.767	0.664 - 2.752
	1.866	1.131 - 2.778
Bubbly to Annular	1.963	1.301 - 6.239

TABLE 4.3.

Co-ordinates for Transition Boundaries of Flow Map shown in Fig. 4.4.

Transition Boundary	U_L^S m/sec	U_G^S m/sec
Stratified to Wavy	0.0165	2.773 - 4.005
	0.033	1.585 - 2.274
	0.0478	1.245 - 1.782
Wavy to Annular	0.0165	9.854 - 19.931
	0.033	8.138 - 19.640
Wavy to Slug	0.478	3.697 - 4.621
Slug to Annular	0.476	14.289 - 19.776
	0.0626	12.446 - 20.006
	0.0755	11.895 - 18.112
	0.0884	11.631 - 19.279
	0.103	11.299 - 19.869
	0.118	11.798 - 18.397
	0.128	10.634 - 17.862
	0.138	9.969 - 16.925
	0.154	10.450 - 17.293
	0.170	9.172 - 16.925
	0.196	8.972 - 16.557
	0.227	7.976 - 17.311
	0.269	8.547 - 17.504
	0.314	8.205 - 16.434
	0.353	8.311 - 17.112

(continued)

Transition Boundary	U_L^S m/sec	U_G^S m/sec
Slug to Annular	0.393	8.878 - 16.903
	0.432	8.523 - 15.724
	0.471	7.458 - 16.026
	0.511	7.103 - 15.225
	0.550	8.095 - 14.963
	0.589	8.559 - 15.654
	0.628	7.874 - 14.830
	0.668	7.903 - 15.661
	0.707	6.698 - 15.801
	0.746	7.230 - 16.199
	0.785	7.778 - 15.323
	0.825	6.540 - 15.323
	0.864	6.088 - 15.004
	0.903	6.155 - 15.242
	0.982	6.222 - 15.070
	1.060	5.445 - 14.792
	1.139	4.900 - 15.693
	1.217	4.232 - 13.979
	1.296	3.387 - 11.010
	1.375	3.462 - 11.178
	1.453	3.078 - 9.036
	1.532	3.145 - 9.175
	1.610	3.145 - 7.352
	1.689	3.145 - 7.228
	1.767	2.772 - 6.227
Plug to Slug	0.755	1.324 - 1.907
	0.0884	0.278 - 0.388

(continued)

Transition Boundary	U_L^S m/sec	U_G^S m/sec
Plug to Slug	0.103	1.186 - 1.803
	0.118	1.076 - 1.798
	0.128	1.182 - 1.645
	0.138	0.938 - 1.787
	0.154	1.131 - 1.916
	0.170	1.182 - 1.765
	0.196	0.990 - 1.575
	0.227	0.772 - 1.749
	0.269	1.175 - 1.678
	0.314	0.985 - 1.794
	0.353	0.982 - 1.760
	0.393	1.115 - 1.595
	0.432	0.924 - 1.546
	0.471	0.924 - 1.423
	0.511	0.969 - 1.533
	0.550	0.915 - 1.441
	0.589	0.753 - 1.730
	0.628	0.753 - 1.657
	0.668	0.702 - 1.335
	0.707	0.751 - 1.428
	0.746	0.824 - 1.424
	0.785	0.846 - 1.408
	0.825	0.742 - 1.019
Bubbly to Slug	1.453	0.550 - 0.950
	1.532	0.615 - 1.138
	1.610	0.682 - 1.066
	1.689	0.629 - 1.057

(continued)

Transition Boundary	U_L^S m/sec	U_G^S m/sec
Bubbly to Slug	1.767	0.661 - 2.772
Bubbly to Annular	1.866	0.832 - 6.811
	1.963	1.083 - 6.521

TABLE 4.4.

Comparison of Void Fractions

obtained from the Optical Probe and Q.C.V.

Experimental	Water Flow Rate (kg/sec)	Air Flow Rate (kg/sec)	Void Fraction (%) Optical Probe	Q.C.V.	Reference
1	0.4	0.0091	37.8	66.6	Fig. 4.7.
2	0.4	0.019	51.0	83.0	Fig. 4.8.

TABLE 4.5.

Comparison of Void Fractions obtained from the Optical Probe, Q.C.V., Homogeneous Model, Premoli's Model, and Zivi's Model.

Experimental	Water Flow Rate kg/sec	Air Flow Rate kg/sec	Pressure KPa	Void Fraction					Ref.
				Optical Probe	Q.C.V.	Homogeneous	Premoli	Zivi	
1	0.44	0.0217	239	0.751	0.774	0.946	0.710	0.819	Fig. 4.9.
2	0.44	0.015	193	0.732	0.767	0.937	0.662	0.802	Fig. 4.10.
3	0.44	0.015	239	0.694	0.692	0.923	0.630	0.775	Fig. 4.11.
4	0.4	0.0215	230	0.769	0.750	0.952	0.733	0.830	Fig. 4.12.
5	0.4	0.0215	230	0.789	0.750	-	-	-	Fig. 4.13.
6	0.4	0.0215	230	0.806	0.750	-	-	-	Fig. 4.14.
7	0.4	0.0215	230	0.779	0.750	-	-	-	Fig. 4.15.

(continued)

Experimental	Superficial Mass Flux (kg/m^2hr)		Quality	Slip Ratio	Distance from O.B.*
	Water	Air			
1	3.20×10^6	1.580×10^5	0.047	5.07	No O.B.
2	3.20×10^6	1.014×10^5	0.033	4.21	No O.B.
3	3.20×10^6	1.014×10^5	0.033	4.9	No O.B.
4	2.65×10^6	1.42×10^5	0.051	5.66	No O.B.
5	2.65×10^6	1.42×10^5	0.051	5.26	9 HD** upstream
6	2.65×10^6	1.42×10^5	0.051	4.73	3 HD downstream
7	2.65×10^6	1.42×10^5	0.051	5.57	9 HD downstream

* O.B.: Obstruction

** HD : Hydraulic Diameter

TABLE 4.6.

Pressure Drop Measurement Data

Exp.	Flow rate(kg/sec)		Liquid phase	TP* press. drop before OB** (KPa/m)		TP press. drop past OB (KPa/m)		TP multiplier Φ_L^2	
	Water	Air	press. drop(KPa/m)	C***	P****	C	P	C	P
1	1.1	0.000775	1.726	4.289	5.293	1.466	2.877	2.48	3.07
2	1.1	0.005	1.726	7.221	8.795	6.841	6.108	4.13	5.09
3	1.1	0.01	1.726	10.098	12.297	9.447	8.904	5.86	7.08
4	1.1	0.0135	1.726	11.238	13.790	10.370	6.624	6.52	7.99
5	0.3	0.0143	0.206	6.244	4.126	6.108	4.670	18.53	12.26
6	0.3	0.025	0.206	8.117	5.673	7.574	5.076	24.09	16.85
7	0.3	0.035	0.206	9.935	7.085	7.438	5.103	29.53	21.05
8	0.3	0.045	0.206	11.021	8.687	10.641	5.483	32.78	25.81
9	0.3	0.055	0.206	12.243	9.230	11.374	6.298	36.34	27.42

* : Two-phase flow

** : Obstruction

***: Central

****: Peripheral

(continued)

Exp.	Superficial velocity (m/sec)		Head loss coeff. Liquid phase		Press. drop across OB(KPa)		Max. press. drop across OB(KPa)		TP multiplier Φ_{HL}^2	
	Water	Air	C	P	C	P	C	P	C	P
1	2.17	0.87	0.798	0.260	4.827	0.896	6.343	1.448	2.57	7.88
2	2.17	3.86	0.798	0.260	5.640	3.103	7.295	5.792	3.00	7.09
3	2.17	6.23	0.798	0.260	6.805	4.206	8.060	6.274	3.62	8.55
4	2.17	7.56	0.798	0.260	7.881	4.482	8.729	6.412	4.19	9.90
5	0.592	13.10	0.798	0.260	2.062	2.069	2.062	2.620	14.73	45.40
6	0.592	18.74	0.798	0.260	3.227	2.689	3.489	2.965	23.05	59.02
7	0.592	22.19	0.798	0.260	4.833	4.137	5.371	3.999	34.58	90.80
8	0.592	24.76	0.798	0.260	5.599	5.206	6.764	5.654	40.03	114.26
9	0.592	28.23	0.798	0.260	6.716	5.792	7.522	5.585	51.92	127.12

APPENDIX

SAMPLE CALCULATION

1. Readings of the Local Void Fractions

Position of the Probe		Void Fractions						
Radial* (mm)	Angular (°)	1	2	3	4	5	6	Average
0		99.8	99.9	99.9	99.9	99.9	99.9	99.9
3	0	99.9	99.9	99.9	99.9	99.9	99.9	99.9
	10	99.9	99.9	99.9	99.9	99.9	99.9	99.9
	20	99.9	99.9	99.9	99.9	99.9	99.9	99.9
	30	99.9	99.9	99.9	99.9	99.9	99.9	99.9
	40	99.9	99.9	99.9	99.9	99.9	99.9	99.9
	50	99.9	99.9	99.9	99.9	99.9	99.9	99.9
	60	99.9	99.9	99.9	99.9	99.9	99.9	99.9
	70	99.8	99.9	99.9	99.9	99.9	99.9	99.9
	80	99.8	99.8	99.8	99.8	99.7	99.8	99.8
	90	99.8	99.8	99.8	99.8	99.8	99.7	99.8
	100	99.7	99.5	99.5	99.5	99.6	99.6	99.6
	110	99.4	99.4	99.3	99.4	99.4	99.6	99.4
	120	99.0	98.9	98.8	99.2	98.4	99.1	98.9
	130	98.1	98.5	98.3	98.2	98.3	98.5	98.3
	140	97.4	97.5	97.4	98.0	97.9	98.0	97.7
	150	96.9	97.3	97.5	97.6	96.6	97.0	97.2
	160	96.0	96.4	96.5	96.4	96.4	97.1	96.5
	170	97.1	96.2	95.7	96.5	96.1	96.5	96.4
	180	96.6	96.6	96.4	96.6	96.3	96.0	96.4

* This is the distance from the center.

Position of the Probe		Void Fractions						
Radial (mm)	Angular (^{o})	1	2	3	4	5	6	Average
6	0	99.9	99.9	99.9	99.9	99.9	99.9	99.9
	10	99.9	99.9	99.9	99.9	99.9	99.9	99.9
	20	99.9	99.9	99.9	99.9	99.9	99.9	99.9
	30	99.9	99.9	99.9	99.9	99.9	99.9	99.9
	40	99.9	99.9	99.9	99.9	99.9	99.9	99.9
	50	99.9	99.9	99.9	99.9	99.9	99.9	99.9
	60	99.9	99.9	99.9	99.9	99.9	99.9	99.9
	70	99.8	99.9	99.8	99.9	99.9	99.9	99.9
	80	99.8	99.8	99.8	99.8	99.8	99.8	99.8
	90	99.6	99.6	99.6	99.7	99.6	99.6	99.6
	100	99.2	99.3	99.1	99.2	99.0	99.1	99.2
	110	98.2	98.4	98.5	98.5	98.2	98.1	98.3
	120	97.2	96.8	96.9	96.8	97.0	97.3	97.0
	130	94.4	94.9	95.3	95.0	94.2	94.7	94.8
	140	91.4	91.6	91.1	90.1	90.7	91.2	91.0
	150	88.3	88.4	89.9	88.3	88.0	87.1	88.3
	160	83.2	84.1	83.9	86.1	85 0	86.0	84.7
	170	83.8	84.4	83.3	84.5	85.9	83.3	84.2
	180	83.9	84.0	83.5	83.8	85.2	84.3	84.1

Position of the Probe		Void Fractions						
Radial (mm)	Angular (^{o})	1	2	3	4	5	6	Average
9	0	99.7	99.7	99.5	99.6	99.5	99.8	99.6
	10	99.8	99.7	99.6	99.8	99.7	99.4	99.7
	20	99.6	99.7	99.6	99.7	99.7	99.6	99.7
	30	99.7	99.7	99.7	99.7	99.7	99.7	99.7
	40	99.6	99.7	99.7	99.6	99.5	99.6	99.6
	50	99.3	99.5	99.3	99.6	99.5	99.5	99.5
	60	99.2	99.5	99.3	99.2	99.1	99.5	99.3
	70	98.9	98.8	98.8	99.1	99.1	98.9	98.9
	80	98.3	98.2	98.5	97.9	98.3	97.8	98.2
	90	97.1	97.5	97.4	96.9	97.4	97.1	97.2
	100	95.4	94.9	95.1	95.1	95.6	94.9	95.2
	110	91.6	92.3	92.7	92.4	91.7	91.6	92.1
	120	87.5	87.2	86.9	87.5	87.1	87.3	87.3
	130	78.4	79.4	78.5	79.4	80.2	77.6	78.9
	140	69.6	69.1	67.5	70.6	67.7	67.0	68.6
	150	54.2	56.0	55.1	56.6	55.9	55.6	55.6
	160	53.0	48.6	48.4	49.2	48.7	47.4	49.2
	170	45.6	43.2	43.5	43.6	44.7	44.4	44.2
	180	44.7	45.8	44.2	43.3	43.6	44.0	44.3

Position of the Probe		Void Fractions						
Radial (mm)	Angular (^{o})	1	2	3	4	5	6	Average
10.5	0	95.6	96.4	96.0	96.0	96.6	96.7	96.2
	10	95.9	96.0	95.9	96.2	96.1	96.1	96.0
	20	95.8	96.6	95.5	94.9	95.8	96.0	95.8
	30	95.2	95.1	96.4	95.7	95.4	96.2	95.7
	40	94.6	94.7	94.9	95.3	94.9	94.5	94.8
	50	94.0	94.7	94.6	94.4	94.6	94.0	94.4
	60	93.0	93.5	92.8	93.6	93.3	92.9	93.2
	70	91.8	92.6	91.8	91.3	92.6	91.8	92.0
	80	90.4	90.1	89.7	89.4	90.2	90.0	90.0
	90	86.9	86.3	86.1	87.0	86.1	86.9	86.6
	100	81.8	81.9	81.7	83.0	81.8	81.8	82.0
	110	74.3	74.2	74.5	74.3	75.0	75.2	74.6
	120	59.4	62.2	61.7	62.4	63.0	62.8	61.9
	130	50.8	49.9	50.3	48.9	50.4	50.9	50.1
	140	37.1	37.7	37.0	37.6	37.4	37.4	37.4
	150	31.3	30.9	31.1	30.8	29.5	31.1	30.3
	160	26.5	27.2	27.7	27.3	27.0	26.5	27.0
	170	24.4	25.9	24.8	25.0	25.7	25.4	25.2
	180	25.7	24.2	25.6	24.9	25.5	24.9	25.1

Position of the Probe		Void Fractions						
Radial (mm)	Angular (^{o})	1	2	3	4	5	6	Average
12	0	57.1	59.0	58.6	57.0	58.2	58.6	58.1
	10	59.1	57.1	57.6	57.6	57.8	58.7	58.0
	20	55.8	57.4	55.9	56.8	56.6	57.5	56.7
	30	56.5	56.9	56.0	56.3	58.2	59.0	57.2
	40	55.3	55.6	56.2	55.1	55.9	55.9	55.7
	50	54.1	52.3	53.6	53.4	52.1	53.1	53.1
	60	49.1	50.6	49.2	49.8	52.5	50.8	50.3
	70	48.0	47.3	46.6	47.8	47.1	47.3	47.4
	80	40.9	40.3	42.3	43.4	41.2	42.5	41.8
	90	33.3	33.4	32.4	31.4	34.0	33.5	33.0
	100	23.9	24.2	24.2	23.6	23.5	24.5	24.0
	110	15.0	15.2	16.7	15.9	16.2	16.3	15.9
	120	11.1	11.6	11.4	11.3	10.9	11.3	11.3
	130	9.6	8.7	8.6	8.6	8.5	8.6	8.8
	140	6.9	7.0	6.6	6.5	6.8	7.3	6.9
	150	6.3	6.0	6.1	6.3	6.0	6.0	6.1
	160	4.9	5.0	4.7	4.8	5.1	4.9	4.9
	170	4.3	4.0	4.5	4.8	4.1	4.5	4.4
	180	4.2	4.4	4.0	3.9	4.2	3.9	4.1

2. Calculation of Integrated Void Fraction.

$$\alpha_i \times A_i = 99.9 \times \frac{7.069}{2} + (99.9 + 96.4) \times \frac{1.571}{2} +$$

$$(99.9 + 99.9 + 99.9 + 99.9 + 99.9 + 99.9 + 99.9 +$$
$$99.8 + 99.8 + 99.6 + 99.4 + 98.9 + 98.3 + 97.7 +$$
$$97.2 + 96.5 + 96.4) \times 1.571 + (99.9 + 84.1) \times$$
$$\frac{3.142}{2} + (99.9 + 99.9 + 99.9 + 99.9 + 99.9 + 99.9 +$$
$$99.9 + 99.8 + 99.6 + 99.2 + 98.3 + 97.0 + 94.8 +$$
$$91.0 + 88.3 + 84.7 + 84.2) \times 3.142 + (99.6 + 44.3) \times$$
$$\frac{4.71}{2} + (99.7 + 99.7 + 99.7 + 99.6 + 99.5 + 99.3 +$$
$$98.9 + 98.2 + 97.2 + 95.2 + 92.1 + 87.3 + 78.9 +$$
$$68.6 + 55.6 + 49.2 + 44.2) \times 4.71 + (96.2 + 25.1) \times$$
$$\frac{2.749}{2} + (96.0 + 95.8 + 95.7 + 94.8 + 94.4 + 93.2 +$$
$$92.0 + 90.0 + 86.6 + 82.0 + 74.6 + 61.9 + 50.1 +$$
$$37.4 + 30.8 + 27.0 + 25.2) \times 2.749 + (58.1 + 4.1) \times$$
$$\frac{2.722}{2} + (58.0 + 56.7 + 57.2 + 55.7 + 53.1 + 50.3 +$$
$$47.4 + 41.8 + 33.0 + 24.0 + 15.9 + 11.3 + 8.8 + 6.9 +$$
$$6.1 + 4.9 + 4.4) \times 2.722 = 20893.6$$

$$A_i = 271.627$$

From Eq.(3.1b)

$$= \frac{\sum(\alpha_i x\ A_i)}{\sum A_i}$$

$$= \frac{20893.6}{271.627}$$

$$= 76.9\ \%$$

3. From Eq. (3.2), the quality is

$$x = \frac{W_G}{W_G + W_L}$$

$$= \frac{0.0215}{0.0215 + 0.4}$$

$$= 0.051$$

4. From Eq. (3.5), the slip ratio is

$$= \frac{x}{1 - x} \quad \frac{\rho_L}{\rho_G} \quad \frac{1 - \alpha}{\alpha}$$

$$= \frac{0.051}{1 - 0.051} \quad \frac{0.9982}{0.002847} \quad \frac{1 - 0.769}{0.769}$$

$$= 5.66$$

5. From Eq. (3.4), the real velocity of water is

$$U_L = \frac{W_L}{\rho_L (1 - \alpha) A}$$

$$= \frac{400}{0.9982 \times (1 - 0.769) \times 5.43}$$

$$= 319.5 \text{ cm/sec}$$

From Eq. (3.5), the real velocity of air is

$$U_G = \eta U_L$$

$$= 5.66 \times 319.5$$

$$= 1808.4 \text{ cm/sec}$$

6. From Eqs. (3.6) and (3.7), the superficial mass fluxes of each phase are

$$G_G^S = \alpha \rho_G U_G$$

$$= 0.769 \times 2.847 \times 18.04 \times 3600$$

$$= 1.42 \times 10^5 \text{ kg/m}^2\text{hr}$$

and

$$G_L^S = (1 - \alpha)\ \rho_L\ U_L$$

$$= (1 - 0.769) \times 998.2 \times 3.195 \times 3600$$

$$= 2.65 \times 10^6 \quad kg/m^2hr$$